OPTICAL MICRO-MANIPULATION IN HIV-1 INFECTED CELLS FOR IMPROVED HIV-1 TREATMENT AND DIAGNOSIS

by

MASIXOLE YVONNE LUGONGOLO

submitted in accordance with the requirements for the degree of

DOCTOR OF PHILOSOPHY

in the subject SCIENCE, ENGINEERING AND TECHNOLOGY

at the

UNIVERSITY OF SOUTH AFRICA

SUPERVISOR: Dr Patience Mthunzi-Kufa

CO-SUPERVISOR: Prof Malik Maaza

CO-SUPERVISOR: Dr Ombinda-Lemboumba

June 2020

Declarations

Name: **Masixole Yvonne Lugongolo**

Student number: **58521968**

Degree: **PhD in Science, Engineering and Technology (TFSET03)**

OPTICAL MICRO-MANIPULATION IN HIV-1 INFECTED CELLS FOR IMPROVED HIV-1 TREATMENT AND DIAGNOSIS

I declare that the above thesis is my own work and that all the sources that I have used or quoted have been indicated and acknowledged by means of complete references.

I further declare that I have not previously submitted this work, or part of it, for examination at UNISA for another qualification or at any other higher education institution.

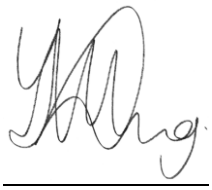

SIGNATURE

30 June 2020

DATE

Abstract

Laser application in the field of biological and medical sciences has significantly grown, thereby strengthening the field of Biophotonics. Research conducted in Biophotonics focuses on the concept of using light especially in the visible and near infrared regions of the electromagnetic radiation for the evaluation of living systems. In this thesis new discoveries are presented about low level laser therapy, optical trapping, transmission spectroscopy, luminescence spectroscopy and structured illumination microscopy (SIM), displaying the impact each technique has on HIV infected cells. The results showed that the irradiation of HIV-1 infected TZM-bl cells with low power red laser reduces HIV-1 infection. The outcomes of this study further proved that when irradiation is used in conjunction with efavirenz, an antiretroviral drug, HIV-1 infection could be reduced to undetectable levels in TZM-bl cells. Through the coupling of transmission spectroscopy with optical trapping, and separately, use of luminescence spectroscopy, label free diagnosis of HIV in infected cell samples was achieved. This finding affirms that HIV-1 infection can be detected in a label free manner when using laser based techniques. Furthermore, the photoluminescence spectrometer system was employed to generate a decay curve, which was necessary so as to have some understanding on lifetime of the luminescent signal in infected TZM-bl cells. Finally, in order to confirm that indeed TZM-bl cells were infected, an established super-resolution microscopy system SIM was used to detect HIV-1 infection in TZM-bl cells. Indeed in the infected cells viral molecules p24 and gp41 were detected through SIM, while they were not detected in uninfected cells. In future studies, super resolution microscopy would be coupled to an optical trapping system in order to confirm that each trapped cells is whether infected or uninfected so as to improve HIV diagnosis.

KEY TERMS:

Human immunodeficiency virus (HIV); TZM-bl cells; Infected cells; Uninfected cells, Label-free detection, Low level laser therapy; Optical trapping, Luminescence, Structured Illumination Microscopy

Acknowledgements

I would like to thank my supervisor, Dr Patience Mthunzi-Kufa and my co-supervisors; Prof Malik Maaza and Dr Saturnin Ombinda-Lemboumba for their immeasurable support, guidance, patience and many other forms of help they gave me during my research. I am grateful to Dr Saturnin Ombinda-Lemboumba and Dr Sello Manoto for assisting me with my experiments. I cannot forget the rest of the Biophotonics Team: Rudzani Malabi, Charles Maphanga and Lebogang Thobakgale for their support and companionship. Much gratitude also goes to the Council for Scientific and Industrial Research (CSIR), National Laser Centre (NLC), National Research Foundation (NRF) for funding my PhD and for also granting me the opportunity to develop my career.

On a more personal note, I would like to thank the following people: My family, relatives and friends especially my mother (Nomatolo Lugongolo), my sister (Nandi Lugongolo) for their prayers and support, Sisters in Jesus (Nancy Meulenberg, Dr Thandeka Khoza, Anna Salimo, Sharon Madzorera) for their prayers and encouragement. Aphiwe Kutshwa who would remind me the reason I am at CSIR when I was busy with other things instead of working. Thanks for your support Sihlobo sam. Qondiswa Cwayi, thanks for your prayers Sisi, uyiSibuso empilweni yam. PCM Class 30, thanks zithandwa for your support and prayer. My Buddies: Hola Bade and Helele Madala! Thanks for the love, encouragement and faith in me.

The biggest “thanks” goes to my God, My Creator, the Giver of life. Ndiswele imilomo ayaba iliwaka, ndibonge ngentlokomo uthando, inceba, intsikelelo engaka kuLowo unamandla onke, kuLizwi elinamandla eliviwa bubumnyama bububaleke. KuLowo ukukuKhanya kwam, Lowo onguMncedi wobomi bam, Lowo owenza indlela apho ingekho khona. Low’ubizwa nazinzulu nengxangxasi zazo. Lowo uLiThemba lam, neKhaka, neNtsika yam. Lowo ububomi bam.

This thesis is based on the following:

This thesis is ba on the following publications:

Publications

1. Lugongolo MY, Manoto SL, Ombinda-Lemboumba S, Maaza M, Mthunzi-Kufa P. The effects of low level laser therapy on both HIV-1 infected and uninfected TZM-bl cells. J. Biophotonics 2017; 10:1335-1344.
2. Manoto SL, Lugongolo M, Govender U, Mthunzi-Kufa P. Point of Care Diagnostics for HIV in Resource Limited Settings: An Overview. Medicina 2018; 54(1):3.
3. Ombinda-Lemboumba S, Malabi R, Lugongolo MY, Thobakgale L, Manoto SL, Mthunzi-Kufa P. Label-free differentiation of HIV-1 infected from uninfected cells using transmission measurement. J. Biophotonics 2019.
4. Lugongolo MY, Manoto SL, Ombinda-Lemboumba S, Maaza M, Mthunzi-Kufa P. The combination of low level laser therapy and efavirenz drastically reduces HIV infection in TZM-bl cells. Biomedical Journal, http://doi.org/10.1016/j.bj.2020.05.022.

Conference Proceedings

1. M. Y. Lugongolo, S. L. Manoto, S. Ombinda-Lemboumba, and P. Mthunzi-Kufa, "Laser irradiation reduces HIV-1 infection in TZM-bl cells," in Frontiers in Optics 2016, OSA Technical Digest (online) (Optical Society of America, 2016), paper FF2A.7.
2. M.Y. Lugongolo, S.L. Manoto, S. Ombinda-Lemboumba, M. Maaza and P. Mthunzi-Kufa, "Could low level laser therapy and highly active antiretroviral therapy lead to complete eradication of HIV-1 *in vitro*?," Proc. SPIE 10075, Biophysics, Biology and Biophotonics II: the Crossroads, 100750B (22 February 2017);

3. S. Ombinda-Lemboumba, R. Malabi, M. Y. Lugongolo, S. L. Thobakgale, S. Manoto, P. Mthunzi-Kufa, "Investigation of HIV-1 infected and uninfected cells using the optical trapping technique," Proc. SPIE 10075, Biophysics, Biology and Biophotonics II: the Crossroads, 100750M (22 February 2017);

4. M.Y. Lugongolo, S. Ombinda-Lemboumba, L.L. Noto, M. Maaza and P. Mthunzi-Kufa, "Label-free detection of HIV-1 infected cells via integration of optical tweezers and photoluminescence spectroscopy," Proc. SPIE 10501, Optical Diagnostics and Sensing XVIII: Toward Point-of-Care Diagnostics, 105011G (20 February 2018).

Patents

1. Lugongolo, MY, Manoto, SL, Ombinda-Lemboumba, S, Mthunzi-Kufa, P, & CSIR 2018, HIV INFECTION, W02018/002836 A1.

2. Ombinda-Lemboumba, S, Malabi, R, Lugongolo, MY, Thobakgale, SL, Manoto, S, Mthunzi-Kufa, P, & CSIR 2018, A method and system for analysing a biological sample of label free cells for presence of an infective agent, WO 2018/138659 A1

Table of Contents

4. Label-free detection of HIV-1 infection using luminescence spectroscopy

Appendix B

Appendix C

List of tables

List of figures

Abbreviations

AIDS	Acquired immunodeficiency syndrome
AP-1	Activator protein-1
ARV	Antiretroviral drug
ATP	Adenosine triphosphate
cAMP	cyclic Adenosine monophosphate
CCD	Charge coupled device
CCO	Cytochrome C oxidase
CCR5	C-C chemokine receptor type 5
CD4	cluster of differentiation 4
cDNA	complementary deoxyribonucleic acid
CRFs	Circulating recombinant forms
D_2O	Heavy water
DC	Drug control
DNA	Deoxyribonucleic acid
FITC	Fluorescein isothiocyanate
HAART	Highly active antiretroviral therapy
HIV	Human immunodeficiency virus,
L	Lens
LDH	Lactate dehydrogenase
LLLT	Low level laser therapy

M	Mirror
mW	milliwatt
NA	Numerical aperture
NC	Negative control
NF-κB	Nuclear factor kappa-light-chain-enhancer of activated B cells
NIR	Near infrared
nm	Nanometer
NNRTI	Non-Nucleoside Analogue Reverse Transcriptase Inhibitor
NO	Nitric oxide
PC	Positive control
PCR	Polymerase Chain reaction
PI	Propidium iodide
RLU	Relative Luminescence Units
RNA	Ribonucleic acid
ROS	Reactive oxygen species
SIM	Structured illumination microscopy
UV	Ultraviolet
W	Watt
WHO	World Health Organization
ZVD	Zidovudine
μm	Micrometer

Chapter 1

Introduction

1.1 Preface

The human immunodeficiency virus (HIV) is a retrovirus which belongs to a group of viruses known as lentiviruses that cause chronic and fatal diseases identified by long incubation periods, in the infected victim [1]. HIV causes acquired immunodeficiency syndrome (AIDS), a condition which occurs in humans due to the failure of the immune system thereby permitting opportunistic infections to flourish [2]. It is transmitted through sexual contact, exchange of bodily fluids such as blood, breast milk, and an infected mother can transmit HIV to the unborn child during pregnancy and at childbirth as the child gets exposed to the mother's blood or vaginal fluid [3]. The average survival time for infected individuals without treatment is estimated to 11 years depending on the HIV type, as HIV has two main types; HIV-1 and HIV-2, with HIV-1 being the most prevalent and the cause of the epidemic [4]. HIV-1 has three distinct groups, which are M, O and N; that have been differentiated based on variations in the envelope (*env*) region. Group M constitutes approximately 90% of HIV-1 infections and is subdivided into subtypes A, B, C, D, F, G, H, I, J, K and circulating recombinant forms (CRFs). With HIV-1 subtype C being the most prevalent in the Sub-Saharan Africa [5].

Despite extensive research that has been conducted in finding a cure for HIV infection, none has become available, therefore it remains a major global health problem and more than 35 million people have died from the infection since the start of the epidemic [6].

According to the UNAIDS latest fact sheet, by the end of 2018 there were approximately 37.4 million people living with HIV and more than 1.8 million became newly infected in 2018 [6].

As per the World Health Organization (WHO) reports, the African continent is the worst stricken region in the globe, with approximately 25.7 million infected people as it can be seen in Figure 1.1, and this accounts for almost two thirds of global HIV infections [7].

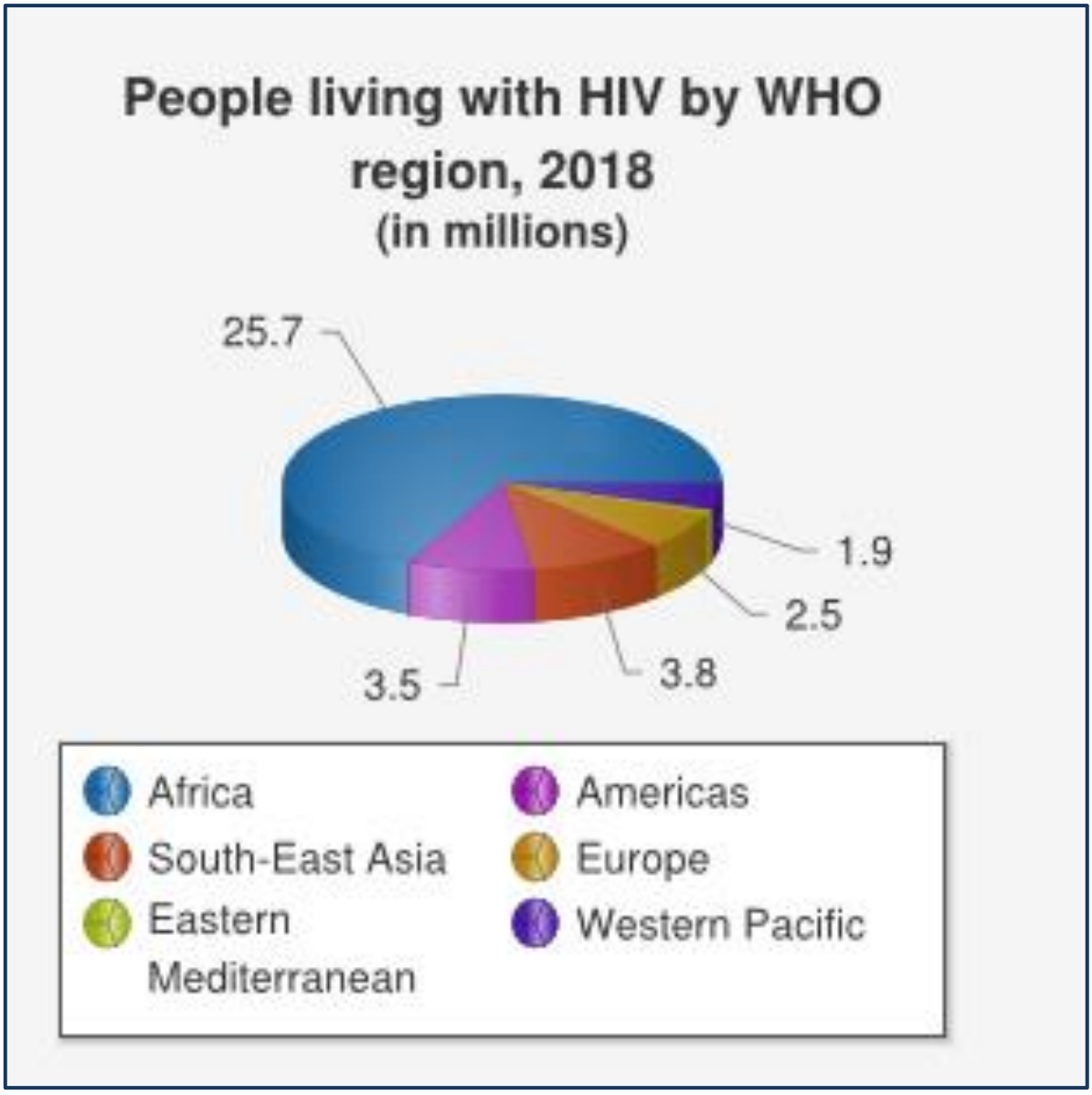

Figure 1.1 The global HIV infection estimates by the World Health Organization showing the estimated number of infected individuals per region [7].

Of note, South Africa has the largest HIV epidemic in the world, with 7.7 million infected individuals, which constitutes 20.4% of the general South African population [9]. In addition, approximately 240,000 new infections and 71,000 AIDS related deaths were reported at the end of 2018 [8]. Even though there is no cure for HIV infection yet, great strides have been made to dampen the detrimental effects of the infection by using antiretroviral (ARV) drugs.

Universally, the use of HIV treatment has improved over the years. Figure 1.2 shows that in 2000 only 0.6 million people had access to treatment, but that number had doubled by the end of 2018 to 23.3 million [9].

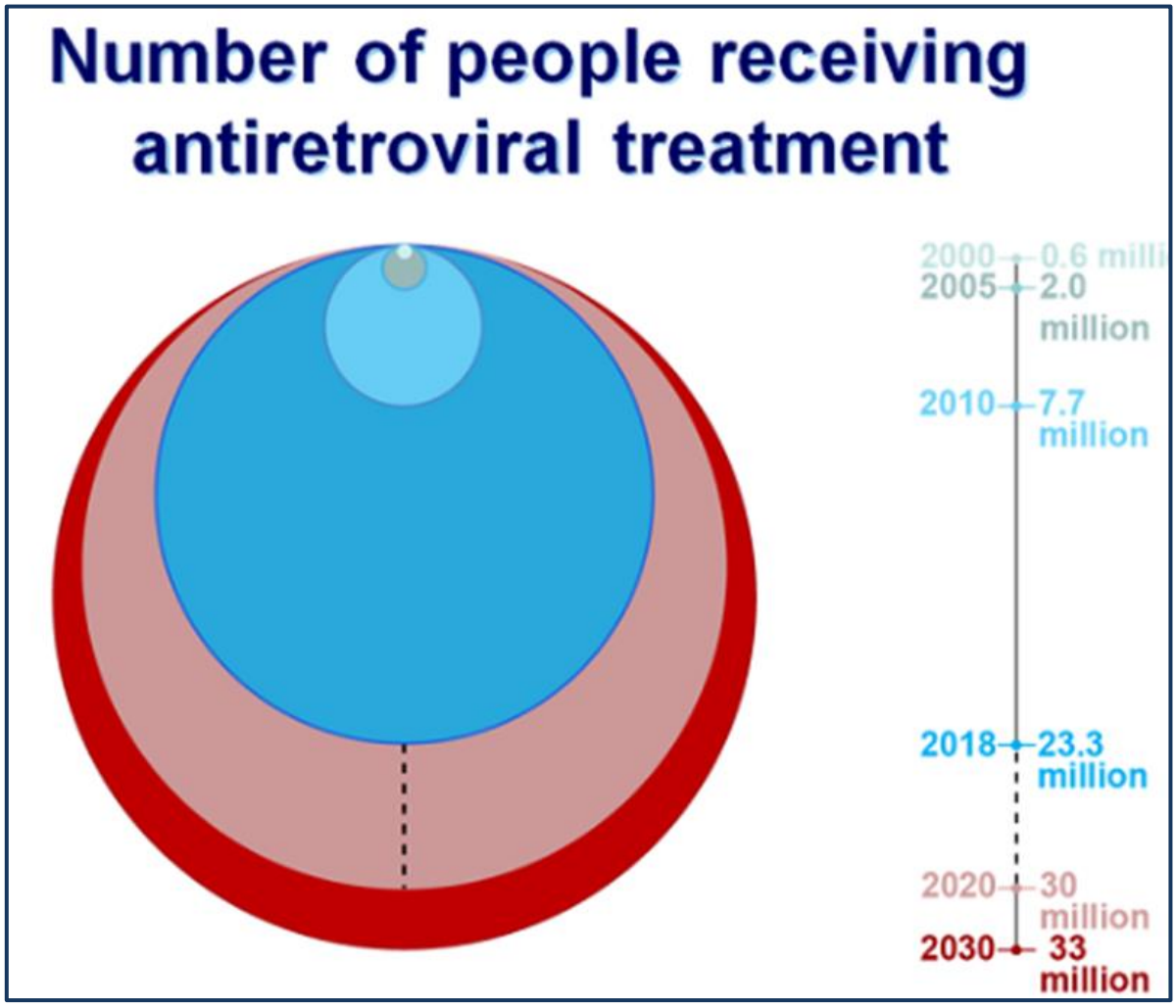

Figure 1.2 Persons living with HIV on antiretroviral treatment around the globe from 2000 to 2018 [9].

The ARV drugs control the infection and prevent transmission so that the infected individuals can have long and productive lives. In South Africa, its effectiveness is further demonstrated by an increase in national life expectancy from 61.2 to 67.7 years. Moreover, lately 3.9 million

HIV infected people are on treatment and that is a significant improvement compared with just over 600,000 individuals that were reported to be on treatment in 2009 (Figure 1.3) [10].

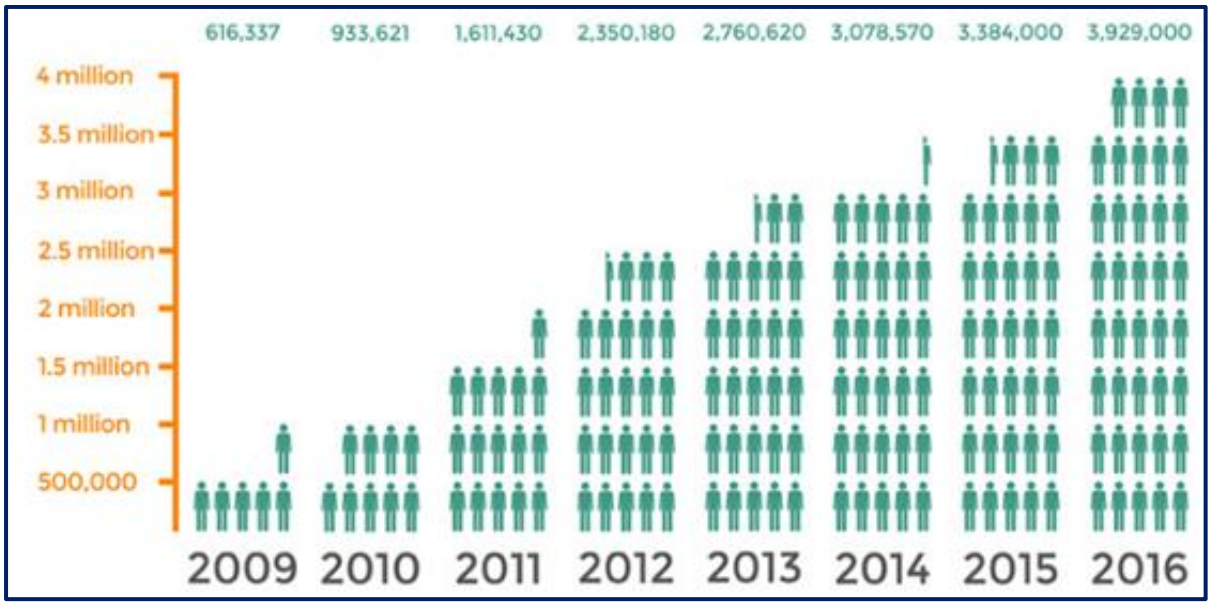

Figure 1.3 The increase in the number of people receiving antiretroviral treatment in South Africa from 2009 to 2016 [10].

These numbers continue to grow after the introduction of the universal test and treat strategy in September 2016 [10]. Since the challenge with HIV-1 is far from over, investigations towards laser based treatment and detection of HIV-1 were pursued and presented for the first time in this thesis. Subsections 1.1.1 to 1.1.3 below give a brief summary on the techniques used for the HIV-1 treatment and detection novel work completed.

1.1.1 Low level laser therapy on HIV infected cells

Obtaining a cure for HIV-1 infection is still an endeavor of many researchers. Approximately six years after the discovery of HIV-1, zidovudine (ZVD), an antiretroviral drug was made available to infected individuals and now more than 20 antiretroviral drugs are in existence [11]. Their usage is effective in reducing the amount of the virus in infected individuals and since they do not cure the infection, they are a lifelong treatment that must be strictly adhered to [12]. For this reason, treatment intake interruption could lead to the emergence of HIV-1 drug resistant strains, which might be difficult to treat [13]. Furthermore, using such drugs can cause some undesirable side effects, even though the drugs have been greatly improved over the years such that the severity of the side effects has been significantly minimized [14]. In an attempt to find a cure and explore the effectiveness of other forms of therapy with more reduced side effects, in this thesis low level laser therapy is used with the aim of reducing HIV-1 infection *in vitro* via measurements conducted on infected TZM-bl cells.

Low level laser therapy (LLLT) is a phenomenon which involves exposing tissue materials or cells to red and/or near infrared laser (light) with wavelengths ranging from 600 to 1,100 nm and low laser output powers of anything between 1 and 500 mW [15]. It has been used in the treatment of various medical conditions including diabetic wound healing, cancer, neurorehabilitation and more, but never on HIV-1 [16-19]. LLLT is an attractive form of therapy as its application stimulates physiological processes such as metabolism and proliferation which then enable the sick cells and tissue to heal naturally and at an optimum rate, thereby increasing the production of new cells, and enhances healing [20]. It is the stimulatory effects of LLLT that has encouraged its use in treating HIV-1 infection in TZM-bl cells as presented in chapter 2 of this thesis, with the anticipation that its use in HIV-1 infected

cells would increase the rate of growth for healthy cells (uninfected) to a point of outgrowing the infected ones.

1.1.2 Optical trapping and spectroscopic analysis of HIV-1 infected cells

Separately, HIV-1 diagnosis is conventionally done either immunologically to detect HIV antibodies or molecularly to detect viral molecules. These techniques have minimal discrepancies, they are effective and their use is valuable. Furthermore, these immunological and molecular methods are complex to run, since their application requires not only special bulky equipment, but also several reagents such as antibodies, antigens, enzymes, substrates, primers and polymerases in order to obtain the desired outcome. In addition, those that do not use sophisticated equipment; require the incorporation of some reagents or labelling for the antibodies in infected samples to be detected [21-23]. In order to simplify the detection of HIV-1 infection, researchers in various fields of science continue to explore various diagnostic methods. Since it has been observed and proven that light in the form of laser can exert pressure or force onto matter in order to study and investigate several substances at cellular and molecular levels, in this thesis optical trapping, transmission spectroscopy and luminescence spectroscopy are employed for the detection of HIV-1 infection in both individual cells and cell suspension.

Optical trapping is a highly sensitive technique that uses laser light forces for the non-invasive influence on nano- and micro- sized particles like cells. Using this technique, it is possible to diagnose diseases based on how light interacts with cells [24]. The dissimilarities detected on cells are commonly based on extracellular characteristics such as size, refractive index and shape [25].

Optical trapping setups can be coupled to other analytical systems for example spectroscopy and imaging setups in order to obtain as much detail as possible about the cell of interest.

1.1.3 Single molecule analysis of HIV-1 infected cells

Diagnosis of diseases is based on the detection of numerous substances on tissues and cells of the infected organisms. The detectable constituents include antibodies, molecules of the diseases causing agents and cellular or tissue damages introduced by the disease causing organism.

In some instances the recognition of a disease requires comparing the condition of a specific molecule in both diseased and healthy states. Similar to the detection of a disease causing agent molecule in infected cells, comparing molecules under two different settings (healthy and diseased) requires comprehensive analysis of either the diseased cells or the molecule of interest (which changes when there is an infection). Such experiments or detection mechanisms are known as single molecule analysis techniques. In the case of HIV-1 infection, single molecule analysis is done by detecting various viral components in infected cells. Since HIV-1 is small with about 120 nm in diameter, the detection and analysis of its components requires the use of super resolution techniques. Such techniques enable the user to visualize fluorescently labelled molecules, thereby affording a platform to enhance disease diagnosis. Understanding the differences caused by a disease in cells has a potential to create platforms for the detection of abnormalities in the infected cells without using labelling dyes. Performing single molecule analysis in this study was a way of confirming the presence of HIV-1 infection as shown by other techniques employed in the work presented in this thesis. Super resolution microscopy has been extensively used in the field of HIV-1 research; however, future plans

include integration with optical trapping to enable studying and intricately interrogating individually trapped cells.

1.2 Synopsis of thesis

This thesis contains six chapters. Chapter 1 gives a brief overview of HIV-1 and epidemic related statistics reports. It continues summarizing the use of low level laser therapy, optical micromanipulation and single molecule analysis in HIV-1 related research.

Chapter 2 focuses on the use of laser light of specific wavelengths in treating HIV-1 infection. Firstly, it gives a brief summary on the history of laser overview and the principles of laser by including the essential components necessary for laser production and modes of laser operation. Then, in a clear manner, chapter 2 describes mechanism of LLLT and the reasons behind its therapeutic effects on living organisms. The chapter also covers the interaction of light with biological matter. Furthermore, the applications of LLLT in the field of medicine are reviewed by looking into various medical areas where LLLT has been used. The chapter moves on to presenting challenges associated with HIV-1 treatment that led to the consideration of LLLT as a potential novel therapy. Finally, chapter 2 contains reports on the LLLT experiments conducted on HIV-1 infected TZM-bl cells and discusses the findings thereof.

Chapter 3 describes in detail the forces governing the optical trapping technique. It begins by expressing mechanisms associated with the two approaches observed in optical tweezing of particles with different sizes, which are the Rayleigh and Mie regimes. The chapter goes on to explain how the optical trap efficiency is determined and also demonstrates optical trapping using a tightly focused 3D Gaussian beam.

In this chapter, the construction of the optical tweezing setup used in the current study is fully described alongside its use in trapping HIV-1 infected TZM-bl cells. The chapter then continues to discuss how optical trapping was coupled with transmission spectroscopy in order to detect HIV-1 infection in TZM-bl cells.

Chapter 4 focuses on the detection of HIV-1 infection in TZM-bl cells using luminescence spectroscopy. Firstly, the chapter zooms in on the general luminescence mechanism as the production of luminescence is explained. Following that, the luminescence spectroscopy overview is defined by stating its principles together with essential elements of luminescence spectroscopy systems. Subsequent to that a brief review on various applications of luminescence spectroscopy is given. The chapter then looks into conventional methods of detecting HIV-1 infection in TZM-bl cells. In closing chapter 4 reports on the findings of the luminescence experiments conducted on HIV-1 infected cells and discusses the findings of the study while elaborating on the attractiveness of label free HIV-1 detection methods.

Chapter 5 focuses on the detection of HIV-1 infection in TZM-bl cells by using structured illumination microscopy (SIM). The chapter opens by giving a historical background on the development of super resolution microscopy and how it has advanced the field of cell biology by allowing users to observe and study nanometer structures that were previously impossible to visualize. As the chapter continues, it then focuses on the mechanisms of SIM by looking into the generation of the Moiré pattern and the application of multi-wavelengths in order to get information inside the cell. This is followed by a brief assessment on how SIM has been used previously.

As the chapter closes, the attention is placed on how SIM was used in the study presented in this thesis and discusses how its use would contribute towards label free detection of HIV-1 for smart diagnosis.

To finish, chapter 6 summarizes the contents of the thesis, while putting special emphasis on its unique aspects and their potential impact in the development of laser driven diagnostic tools and laser based treatment modalities.

References

1. "What is Lentivirus?" https://www.news-medical.net/life-sciences/What-is-Lentivirus.aspx; [Accessed 18 May 2019].
2. Weiss RA. How does HIV cause AIDS? Science 1993; 260(5112):1273–1279.
3. Mabuka J, Nduati R, Odem-Davis K, Peterson D, Overbaugh J. PLOS Pathogens 2012; 8(6):e1002739.
4. Venner CM, Nankya I, Kyeyune F, Demers K, Kwok C, Chen PL, Arts EJ. Infecting HIV-1 subtype predicts disease progression in women of Sub-Saharan Africa. EBioMedicine 2016; 13:305–314.
5. Buonarguro L. Human Immunodeficiency Virus Type 1 subtype distribution in the worldwide epidemic: pathogenetic and therapeutic implications. Journal of Virology 2007; 81(19):10209-10219.
6. Global HIV & AIDS statistics — 2019 fact sheet, http://www.unaids.org/en/resources/fact-sheet; [Accessed 24 January 2020].
7. Data and stats, http://www9.who.int/hiv/data/en/; [Accessed 24 January 2020].

8. South Africa, https://www.unaids.org/en/regionscountries/countries/southafrica; [Accessed 24 January 2020].

9. Antiretroviral therapy coverage among all age groups, https://www.who.int/gho/hiv/epidemic_response/ART/en/; [Accessed 24 January 2020].

10. UNAIDS Strategy, http://www.unaids.org/en/goals/unaidsstrategy, [Accessed 18 May 2018].

11. Fischl MA, et al. The efficacy of azidothymidine (AZT) in the treatment of patients with AIDS and AIDS-related complex. A double-blind, placebo-controlled trial. The New England Journal of Medicine 1987; 317(4):185–191.

12. Buell KG, Chung C, Chaudhry Z, Puri A, Nawab K, Ravindran RP. Lifelong antiretroviral therapy or HIV cure: The benefits for the individual patient, AIDS Care 2016; 28(2):242-246.

13. Condra JH, Schleif WA, Blahy OM, Gabryelski LJ, Graham DJ, Quintero JC, Emini EA. *In vivo* emergence of HIV-1 variants resistant to multiple protease inhibitors. Nature 1995; 374(6522):569–571.

14. Guidelines for the Use of Antiretroviral Agents in Adults and Adolescents Living with HIV, https://aidsinfo.nih.gov/guidelines/html/1/adult-and-adolescent-arv/31/adverse-effects-of-arv; [Accessed 20 May 2018].

15. Bolton P, Young S, Dyson M. The direct effect of 860 nm light on cell proliferation and succinic dehydrogenase activity of human fibroblast *in vitro*. Laser Therapy 1995; 7:55-60.

16. Hashmi JT, Huang YY, Osmani BZ, Sharma SK, Naeser MA, Hamblin MR. Role of Low-Level Laser Therapy in Neurorehabilitation. PM&R the journal of injury, function, and rehabilitation 2010; 2:S292-S305.

17. Dastanpour S, Momen BJ, Saber K. The Effect of Low-Level Laser Therapy on Human Leukemic Cells. Journal of Lasers in Medical Sciences 2015; 6(2):74-79.

18. Kajagar BM, Godhi AS, Pandit A, Khatri S. Efficacy of Low Level Laser Therapy on Wound Healing in Patients with Chronic Diabetic Foot Ulcers—A Randomized Control Trial. The Indian Journal of Surgery 2012; 74(5):359-363.

19. Stona P, da Silva VE, dos Santos PL, Blessmann WJB, Floriani KP. Recurrent Labial Herpes Simplex in Pediatric Dentistry: Low-level Laser Therapy as a Treatment Option. International Journal of Clinical Pediatric Dentistry 2014; 7(2):140-143.

20. Karu TI. Photobiology of low-power laser effects. Health Physics 1989; 56:691–704.

21. Bartlett JG, Gallant JE. 2000-2001 Medical Management of HIV Infection. Baltimore: Port City Press, 2000.

22. Centers for Disease Control and Prevention. Revised guidelines for HIV counseling, testing, and referral. MMWR Recomm Rep 2001; 50:1-57.

23. Zhang M, Versalovic J. HIV update. Diagnostic tests and markers of disease progression and response to therapy. Pathology Patterns Reviews 2002; 118:S26-32.

24. Ashkin A, Dziedzic JM. Optical trapping and manipulation of viruses and bacteria. Science 1987; 235:1517–1520.

25. Gongora JST, Fratalocchi A. Optical force on diseased blood cells: Towards the optical sorting of biological matter. Optics and Lasers in Engineering 2016; 76:40-44.

Chapter 2

The effects of low level laser therapy on HIV-1 infection in the presence or absence of efavirenz

Introduction

The beginning of this chapter deals with the history of lasers and principle of laser production. Following this is the history of light therapies in conjunction with the mechanism of low level laser therapy (LLLT). Then a review on the suitable wavelengths for LLLT is given together with how biological matter absorbs laser during LLLT. Next, the use of LLLT in the treatment of various medical conditions is covered. Thereafter, challenges (leading to the investigation of how LLLT can affect HIV infection) associated with HIV-1 treatment are described. Furthermore, the construction of a simple LLLT experimental setup used is demonstrated and all its components such as the laser wavelength and power are described. Later in the chapter, the outcomes of using LLLT to treat HIV-1 infection in the presence or absence of antiretroviral treatment in a model system (TZM-bl cells) are discussed.

2.1 Laser history and production

2.1.1 Brief history of lasers

Lasers are instruments producing intense beams of light that are monochromatic, highly collimated and coherent.

Owing to their properties, lasers are used in a variety of fields such as guidance systems, communication, photography, scanners, holography and medicine [1]. Their existence is attributed to Albert Einstein who hypothesized the process that makes laser possible by suggesting that besides absorbing and emitting light spontaneously, electrons could be stimulated to emit light of a specific wavelength [2]. Hence the invention of the acronym LASER, which stands for Light Amplification by Stimulated Emission of Radiation, as coined by Gordon Gould [3]. Einstein's hypothesis was successfully put into practise by Theodore Maiman in 1960 when he constructed the first working ruby laser, which had silver-coated ends that were reflective to effectively serve as an optical resonator. Maiman's laser was based on optical pumping of ruby crystal with a flash lamp, which generated a 694 nm red laser [4].

2.1.2 Principles of lasers

Laser production is dependent on three basic components, which are the gain medium, energy source and optical resonator. Firstly, the gain medium; the source of optical gain within the laser and is capable of undergoing population inversion. It also determines both the laser type and laser wavelength. The medium can either be solid, gas, liquid or semiconductor diode. Secondly, the energy source, which provides the necessary energy and can either be optical, electrical or chemical. Finally, the optical resonator contains two parallel mirrors, which act as the feedback mechanism for the amplification of light. Mirror 1 denoted as M1 in figure 2.1 is highly reflective and allows no light to pass through, whereas mirror 2 denoted as M2 in Figure 2.1 is partially reflective [2,3,5].

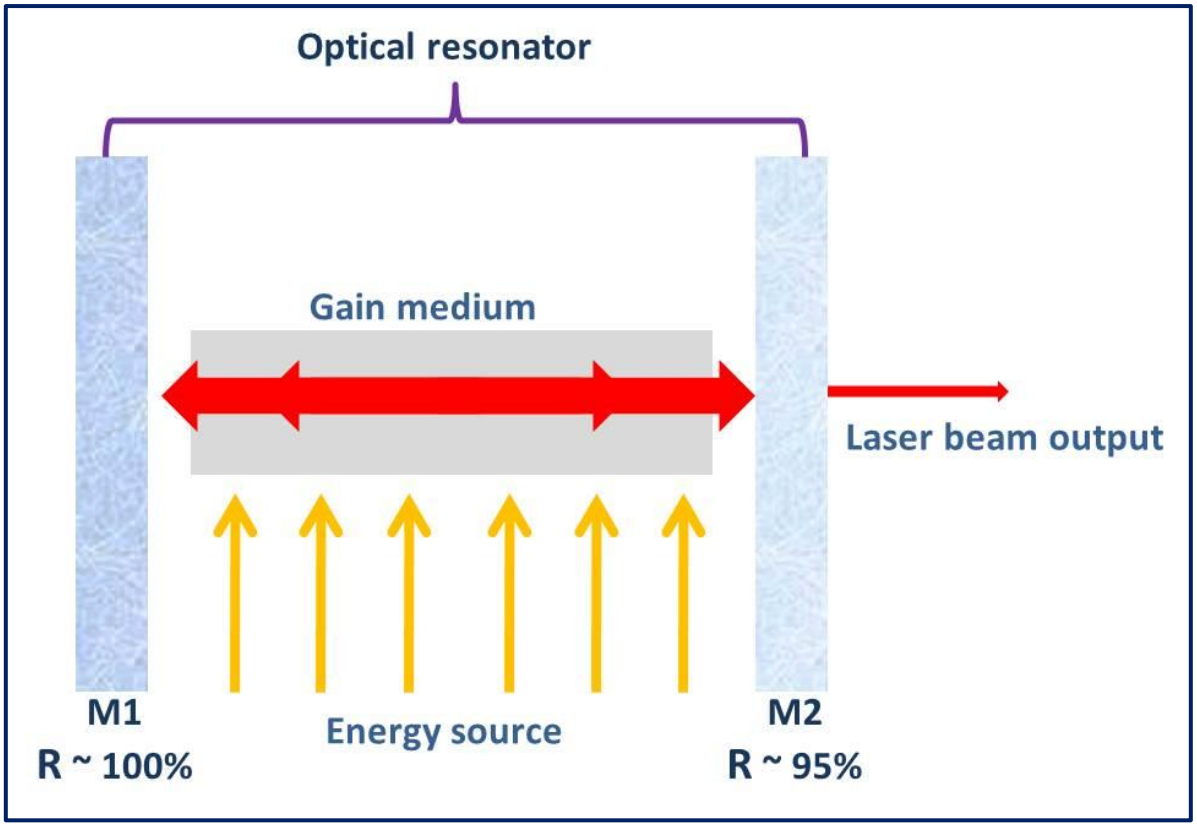

Figure 2.1 Schematic representation of the principle of laser showing laser cavity and the laser operation, where R is the level of reflectivity [2,3,5].

The lasing medium has atoms, and any atom has a central nucleus which contains protons and neutrons that are surrounded by electrons in different orbitals. These electrons jump from one orbital to another, as long as they absorb and emit energy in the form of photons, as determined by the equation:

$$E = hv \tag{2.1}$$

Where E is the photon energy, h is Planck's constant (6.63 x 10^{-24} J/s) and v is the photon frequency. Electrons in atoms are normally in a lower ground state and when they absorb light from the excitation source, the majority of electrons become excited and jump to a higher energy state, a process called population inversion. Electrons in this state are unstable and they quickly move back to the ground lower energy level through the emission process, which

happens in two ways. In spontaneous emission, electrons jump to their ground state while emitting photons in a random direction and a random phase, with a wavelength determined by the difference in energy of the two states. On the other hand, stimulated emission occurs when a photon collides with an atom in the excited state thereby releasing another stimulated photon, identical to the incident photon in its direction, phase and wavelength. The light energy is amplified until sufficient energy is built up for the release of laser light through the partially reflective mirror [5, 6].

Lasers are classified according to their modes of operation, which are determined by the power output as well as their mode of operation i.e. continuous wave mode or pulsed mode. In the continuous wave (Figure 2.2A), the power output is continuous over time, whereas in the pulsed mode (Figure 2.2B) of operation the laser beam power output varies with respect to time, thereby giving high peak powers [7].

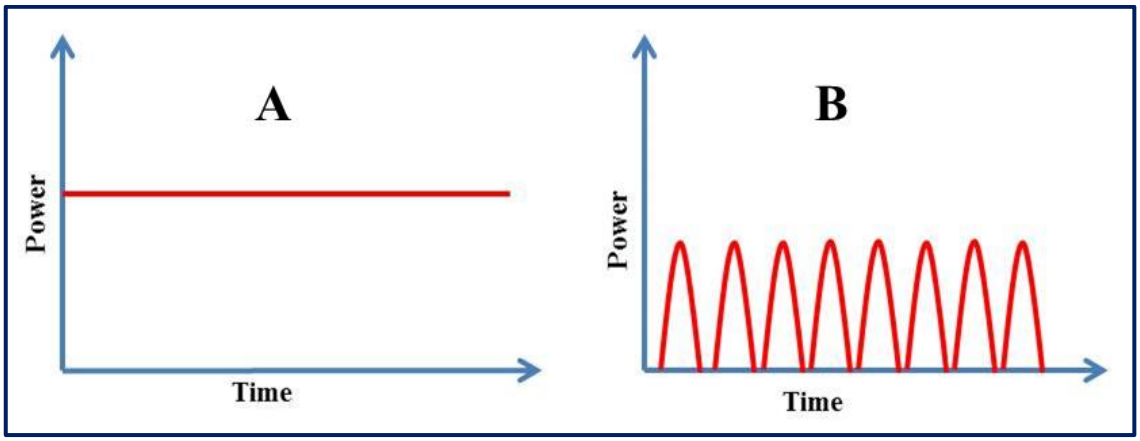

Figure 2.2 Two modes of laser operation: (A) profile of continuous wave laser output and (B) represents the profile output of a pulsed laser which are normally high power lasers [7].

Both these modes of laser operation have been widely used in laser therapy and in various applications in the Biophotonics field of study [8,9].

2.2 Overview of low level laser therapy

2.2.1 Discovery of light therapies

The use of electromagnetic radiation (light) for medicinal purposes was established on the interaction of light from sources such as the sun, fire, electric discharge and bulbs with biological matter. The ancient Romans, Greeks, Egyptians, Chinese, Indians used sunlight for phototherapy and photo-chemotherapy to treat various skin ailments such as leukoderma, rickets and skin cancer [10]. Following the invention of the first laser by Theodore Maiman in 1960, physicists and engineers began to investigate the potential applications of lasers for therapeutic purposes [8]. Only much later after this breakthrough, was the efficacy of laser as a form of treatment discovered [11]. The discovery was made when Endre Mester wanted to treat cancerous tumour cells on rats using laser. He instead noticed that applying laser light was not killing the tumour cells, but accelerated wound healing on surgical sites and also stimulated hair growth on shaved mice [11].

2.2.2 Mechanism of low level laser therapy

Low level laser therapy is the application of red and near infrared lasers with wavelengths of 600 to 1,100 nm at low powers of 1 to 500 mW for therapeutic purposes [12,13]. The mechanism of LLLT in the treatment of different medical conditions is not fully understood. However, unlike high power lasers that generate a thermal effect, low power lasers are used in LLLT to induce photochemical effects in cells, a phenomenon known as photo-bio-modulation or bio-stimulation.

Photobiology principle states that when light hits a chromophore the energy of the photons causes electrons to be excited and they move from a lower to a higher orbit. Several pieces of evidence show that these photochemical effects and electron shifts from one orbital level to another take place when mammalian cells absorb red and near infrared (NIR) light by mitochondrial chromophore, cytochrome c oxidase (CCO), and also by the photo-acceptors in the cell plasma membrane [14].

In cells, LLLT causes the photo-dissociation of nitric oxide (NO) from CCO. Normally, stressed cells produce NO by mitochondrial NO synthase, displacing oxygen from CCO, which leads in a down regulation of cellular respiration and decrease in the production of adenosine triphosphate (ATP). So the dissociation of NO from CCO as a consequence of LLLT prevents oxygen displacement from CCO and promotes unobstructed cellular respiration. Therefore, the absorption of light stimulates the electron transport chain, which leads to the synthesis of ATP and cyclic adenosine monophosphate (cAMP), production of reactive oxygen species (ROS) and release of nitric oxide (Figure 2.3) [14-16].

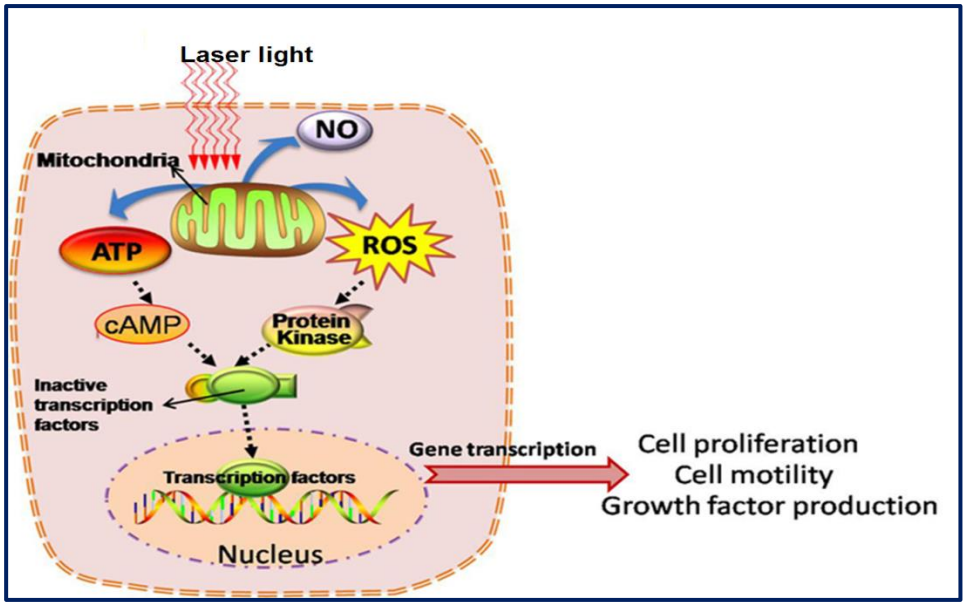

Figure 2.3 Low level laser therapy mechanisms showing the different molecules involved in the therapeutic process [17].

Reactive oxygen species are the free radicals and reactive molecules that originate from molecular oxygen produced during electron transport as by-products [18]. It was presumed that these molecules only have damaging effects in cell components, however, recently it has been demonstrated that ROS play significant and beneficial roles in cell signalling processes and other physiological processes [19-20]. The induction of these molecules by LLLT have positive effects as they induce transcription factors like nuclear factor Kappa B (NF-κB) and activator protein-1 (AP-1), which in turn promote gene expression, thereby increasing protein synthesis, cell proliferation, cell migration, production of cytokines and growth factors, as well as increased tissue oxygenation [12-13,21-22]. Furthermore, the absorption of photons by mammalian cells regulates enzymatic activity and balances both intracellular and extracellular pH [23].

Yaakobi *et al*, 2001 [24] have also reported that LLLT increases antioxidant levels and plays a significant role in protein-protein interactions and establishing proper protein conformation as it stimulates the expression of heat shock proteins.

2.3 Laser wavelength and biological material

2.3.1 Laser light absorption in cells

Biological materials such as cells are rich in proteins which are responsible for various roles; from transporting oxygen to intricate processes for example supplying a light-induced neurological response for vision. Amino acids as building blocks of proteins are aliphatic or aromatic [25]. The aliphatic amino acids absorb light of wavelengths shorter than 240 nm. On the other hand, aromatic amino acids absorb at wavelengths longer than 240 nm, but not within the visible region of the light spectrum. In addition to light absorption by amino acid residues, protein bonding in the form of polypeptide bonds and disulphide bonds are absorptive thus contributing to the total protein absorption of light [26]. To demonstrate classic absorption coefficients for various materials (water, whole blood, skin, cells), Figure 2.4 illustrates the absorption qualities of these materials [27].

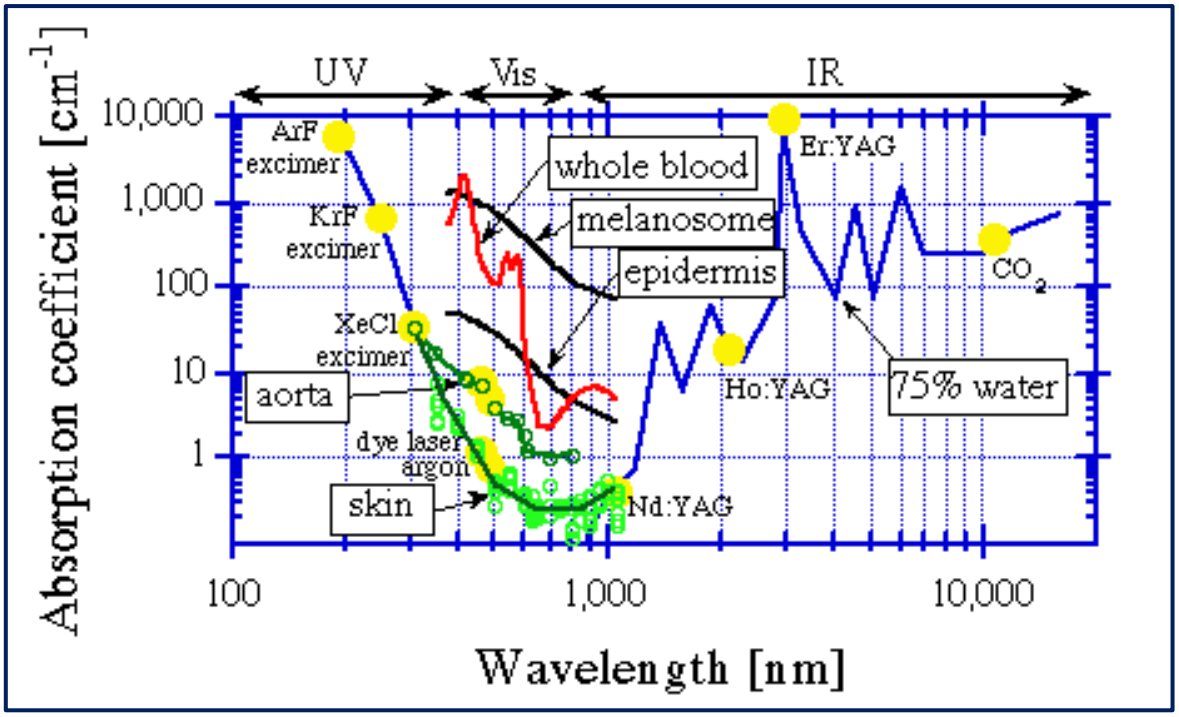

Figure 2.4 The absorption spectra of some biological species. In the UV region, there is an increase in absorption of light with shorter wavelengths due to protein, DNA and other molecules. In the IR region, the increase in absorption of light with longer wavelengths results from the tissue water content. There is minimal absorption in the red and NIR [27].

Other biological materials that absorb light are purines and pyrimidines, which are building blocks of deoxyribonucleic acid (DNA) and ribonucleic acid (RNA). They absorb light between 230 nm and 300 nm, whereas carbohydrates absorb lower than 230 nm [28-29]. Despite the inability of water to absorb radiation in the between ultra-violet (UV) and the NIR, its absorption peaks emerge weakly above 1300 nm and its peaks are more pronounced at ≥ 2900 nm and very strong absorption is at 10 000 nm [30]. Characteristically, cells exhibit notable transparency between 800 and 1100 nm; as such the majority of biological studies are done with lasers at these wavelengths [31].

2.3.2 Laser wavelengths suitable for LLLT

Generally, the interaction of light with matter results in the scattering of the incident light rays, reflection, refraction, as well as absorption. For biological materials such as tissues, cells or organelles; the interaction of light with matter tends to induce a chain of events, which result in the manifestation of thermal, physical, chemical and mechanical effects or their combination [32]. To avoid undesirable outcomes and to ensure effective treatment when doing LLLT experiments, a suitable wavelength must be carefully selected. Tissues have an "optical window or therapeutic window" which runs between 650 nm and 1200 nm where the tissue permeation is optimal [32]. It should therefore be noted that LLLT in mammals, mammalian tissues and cells should be done using wavelengths between 600 nm and 1100 nm; covering the red and near infrared region of the electromagnetic spectrum [31]. Within the therapeutic window, various regions are more effective when used for a specific purpose, for instance, the 600 to 660 nm treatment stretch is the best option for superficial scar tissue as it is absorbed close to the surface [33].

It is also the preferred choice when treating more complex problems with no knowledge of the exact treatment location. The energy of this region can move through the body and interact with damaged cells in several body parts [33]. The 800 to 850 nm region is the best for deeper penetration and cellular interaction [32]. Lasers in this range are adjusted to interact with the mitochondria and elicit an increase in CCO and ATP, the two substances required in the remedial process [34]. While lasers within 905 nm interact with iron in hemoglobin and oxygenate the sick area. Oxygen is one of the essential molecules required for healing to successfully take place [35]. The 980 nm region is the peak of light interaction with water in the body and the energy generated here creates thermal gradient leading to an increase in circulation and blood flow.

The increase in circulation accelerates the natural healing process. However, the 980 nm lasers are great for laser surgery and less ideal for therapy because high energy level contained in this wavelength is converted into heat [36].

2.4 Applications of low level laser therapy in biomedical sciences

Few years after the invention of lasers in 1960, lasers were demonstrated to have therapeutic effects through the application of low power laser [8]. Since then LLLT has been used to treat various medical conditions including diabetic wounds, cancer, neurological challenges and many more. Section 2.4 focuses on reviewing the work that has been previously done with LLLT towards treating medical disorders in order to highlight its potential as it is used for HIV-1 infection therapy in this study.

2.4.1 Low level laser therapy in diabetic wound healing

Diabetes mellitus is a metabolic disease in which glucose is underused and characterized by hyperglycaemia. Diabetes is a growing health concern worldwide, which is aggravated by poor diet in the modern culture due to an increase in fat intake and reduction in the consumption of fruit and vegetables leading to obesity. [37]. Diabetes sufferers are predisposed to several complications for example diabetic foot wounds, as they have been shown in many experimental and clinical studies [38]. Diabetic wounds are chronic due to impaired healing process and slow recovery because of physiological defects. Furthermore, diabetic ulcers are prone to poly-microbial infections; as diabetic patients have altered immune function and therefore increased susceptibility to infection and structural deformity [39]. Because of wound infections patients later develop gangrene, which normally results in limb amputation. Several factors such as decreased synthesis of collagen, production of growth factors, keratinocyte and

fibroblast proliferation contribute to poor wound healing in diabetic patients. Non-healing wounds are associated with high treatment costs with little or no success [40]. Due to these challenges, the medical fraternity is looking into other alternative ways in order to improve and hasten tissue restoration in diabetic wounds.

Owing to its photochemical effects, low level laser therapy is gaining popularity in treating diabetic wounds. Several studies have shown that low level laser therapy has great healing effects on diabetic wounds [41]. It has been reported that LLLT stimulates microcirculation and angiogenesis, which lead to improved blood circulation and reduced tissue damage. In both *in vitro* and *in vivo* studies, experimental and clinical studies, LLLT has been successfully used. *In vitro* the positive impact of phototherapy in cell cultures has been displayed in several ways. In a study conducted by Ayuk *et al* 2012 [41], the healing effect of LLLT was shown by a significant increase in cell viability, cell proliferation, collagen content and cell migration. In that study wounded fibroblasts were irradiated with 5 J/cm^2 at 660 nm. In other study using human fibroblast, the wounded cells were exposed to a 636 nm diode laser at a density of 5 J/cm^2 and accelerated wound closure, normalization of cell function and increased proliferation were observed [42].

Great success when using LLLT has also been shown in *in vivo* studies: Yamany and co-workers 2012 [43] performed a study with 30 females and male diabetic patients who were treated with a 850 nm laser for a period of four weeks. The laser treated group experienced reduction in pain and a significant improvement in foot skin microcirculation. In another experimental trial 13 patients who were unresponsive to other forms of treatment were treated with phototherapy combining both 660 nm and 890 nm.

Their leg ulcers were irradiated twice a week for three months and the wounds achieved 90 to 100% recovery by day 90 in 75% cases, the healing was due to an increase in tissue granulation [44]. Literature suggests that for diabetic wound healing the best dose is 0.5 - 5 J/cm^2 with wavelengths ranging between 600 and 700 nm, even though there are a number of successful treatments outside of this range [45].

2.4.2 Low level laser therapy in cancer

Cancer is a disease distinguished by abnormal growth and uncontainable cell division, which has a potential to infiltrate other parts and destroy normal body tissues [46]. It is caused by various factors such as inherited genetic defects, environmental factors, lifestyle and microbial infections [47]. Cancer affects any part of the body and usually named according to the affected body part. There are several available cancer treatments and the choice of treatment is dependent on factors such as cancer type, stage, patient's state of health, and in some instances treatments are combined. Treatment options include chemotherapy, radiotherapy, immunotherapy, surgery, stem cell transplant, hormone therapy and targeted drug therapy. Other alternative means of treatment are being explored including LLLT. However, practitioners do not encourage the use of LLLT for cancer treatment with the fear that it might promote the proliferation of malignant cells, and worsen the condition. In cancer related cases, LLLT has been successfully used to prevent and manage the complications caused by the treatment and also to treat other conditions that the cancer sufferers might be burdened with [48-49].

2.4.3 Low level laser therapy in neurorehabilitation

Neurorehabilitation is a complicated medicinal path aiming to encourage recovery from a nervous system injury or sickness to lessen any functional alterations resulting from it [50]. Disturbances associated with the nervous system result in various neurological disorders such as stroke, brain tumours, epilepsy, dementia and many others [51]. Various effective treatments for neurological disorders are available. In addition to these available treatments, LLLT is also recommended and has been successfully used in many studies. In most studies associated with the application of LLLT, the radiation is applied to the head and that is known as transcranial LLLT [52]. Transcranial LLLT was shown to improve outcomes in patients with acute stroke when applied over the entire head surface (20 points in the 10/20 electroencephalographic system) nearly 18 hours after the stroke had occurred. This significant change was observed after only LLLT treatment and the improvement was still present even 90 days later. In that study a near infrared 808 nm laser delivering a fluence of 0.9 J/cm^2 was used [52].

Transcranial LLLT has also been shown to successfully keep traumatic brain injury related neurological disorders in check with continuous treatments. In one case a 52 year old retired woman who had experienced multiple traumatic brain injuries and her brain MRI showed front parietal atrophy. Before beginning with transcranial (light emitting diode) LED treatments she had been medically incapacitated for 5 months. Following 4 months of nightly LED treatments, she went back to work full-time and discontinued medical disability leave [53]. For neurological abnormalities**,** the best wavelength range seems to be between 800 nm and 1000 nm, as these wavelengths can penetrate the scalp and skull and reach the brain [54].

2.4.4 Low level laser therapy in other medical conditions

Above and beyond the three medical conditions discussed above, LLLT has been utilized for the treatment of many other medical conditions such as hair loss, skin related problems, and pain. In this section I will give a short review of what has been achieved with LLLT for the treatment of other medical conditions. After Mester's observation of mice hair growth due to laser irradiation [8], several other studies using mice models demonstrated the hair growth effects of LLLT [55-56]. The stimulatory effects of LLLT on hair growth were also observed in clinical trials: In one study 24 male patients suffering from androgenetic alopecia were treated with 655 nm and 780 nm laser for ten minutes a day over a period of 14 weeks. Subsequent to the treatment an increase in hair density was observed and 83 % of the patients were pleased with the treatment [57]. When the HairMax LaserComb® device was used in two different studies; all the 145 patients who participated experienced a substantial improvement in overall hair growth and significant reduction in hair loss [57-59].

A study conducted by Aziz-Jalali *et al*, 2012 [33], where LLLT using a 630 nm InGaAs laser at 12 J/cm^2 showed considerably reduced active acne abrasions after several weeks of therapy over a 10 week period on 28 study participants. The success of this study was attributed to the red light's ability of regulating the secretion of sebum by sebaceous glands and also changing keratinocyte behavior. Moreover, irradiation with red laser is associated with a reduction in inflammation due to the modulation of cytokines by macrophages and others cells [60]. In one study sunburn symptoms associated with skin burning, redness, peeling and swelling were significantly reduced after the 10 patients had received 590 nm LED treatment for three days [61]. Skin rejuvenation has also been achieved when using LLLT. It has been shown by the reduction in the appearance of wrinkles and it is associated with an increase in the production of pro-collagen, collagen, proliferation of fibroblasts following exposure to low power laser

irradiation in both *in vitro* and *in vivo* studies [62-64]. The efficacy of LLLT on skin related disorders has been seen in the treatment of psoriasis that had been resistant to conventional therapy. That was achieved by sequentially treating the patients with 830 nm and 630 nm wavelengths with 20 minute sessions over a 4 weeks and no adverse side effects were observed [65].

LLLT has been extensively used for various kinds of pain such as osteoarthritis, neck pain frozen shoulder and orthodontic pain [66-76]. In a double-blinded randomized placebo-controlled trial, participants who were treated with LLLT experienced a significant reduction in knee associated pain compared to those who were treated with sham treatment [68]. The pain associated with frozen shoulder can be effectively reduced by LLLT while the inability to move the arm can be treated by corticosteroid injections and other forms of treatment [72]. Orthodontic procedures are usually followed by pain which usually forces patients to interfere with their treatment [75-76]. However, LLLT has been shown to successfully produce analgesic effects in various clinical applications in controlling orthodontic post adjustment pain [76].

It is worth noting that the majority, if not all the medical conditions that have been treated with LLLT are non-communicable disease. The focus of the work presented in this thesis is the use of LLLT in the treatment of HIV-1, which is a communicable disease that has burdened the global health sector for more than three decades.

2.5 Challenges with HIV-1 treatment

Great strides have been made to treat HIV-1 since its discovery in the early 1980s. These victories are largely due to the availability and use of effective antiretroviral drugs. However, HIV-1 treatment struggles are far from being over because even the current HIV-1 treatment has a few challenges such as high cost, lifelong intake and the development of resistant strains of HIV-1 that render some antiretroviral drugs ineffective. In sections 2.5.1 to 2.5.3; these challenges will be discussed.

2.5.1 Antiretroviral Spending in South Africa

South Africa has the highest expenditure on HIV-1 treatment programme in the world [77]. Between 2014 and 2015 the national department of health spent $350 million on antiretroviral treatment for just over 3 million people living with HIV-1 [78-79]. By the end of 2016 that number had increased to 3.9 million individuals. However, this bleak picture of expensive treatment was changed when a pricing agreement was reached between the Kenyan and South African governments in collaboration with UNAIDS, the Clinton Health Access Initiative, Unitaid, the Bill & Melinda Gates Foundation, the United Kingdom's department for International development, the Global Fund to fight AIDS, TB & Malaria and the U.S. Agency for International Development. This new collaboration aimed to accelerate and bring about significant reduction in the national expenditure on the antiretroviral therapy programme by the introduction of a state-of-the-art pill which is a combination of three antiretroviral drugs. The backbone of this pill is dolutegravir, which is combined with tenofovir and lamivudine and is commonly referred to as TLD representing the first letters of each drug contained in the pill.

Its introduction will not only bring about economic benefits, but it will also come with clinical benefits as it has less side effects and therefore better tolerated than efavirenz and nevirapine [80-83]. With this new pill the South African government is estimated to save $900 million over six years [81].

2.5.2 Antiretroviral therapy as a lifelong treatment

Since HIV infection is a chronic medical condition, it requires a lifetime treatment and the current treatment is not a cure, but a means of keeping the virus in check without being able to replicate. The presence of latent viral reservoirs in infected individuals makes the virus incurable. In the reservoirs the virus lies dormant, transcriptionally silent without replication and production of viral progeny until reactivation by stimuli. Some infected cells in the reservoirs escape immune detection and elimination. Reservoirs can be found all over the body, including digestive tract, brain and lymph nodes. Due to the presence of these dormant sites, antiretroviral drugs must be taken with strict adherence without any interruption. Treatment interruption poses a major risk of activating the dormant virus to start replicating [84-85].

Furthermore, due to the error prone character of HIV-1 reverse transcriptase enzyme, every lytic cycle gives rise to virions containing 5 to 10 bases that are different from the parent virus. This variation in viral sequence is commonly known as drug resistance mutation, which can cause treatment failure [86]. With the emergence of drug resistant strains of HIV, there is an increase in costs as drug resistance tests must be conducted to establish which of the drugs in the cocktail has become ineffective. In addition, a new treatment regimen would have to be used and in some instances, it might be challenging to treat the infection with the already in use drug combinations [87].

Due to the challenges associated with HIV-1 treatment, the study presented in this chapter was designed as means of looking into other forms of therapy for HIV-1 infection. Similar to other research studies in HIV-1 treatment, the current study is looking into discovering treatment that can either completely eradicate HIV-1 infection or reduce costs and any other complications associated with HIV-1 treatment. From section 2.6 to 2.9, I will address the aims of the study, the experiments conducted and the outcomes thereof.

2.6 Applications of low level laser therapy in HIV-1 in the absence or presence of efavirenz

To date, extensive research has been conducted towards finding treatment for HIV-1 infection and antiretroviral drugs that reduce the virus to undetectable levels are available [88]. Since no cure has come to the fore, researchers continue with investigations towards obtaining treatment that would completely eradicate HIV. The current study then seeks to unpack the significance of applying LLLT only on HIV-1 infection and also combining LLLT with antiretroviral drugs as a potential therapy; in this case efavirenz was the drug of choice. Efavirenz is always used in conjunction with other drugs in highly active antiretroviral therapy (HAART) [89]. It is a non-nucleoside reverse transcriptase inhibitor (NNRTI), which binds at a distinct site away from the enzyme active site thereby hindering the enzyme polymerase activity [90]. It prevents HIV-1 replication by blocking the reverse transcriptase enzyme from converting the viral genomic RNA into complementary DNA (cDNA), which then becomes integrated into the host DNA [91].

The experiments comprized of three groups of TZM-bl cells (HIV infection model); the first group was uninfected TZM-bl cells that were not infected with the pseudovirus (G1), the second group were infected cells (G2) and the third group were infected cells that were

incubated with efavirenz (G3). During the experiments, for G2 and G3, the TZM-bl cells were infected by the ZM53 pseudovirus in a tissue culture dish containing cells and growth media. Both the infected (G2 and G3) and uninfected (G1) TZM-bl cells were incubated at 37°C, 5% CO_2 and 85% humidity for 48 hours. After 48 hours of incubation, the G3 cells were prepared by adding 20 µg/ml of efavirenz to the infected cells and further incubated for 30 minutes at 37°C. The G1, G2 and G3 cell samples were separately irradiated at doses 2 to 10 J/cm^2. Irradiation using a 640 nm laser was conducted in a dark room in order to prevent contamination from background light.

All experiments were conducted in triplicates and repeated three times (n = 3), with average values used to plot the graphs. Non-parametric one way analysis of variance was used to investigate the statistical significance of data and shown on graphs by asterisks*. The results were considered significantly different when $P < 0.05$. Statistical differences between the untreated controls and experimental groups are shown in graphs as * $P < 0.05$, ** $P < 0.01$, and *** $P < 0.001$ and dispersion bars represent standard error. All the non-irradiated cells were used as controls; with uninfected cells being the negative control (G1 = NC), infected cells being the positive control (G2 = PC) and the infected cells incubated efavirenz considered the drug control (G3 = DC).

2.7 Low level laser therapy experimental setup

The TZM-bl cells were irradiated using a 640 nm diode laser (Coherent), with a laser power of 30 mW at the sample area using fluences of 2 to 10 J/cm^2. Table 1.1 shows laser parameters used for irradiation experiments.

Table 2.1 Laser irradiation parameters

Laser parameters	
Wavelength (nm)	640
Power Output at the sample (mW)	30
Type of emission	Continuous wave
Illuminated area (cm^2)	4.2
Irradiation times (s)	606, 1263, 1920, 2526, 3183
Fluences (J/cm^2)	2, 4, 6, 8 and 10
Beam profile	Gaussian

The fluence (∅), power (P) and the irradiated area A were parameters used to determine the duration of cell exposure to laser using the following formula:

$$t = \frac{\emptyset \times A}{P} \qquad (2.2)$$

Through the laser pulse energy in joules J and the effective focal spot area in cm^2, it was possible to determine different fluences used, via this formula:

$$\text{Fluence} = \frac{\text{J}}{\text{cm}^2} \qquad (2.3)$$

After laser irradiation of cells through the setup shown in Figure 2.5, the culture dishes were incubated for 24 hours at 37 °C in 5% CO_2 and 85% humidity, followed by biological assays.

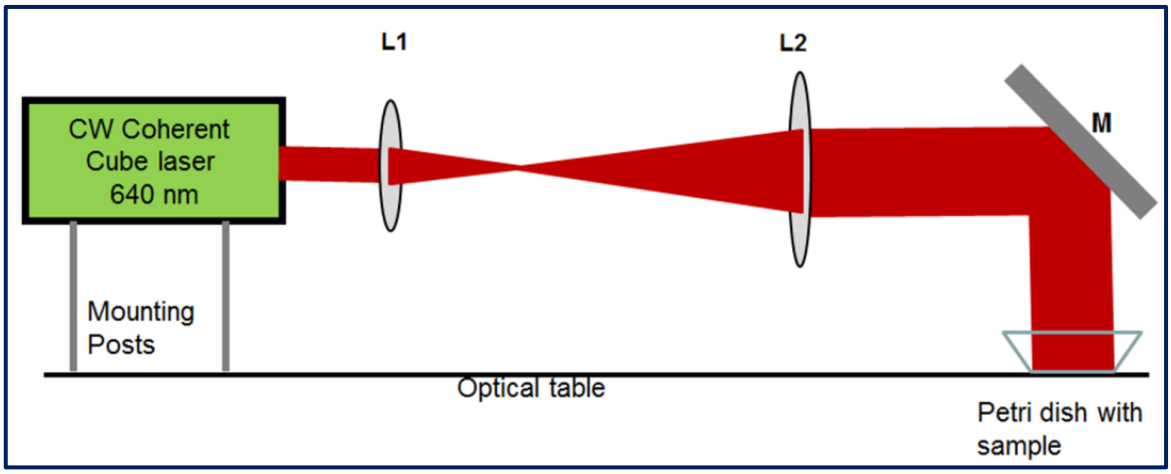

Figure 2.5 The experimental setup for the LLLT studies depicted. The diameter of the 640 nm diode laser was expanded using a two lens telescope (L1 = 25.4 mm and L2 = 500 mm) from 1.2 mm to 24 mm. The laser beam was reflected using a highly reflective silver mirror (M) to fill the surface area of the petri dish with a monolayer of TZM-bl cells.

2.8 The effects of LLLT in HIV-1 infected TZM-bl cells

2.8.1 Assays for the effects of LLLT, HIV-1 infection and efavirenz on cells

2.8.1.1 Cell morphology and Reactive Oxygen Species

The results in Figure 2.6 show the changes in cell morphology and production of the reactive oxygen species (ROS) following HIV-1 infection, laser irradiation and addition of efavirenz on TZM-bl cells. The assessment of cell morphology using the bright-field microscope showed that both irradiated and non-irradiated uninfected cells in Figures 2.6 A and G were healthy and grew as a monolayer. Also, there was no ROS production in both irradiated and non-irradiated uninfected cells as exhibited by the absence of green fluorescence in Figures 2.6 D and J.

Both the irradiated and non-irradiated infected cells in Figures 2.6 B and H showed signs of cell stress as the cells became round with some detached and floating around. A similar pattern of stressed cells was observed in both irradiated and non-irradiated infected cells in the presence of efavirenz at Figures 2.6 C and I. With regards to ROS production in infected irradiated and non-irradiated cells in Figures 2.6 E and K there was increased ROS production. ROS production also took place in both irradiated and non-irradiated infected cells with drug as demonstrated in Figures 2.6 F and L.

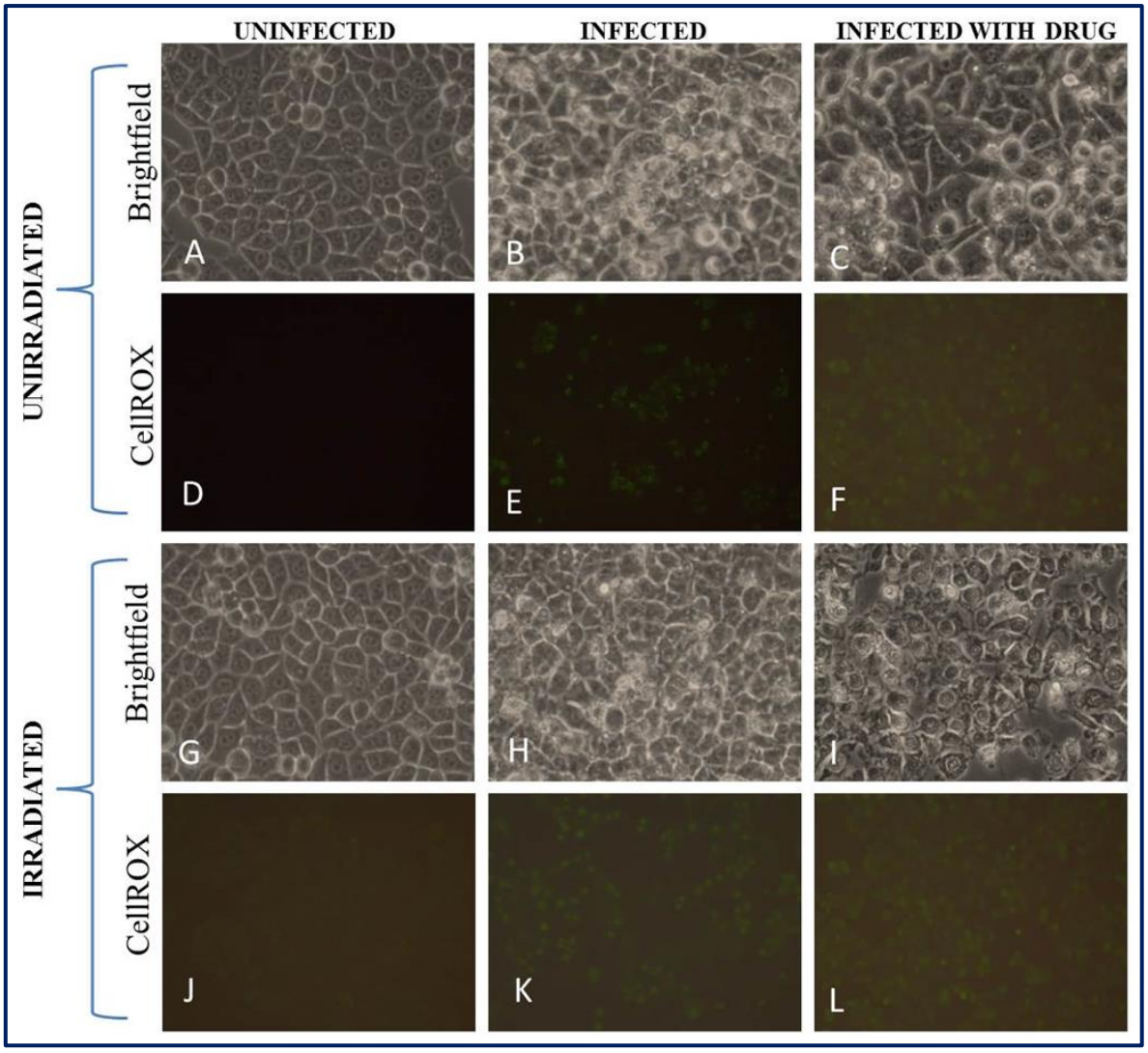

Figure 2.6 Cell morphology and ROS production in TZM-bl cells: pictures A to C and G to I show the cell morphology of (A and G) uninfected non-irradiated, (B and H) infected non-irradiated and (C and I) non-irradiated infected with drug. Images D to F and J to L are the ROS production images where, (D and J) uninfected non-irradiated, (E and K) infected non-irradiated and (F and L) non-irradiated infected with drug.

2.8.1.2 Cell viability detection by adenosine triphosphate assay

Cell viability was assessed using the ATP assay (Figure 2.7) in order to determine the effects of HIV infection, exposure to efavirenz and laser irradiation on the cells. The results obtained showed that uninfected cells irradiated at 2 to 6 J/cm^2 displayed no significant changes in cell viability as compared to the negative control (NC).

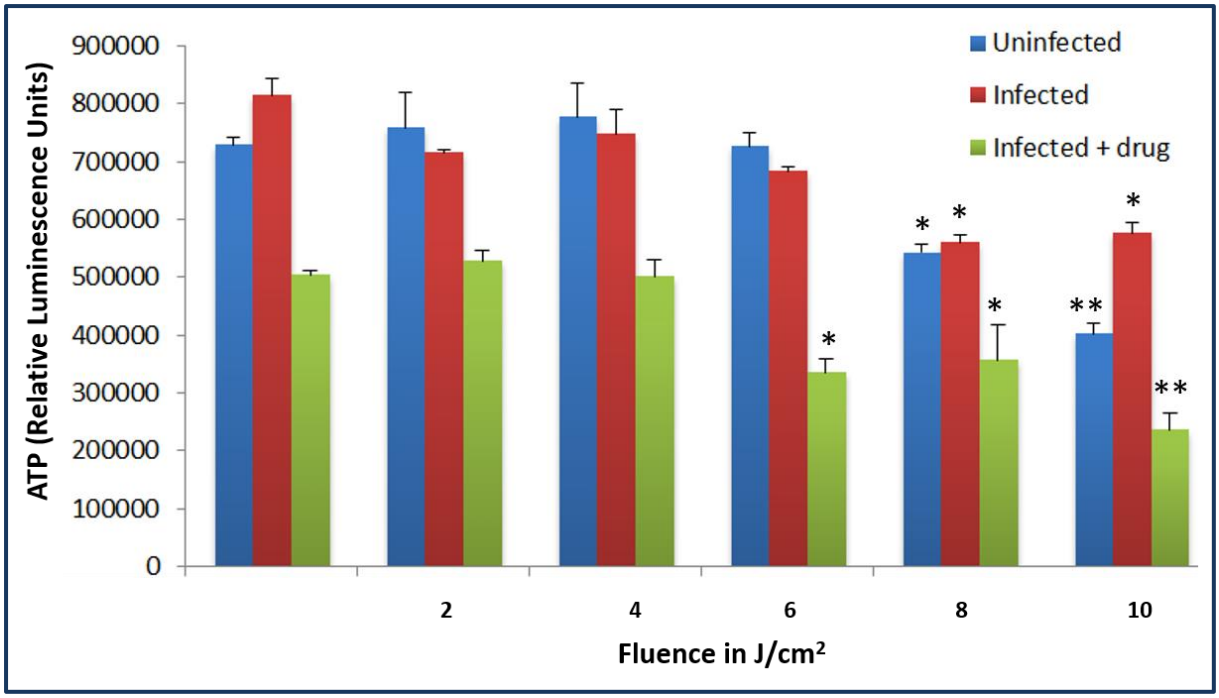

Figure 2.7 Cell viability results of uninfected, HIV-1 infected and HIV-1 infected TZM-bl cells treated with efavirenz. Cells were irradiated with increasing fluences of 2, 4, 6, 8 and 10 J/cm^2. Significant differences between controls (NC = negative control, PC = positive control and DC = drug control) and experimental groups are represented on the graph as (*) = $P < 0.05$ and (**) = $P < 0.01$. Error bars represent the standard error of the mean where n = 3.

On the contrary, at fluences 8 and 10 J/cm^2 there was a significant reduction in ATP levels in uninfected cells. Infected cells irradiated at fluences of 8 and 10 J/cm^2 also showed significant changes in cell viability when compared to positive control (PC).

No significant changes in cell viability were noted in infected cells irradiated at fluences of 2, 4, and 6 J/cm^2 when compared to PC. Infected cells containing efavirenz and laser irradiated at 6, 8 and 10 J/cm^2 showed a significant reduction in cell viability when compared to the drug control (DC), while laser irradiation at 2 and 4 J/cm^2 showed no significant changes. The PC (cells infected with virus) showed the highest cell viability followed by NC (cells with no infection) and then DC (cells infected and treated with efavirenz).

Infected cells irradiated at 2, 4, 6 J/cm^2 showed a decrease in ATP levels as compared to uninfected cells irradiated with the same fluence, while at fluences 8 and 10 J/cm^2, infected cells showed an increase in ATP levels. Infected cells containing efavirenz showed the lowest ATP levels both in the presence and absence of laser irradiation when compared to the uninfected and infected cells.

2.8.1.3 Cell proliferation detection by MTT assay

Cell proliferation (Figure 2.8) was assessed using the MTT assay in order to determine the effects of HIV infection, treatment with efavirenz and exposure to laser irradiation on the proliferation of TZM-bl cells. The MTT assay absorbance was measured at 600 nm using a luminometer.

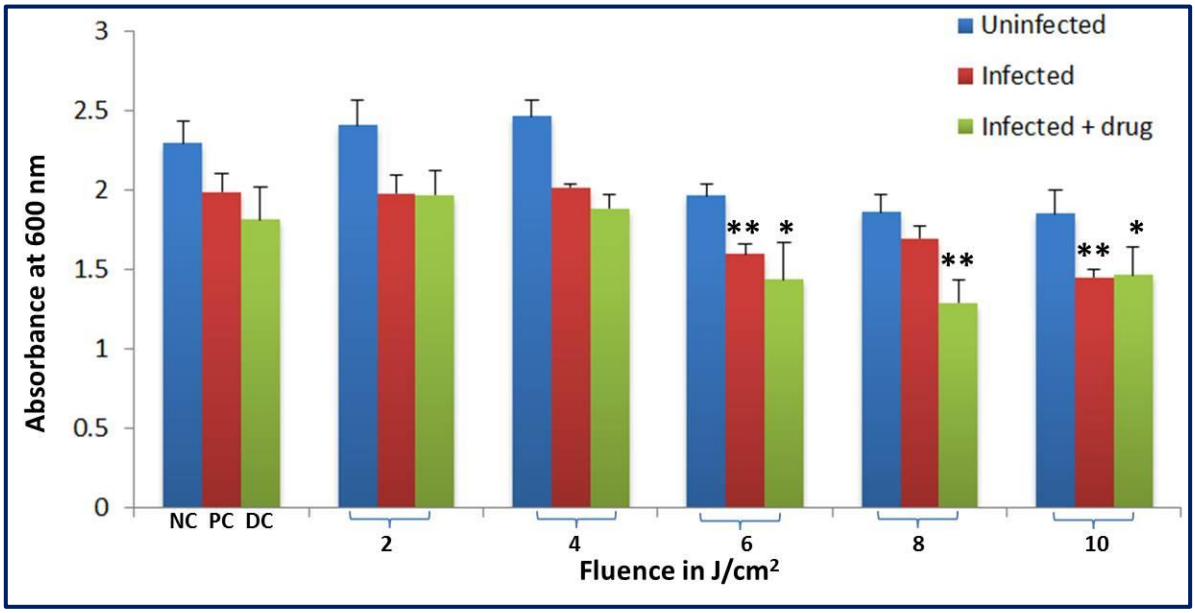

Figure 2.8 Cell proliferation of uninfected, HIV infected and HIV infected TZM-bl cells with efavirenz. The cells were irradiated with increasing fluences of 2, 4, 6, 8 and 10 J/cm^2. Significant differences between controls and their respective control groups are represented on the graph as (*) = $P < 0.05$ and (**) = $P < 0.01$. Error bars represent the standard error of the mean where n = 3.

Data obtained confirmed that uninfected cells irradiated at 2 to 10 J/cm^2 showed no significant changes in cell proliferation in comparison to the NC. Infected cells irradiated with fluences 6 and 10 J/cm^2 showed a significant reduction ($P < 0.01$) in cell proliferation when compared to the PC. However, there was no significant difference between the infected cells irradiated at 8 J/cm^2 and the PC. Infected cells containing efavirenz and laser irradiated at 2 and 4 J/cm^2 showed no significant differences in cell proliferation as compared to the PC, while those irradiated at 6 to 10 J/cm^2 proliferated significantly poor ($P < 0.05$). The negative control had the highest proliferation rate followed by the PC and then DC. A similar pattern was also observed in irradiated cells at fluences 2 to 10 J/cm^2.

2.8.1.4 Cell membrane integrity detection by lactate dehydrogenase assay

The cell membrane integrity was examined using lactate dehydrogenase (LDH) assay (Figure 2.9) in order to determine the effects of HIV infection, efavirenz and treatment with laser light of different doses on TZM-bl cells.

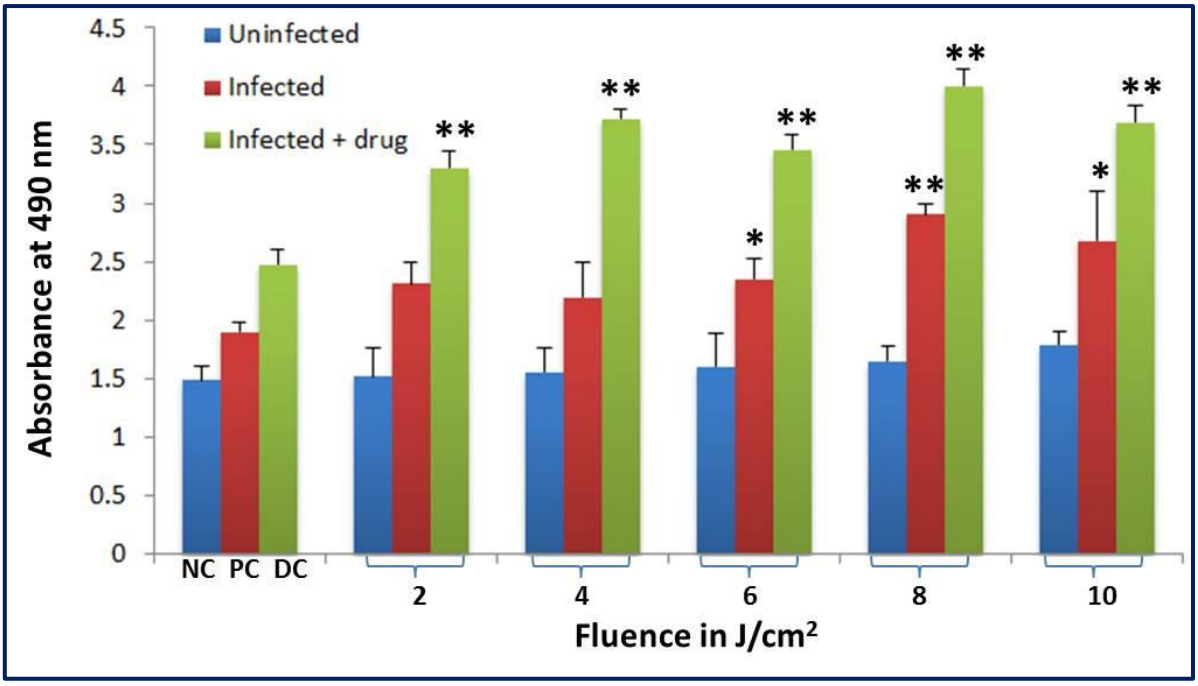

Figure 2.9 Cell membrane damage of uninfected, HIV infected and HIV infected TZM-bl cells with the drug efavirenz. Cells were irradiated with increasing fluences of 2, 4, 6, 8 and 10 J/cm^2. Significant differences between the controls and the respective experimental groups are represented in the graph as (*) = $P < 0.05$ and (**) = $P < 0.01$. Error bars represent the standard error of the mean where n = 3.

LDH is a cytosolic enzyme that is released from cells when cell membranes are damaged. Uninfected cells irradiated at 2 to 10 J/cm^2 showed no significant differences in LDH levels in comparison to the NC. Infected cells irradiated with fluences of 6, 8 and 10 J/cm^2 showed significantly high LDH levels as compared to PC ($P < 0.05$, $P < 0.01$ and $P < 0.05$), while there were no significant differences between PC and infected cells irradiated at 2 and 4 J/cm^2. Infected cells containing efavirenz and laser irradiated at fluences of 2 to 10 J/cm^2 showed significantly high LDH levels when compared to the DC ($P < 0.01$ and $P < 0.05$). The DC had the highest LDH levels followed by PC and NC, and a similar pattern was also seen in all experimental groups.

2.8.2 Luciferase assay to detect effects of LLLT and efavirenz on HIV-1 infection in TZM-bl cells

Luciferase assay is a tool generally used to study gene expression and it gives quantitative measurements. In this study the luciferase assay was used to monitor HIV-1 infection (Figure 2.10) and to evaluate the effects of combining the drug efavirenz and laser irradiation as potential treatment for HIV-1 infection. It was used because TZM-bl cells contain a luciferase gene which is expressed when HIV-1 infection has taken place. By measuring luciferase activity, which is directly proportional to viral particles that infected a cell using relative luminescence units (RLUs) HIV-1 infection can be determined. The higher RLUs indicate high levels of infection, whereas lower RLUs indicate low infection levels. In the absence of infection there is no luminescence produced because the luciferase gene in cells would not be expressed [92-93].

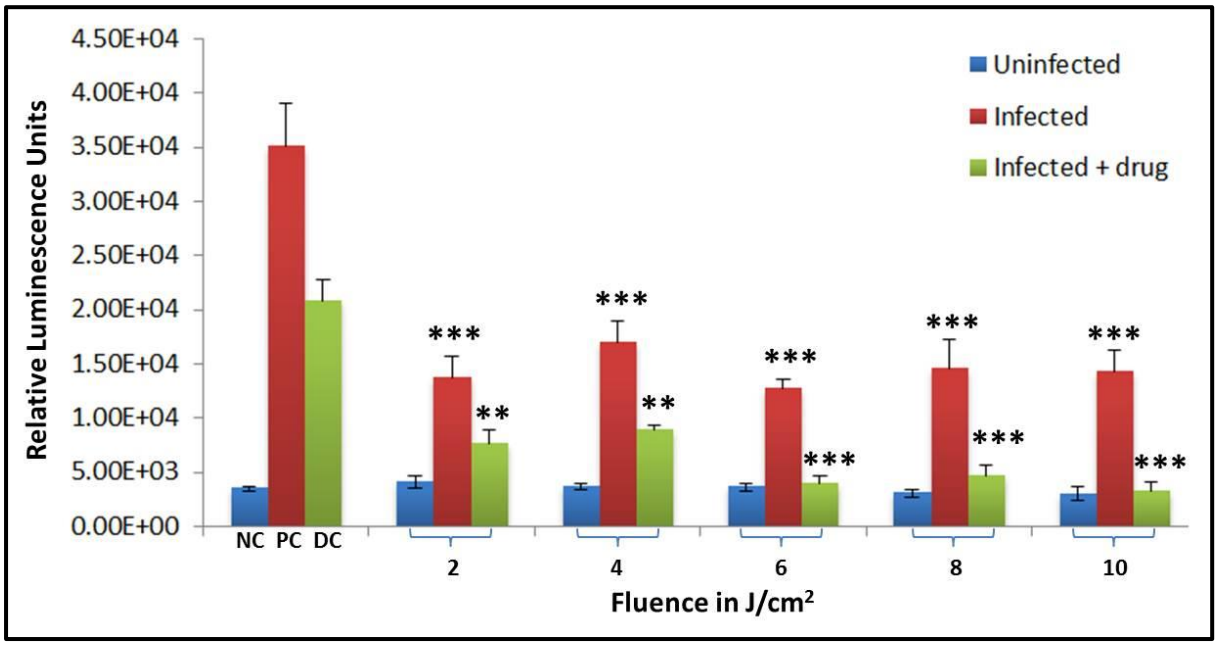

Figure 2.10 Luciferase assay monitored HIV infection in TZM-bl cells. TZM-bl cells were irradiated at 2 to 10 J/cm^2. Significant differences between controls and their respective control groups are represented on the graph as (**) = $P < 0.01$ and (***) = $P < 0.001$. Error bars represent the standard error of the mean where n = 3.

Briefly, uninfected cells irradiated at 2 to 10 J/cm^2 showed no significant differences in luciferase activity as compared to the NC as shown in Figure 2.10. Infected cells irradiated at 2 to 10 J/cm^2 showed a significant reduction in luciferase activity (HIV infection) when compared to PC ($P < 0.001$). Infected cells containing efavirenz and laser irradiated at 2, 4, 6, 8 and 10 J/cm^2 also showed significantly low levels of HIV infection when compared to DC ($P < 0.01$, $P < 0.01$, $P < 0.001$ and $P < 0.001$ respectively). PC showed the highest levels of HIV infection followed by DC and then NC and a similar pattern was seen in all laser irradiated cells.

2.8.3 Flow cytometry for the detection of cell death pathway induced by HIV infection, LLLT and efavirenz

The Annevin V-Flourescein isothiocynate commonly known as Annexin V-FITC apoptosis kit was used to distinguish between apoptotic and necrotic cells using flow cytometry. Figure 2.11 shows flow cytometric dot plots differentiating between live, necrotic, late apoptotic (dead) and early apoptotic cells.

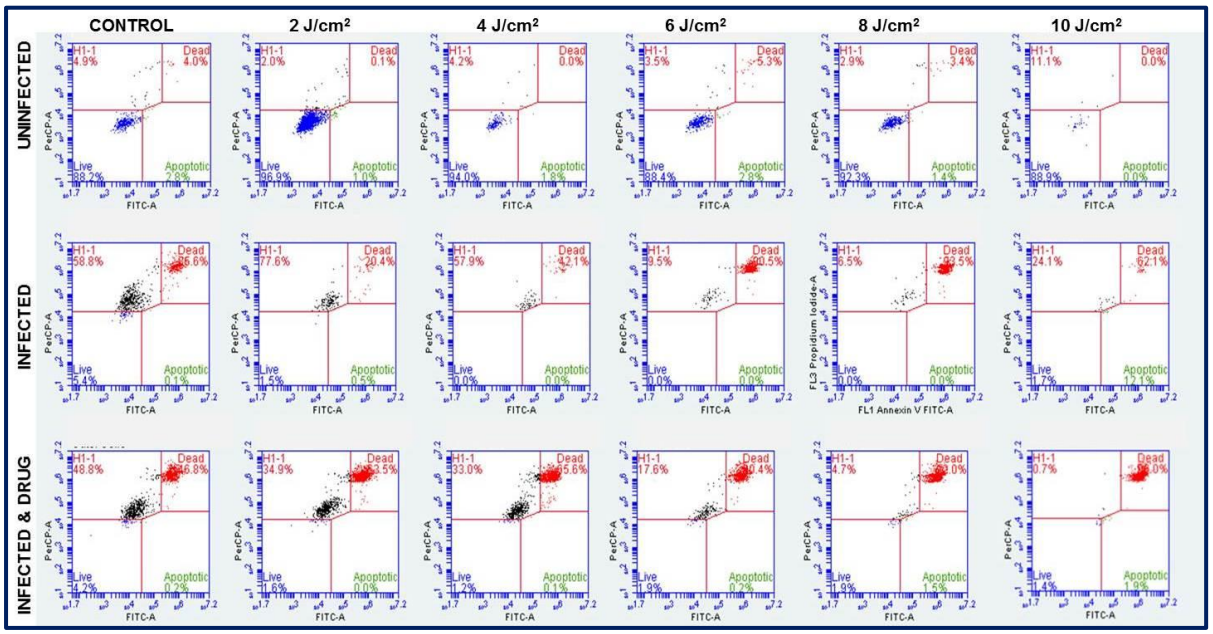

Figure 2.11 Propidium iodide/Annexin V FITC staining used to assess the mode of cell death in both irradiated and non-irradiated cells.

Early apoptotic cells were positively stained with annexin V-FITC (lower right quadrant), necrotic cells were positively stained with propidium iodide (PI) (upper left quadrant), dead cells were stained with both annexin V-FITC and PI (upper right quadrant) while live cells are not stained (lower left quadrant). Uninfected cells irradiated at 2 to 10 J/cm^2 showed no changes in cell population when compared to the uninfected control cells and the majority of the cell population was live cells. Infected cells irradiated at 2 to 10 J/cm^2 also showed no changes in cell population when compared to infected control cells, except for cells irradiated with 8 J/cm^2. These cells had a significantly reduced proportion of viable cells 1.3% ($P < 0.05$) and a significant increase in dead cells 86.6% ($P < 0.001$) and necrotic cells 11.7% ($P < 0.001$).

Table 2.2 Percentage of various cell populations after staining with propidium iodide/annexin V-FITC

Groups	Lives cells (%)	Dead cells (%)	Apoptotic cells (%)	Necrotic cells (%)
Uninfected	93.6 ± 2.7	1.37 ± 1.3	1.27 ± 0.81	3.7 ± 0.84
2	95 ± 0.9	1.1 ± 0.5	0.7 ± 0.35	3.17 ± 0.84
4	92.2 ± 2	2.26 ± 1.39	1.4 ± 0.23	4.1 ± 1.07
6	92.3 ± 2.01	2.46 ± 1.46	1.83 ± 0.61	3.33 ± 0.38
8	93.5 ± 0.63	1.83 ± 0.99	1.23 ± 0.12	3.36 ± 0.73
10	92.3 ± 1.6	1.6 ± 0.8	1.06 ± 0.5	5.16 ± 2.96
Infected	6.43 ± 1.29	38.33 ± 1.56	0.43 ± 2.72	54.96 ± 2.72
2	4.53 ± 1.71	28.73 ± 4.29	0.36 ± 0.08	66.33 ± 5.91
4	2.3 ± 1.21	46.13 ± 3.13	0.3 ± 0.15	51.23 ± 3.89
6	2.3 ± 1.38	73.37 ± 8.58	0.03 ± 0.03	24.2 ± 7.46*
8	1.3 ± 0.68*	86.8 ± 3.66***	0.2 ± 0.1	11.7 ± 3.09***
10	1.9 ± 0.11	58.46 ± 6.91	0.46 ± 0.36	35.53 ± 8.74
Infected and drug	3.67 ± 0.29	37.2 ± 5.48	0.2 ± 0.11	58.97 ± 5.65
2	2.2 ± 0.34*	55.56 ± 4.08	0.4 ± 0.31	41.83 ± 3.51
4	3.53 ± 1.52	56.87 ± 8.48	0.33 ± 0.28	39.17 ± 6.83
6	1.83 ± 0.06*	74.83 ± 4.10**	0.37 ± 0.12	22.97 ± 4.18
8	3.1 ± 1.00	78.33 ± 7.97*	1.37 ± 0.35	17.2 ± 7.27*
10	1.97 ± 0.42*	87.9 ± 4.07**	0.9 ± 0.55	9.23 4.27**

Significant differences between controls and their respective control groups are represented on the graph as (**) = $P < 0.01$ and (***) = $P < 0.001$. Experiments were repeated 3 times (n=3).

All the infected cells that were treated with efavirenz showed a reduction in the live cell population. However, the number of dead cells increased with the increase in fluence, with non-irradiated group showing smallest populations of both dead and apoptotic cells, but the highest on necrotic cells. In Table1.2, percentages of various cell populations i.e. live, dead, apoptotic and necrotic cells are shown. The data explicitly shows that the uninfected group of cells (G1) had a higher number of live cells compared to the infected groups (G2 and G3). Both G2 and G3 had a higher number of necrotic cells and dead cells.

2.9 Discussion

The introduction of antiretroviral agents has seen a million lives spared from the unmerciful scourge of HIV-1 infection on the human race. Nonetheless, there is still a dire need to find a form of therapy that would completely eradicate HIV and minimize the side effects caused by the combination of different drugs in each HAART regimen. The efavirenz used in the current study is a first generation NNRTI that has been in use as a first line regimen [94-96]. Since its first use in the late 1990s, efavirenz is still part of the treatment used by HIV infected individuals resulting in viral suppression even after years of using it and this is a clear indication that it is effective against HIV [96]. In this study, we tested a combination of two unrelated therapies i.e. LLLT and the drug efavirenz against HIV infection in TZM-bl cells (model of HIV infection) for the first time.

The TZM-bl cells are susceptible to HIV primary isolates and molecularly cloned Env-pseudotyped viruses, like the ZM53 virus used in the current study. When HIV infection has taken place in TZM-bl cells, the reporter gene expression is induced by the HIV Tat protein, as the reporter genes are tat-inducible. The presence of reporter genes in TZM-bl cells enables the user to determine whether there is HIV infection or not. Both the negative control and all the irradiated uninfected cells showed no luciferase activity, which was expected as luciferase activity in TZM-bl cells is only induced when HIV infection has taken place [92].

The little luminescence detected in uninfected cells is attributed to the auto-luminescence which is present at negligible levels in most mammalian cells [97]. The notably high levels of luciferase activity as shown by RLUs in the presence of HIV was a clear indication that TZM-bl cells are permissive to HIV infection and the ZM53 virus used was infectious.

A significant reduction in HIV-1 infection ($P < 0.001$) was observed in irradiated infected cells as shown by a red bar in Figure 2.10. A further reduction ($P < 0.01$ and $P < 0.001$) was seen when the infected cells were exposed to efavirenz and laser irradiation as shown by the green bar in Figure 2.10, when compared with the drug control, where infected cells were exposed to the drug for 30 minutes, but were not irradiated. Even though the reduction of HIV infection was expected in the presence of an antiretroviral agent, the noteworthy reduction of infection when the two therapies were combined was a rejuvenating factor, as it is apparent that the combination of the two therapies has potential in fighting HIV infection.

Having assessed how irradiation and efavirenz affect HIV infection in TZM-bl cells, it was essential to establish how the two therapies affected the health of TZM-bl cells. This was done by evaluating cell morphology using light microscope, ROS production detected with fluorescence microscope, cell viability (ATP assay), cell proliferation (MTT assay) and cell membrane damage (LDH assay). In Figure 2.6 cell morphology results showed visible differences between infected and uninfected cells, and the presence of floating cells as shown in Figure 2.6 B, C, H and was a clear evidence that HIV has cytopathic effects on virus permissive cells [98]. The cell morphology results compare with the MTT assay results in Figure 2.8 as the uninfected cells proliferated better than the infected cells.

Furthermore, the absence of significant differences between the negative control and uninfected cells irradiated at 2 to 10 J/cm^2 was indicative of irradiation having no noteworthy effects on uninfected TZM-bl cells. The lack or minimal effects of irradiation on cells has been previously observed on other cell lines as the impact of irradiation on different cell types differs

from one cell type to another [99]. Various factors such as wavelength and fluence have an impact on the response of cells and determine the success or failure of LLLT [12].

According to MTT results, infected cells in the presence or absence of efavirenz showed no significant changes in cell proliferation after irradiating at 2 and 4 J/cm^2 when compared to their respective control groups (PC and DC). On the contrary, a significant reduction in cell proliferation was seen at fluences of 6 to 10 J/cm^2 except for infected cells irradiated at 8 J/cm^2. The reduction can be attributed to the increase in fluence, which would have enhanced the undesirable effects of the infection and efavirenz on the cells. A similar observation was noted in the LDH assay for infected cells in the absence of efavirenz, as there were no significant differences between the PC and infected cells irradiated at 2 to 4 J/cm^2, while there was a significant increase in LDH levels at fluences 6 to 10 J/cm^2. However, in the LDH results there were significantly high levels of LDH at all fluences in cells that contained efavirenz, which clearly shows the detrimental effects that the drug had on the cells. The undesirable effects associated with the use of efavirenz in mammalian cells include endoplasmic reticulum stress and autophagy in endothelial cells and the generation of ROS [100-101].

With the understanding that HIV infection causes cytopathic effects in cells, one would have expected that HIV infected cells would have significantly lower ATP levels in comparison to the uninfected cells. However, the results showed that there were no significant differences between ATP levels in infected and uninfected cells as well as at fluences of 8 and 10 J/cm^2. ATP levels in infected cells were slightly higher than in uninfected cells, and this was attributed to the role of the HIV-1 p2 peptide, which intensifies the virus' acute infection as it increases intracellular ATP production [102].

The significant reduction in cell viability levels in the presence of efavirenz is in correlation with what is known about the detrimental effects of efavirenz in cells [101].

Flow cytometry was done to determine the mode of cell death associated with HIV infection, LLLT and the use of efavirenz. The flow cytometry results of uninfected cells in Figure 2.11 showed expected results as there was a high number of live cells (88 to 96%) compared to apoptotic, necrotic and dead cells that had low populations ranging from 0.1% to 11%. The presence of dead or dying cells in a healthy sample is also not an alarming observation as cells die when they are old and are replaced by new ones or when they have been damaged [103]. The dying of old cells in order to be replaced by new ones is a programmed form of cell death that is commonly known as apoptosis. In addition, since TZM-bl cells are adherent, during passaging they get exposed to trypsin-EDTA to enable them to detach from the culture flask and a small population of cells gets damaged during this process, thereby leading to cell death. Unlike uninfected cells, the infected cells had a small population of live cells ranging from 0 to 5.4%, while necrotic and dead populations had the highest numbers and the apoptotic population had no greater than 13%. This observation correlates with the other assays where HIV infection, addition of efavirenz and laser irradiation at some fluences had detrimental effects on TZM-bl cells. It also became apparent that cell death in this study was mainly due to necrosis which correlates with literature where necrosis has been mostly observed *in vitro*, while apoptosis seems to be the most common form of cell death observed *in vivo* [104]. Furthermore, cell death by necrosis is also in correlation with the fact that necrosis occur as a consequence of infection or injury.

There was no ROS detected in both irradiated and non-irradiated uninfected cells Figure 2.6 D and J, which is similar to what was previously observed by Basso, where there was no detectable ROS production in healthy irradiated cells [99]. This result also correlates with what was observed in other biological assays conducted in this study, where there were no significant changes and differences between irradiated and non-irradiated uninfected cells. On the other hand, the results showed what was speculated in the late 1980s that HIV infection is associated with ROS production, as cells infected with HIV (both irradiated and non-irradiated) showed the generation of ROS [105]. Non-irradiated infected cells with or without efavirenz showed the same fluorescence pattern with irradiated cells indicating production of ROS. Based on these findings, it is clear that the ROS production was caused by HIV infection. Finally, following combining LLLT and the drug efavirens for the first time in HIV treatment, an elaborate decrease in infection was detected calling for future research via this novel treatment regime even *in-vivo.*

References

1. Singh, Subhash Chandra, et al. Nanomaterials: Processing and Characterization with Lasers. Wiley-VCH Verlag & Co. KGaA, 2012.
2. Einstein A. The Quantum Theory of Radiation. Physikalische Zeitschrift 1917; 18:121.
3. Gordon, Gould. The LASER, Light Amplification by Stimulated Emission of Radiation. University of Michigan Press, 1959.
4. Maiman TH. Optical and microwave- optical experiments in ruby. Physical Review Letters 1960; 4:564–566.
5. Steen WM, Mazumder J. Laser Material Processing. Basic Laser Optics. Springer-Verlag London; 2010.

6. How Lasers Work, https://science.howstuffworks.com/laser.htm; [Accessed 20 May 2018].

7. Lasers: Understanding the Basics, https://www.photonics.com/Article.aspx?AID=25161; [Accessed 20 May 2018].

8. Mester E, Szende B, Tota, JG. Effect of laser on hair growth of mice. Kiserl Orvostud. 1967; 19:628–631.

9. Ashkin A. Acceleration and Trapping of Particles by Radiation Pressure. Physical Review Letters 1970; 24:156-159.

10. Bertolotti, Mario. The History of the Laser. IOP Publishing, 2005.

11. Mester E, Spiry T, Szende B, Tota JG. Effect of laser rays on wound healing. The American Journal of Surgery 1971; 122:532–535.

12. Chung H, Dai T, Sharma SK, Huang YY, Carroll JD, Hamblin MR. The nuts and bolts of low-level laser (light) therapy. Annals of Biomedical Engineering 2012; 40(2):516-533.

13. Baxter, G. David. Therapeutic Lasers: Theory and Practice. Churchill Livingstone; 1994.

14. Passarella S, Casamassima E, Molinari S, Pastore D, Quagliariello E, Catalano IM, Cingolani A. Increase of proton electrochemical potential and ATP synthesis in rat liver mitochondria irradiated *in vitro* by helium-neon laser. FEBS Letters 1984; 175:95–99.

15. Chen ACH, Arany PR, Huang YY, Tomkinson EM, Sharma SK, Kharkwal GB, Saleem T, Mooney D, Yull FE, Blackwell TS, Hamblin MR. Low-Level Laser Therapy Activates NF-kB via Generation of Reactive Oxygen Species in Mouse Embryonic Fibroblasts. PLoS ONE 2011; 6(7):e22453.

16. Ball KA, Castello PR, Poyton RO. Low intensity light stimulates nitrite-dependent nitric oxide synthesis but not oxygen consumption by cytochrome c oxidase: Implications for phototherapy. Journal of Photochemistry and Photobiology B. 2011; 102(3):182–191.

17. Huang Y, Chen A, Hamblin M. Low level laser therapy: an emerging clinical paradigm. SPIE Newsroom 2009; 9:1-3.

18. Hancock JT, Desikan R, Neill SJ. Role of Reactive Oxygen Species in Cell Signaling Pathways. Biochemical and Biomedical Aspects of Oxidative Modification 2001; 29(2):345-350.

19. Cini M, Moretti A. Studies on lipid peroxidation and protein oxidation in the aging brain. Neurobiol Aging 1995; 16:53–57.

20. Schieber M, Chandel NS. ROS function in redox signaling and oxidative stress. Current Biology 2014; 24(10):R453–R462.

21. Kam T, Kalendo GS, Letokhov VS, Lobko VV. Biostimulation of HeLa cells by low-intensity visible light II. Stimulation of DNA and RNA synthesis in a wide spectral range. Nuevo Cimento 1984; 309–318.

22. Karu TI, Kolyakov SF. Exact action spectra for cellular responses relevant to phototherapy. Photomedicine Laser Surgery 2005; 23(4):355-361.

23. Zhang Q, Piston DW, Goodman RH. Regulation of corepressor function by nuclear NADH. Science 2000; 295(5561):1895-1897.

24. Yaakobi T, Shoshany Y, Levkovitz S, Rubin O, Ben Haim SA, Oron U. Long-term effect of low energy laser irradiation on infarction and reperfusion injury in the rat heart. Journal of Applied Physiology 2001; 90:2411-2419.

25. O'Connor Clare and Adams JU. Essentials of Cell Biology. NPG Education, 2010.

26. Beaven GH, Holiday ER. Ultraviolet absorption spectra of proteins and amino acids. Advances in protein chemistry 1952; 7:319-386.

27. Absorption spectra for biological tissues, ttps://omlc.org/classroom/ece532/class3/muaspectra.html, [Accessed 22 May 2018].

28. Ploeser JM, Loring HS. Ribonucleotides ribonucleosides and spectra of the pyrimidine the ultraviolet absorption. Journal of Biological Chemistry 1949; 178:431-437.

29. Houle MJ, Powell RL, Fintschenko P. Absorbance of UV light by various carbohydrates in strong sulfuric acid. Analytical Biochemistry 1967; 21(3):462-466.

30. Wozniak, Bogdan and Dera Jerzy. Light Absorption in Sea Water. Springer New York, 2007.

31. Karu TI, Afanas'eva NI. Cytochrome c oxidase as the primary photoacceptor upon laser exposure of cultured cells to visible and near IR-range light. Dokl Akad Nauk 1995; 342(5):693–695).

32. Esnouf A, Wright PA, Moore JC, Ahmed S. Depth of penetration of an 850nm wavelength low level laser in human skin. Acupuncture & Electro-Therapeutics Research 2007; 32(1-2):81-6.

33. Aziz-Jalali MH, Tabaie SM, Djavid GE. Comparison of Red and Infrared Low-level Laser Therapy in the Treatment of Acne Vulgaris. Indian Journal of Dermatology. 2012; 57(2):128–130.

34. Sobol EN, Baum OI, Shekhter AB, Guller A, Baskov AV. Laser-induced regeneration of cartilage. Journal of Biomedical Optics, 2011; 16(8):080902.

35. .An Analysis of the Operating Wavelengths for Cold Lasers, https://www.coldlasers.org/therapy/wavelength/; [Accessed 22 March 2019].

36. Desiate A, Cantore S, Tullo D, Profeta G, Grassi FR, Ballini A. 980 nm diode lasers in oral and facial practice: current state of the science and art. International Journal of Medical Sciences 2009; 6(6):358-364.

37. Wild S, Roglic G, Green A, Sicree R, King H. Global prevalence of diabetes: estimates for the year 2000 and projections for 2030. Diabetes Care 2004; 27:1047-1053.

38. Boulton AJ, Vileikyte L, Ragnarson TG, Apelqvist J. The global burden of diabetic foot disease. Lancet 2005; 366:1719-1724.

39. Reiber GE, Pecoraro RE, Keopsell TD. Risk factors for amputation in patients with diabetes mellitus: A case control study. A case control study. Annals of Internal Medicine 1992; 117: 97-105.

40. Lazarus GS, Cooper DM, Knighton DR, Margolis DJ, Pecoraro RE, Rodeheaver G, Robson MC. Definitions and guidelines for assessment of wound and evaluation of healing. Archives of Dermatology 1994; 130(4):489-493.

41. Ayuk SM, Houreld NN, Abrahamse H. Collagen production in diabetic wounded fibroblasts in response to low-intensity laser irradiation at 660 nm. Diabetes Technology & Therapeutics 2012; 14(12):1110-1117.

42. Sekhejane PR, Houreld NN, Abrahamse H. Irradiation at 636 nm positively affects diabetic wounded and hypoxic cells *in vitro*. Photomedicine and Laser Surgery 2011; 29(8):521-530.

43. Yamany AA, Sayed HM. Effect of low level laser therapy on neurovascular function of diabetic peripheral neuropathy. Journal of Advanced Research. 2012; 3(1): 21-28.

44. Minatel DG, Frade MAC, Franca SC, Enwemeka CS. Phototherapy promotes healing of chronic diabetic leg ulcers that failed to respond to other therapies. Lasers Surg Med. 2009; 41(6):433-441.

45. AlGhamdi KM, Kumar A, Moussa NA. Low level laser therapy: a useful technique for enhancing the proliferation of various cultured cells. Lasers in Medicine Science 2012; 27(1): 237-249.

46. World Health Organization (WHO), Cancer Fact Sheet (N 297), http://www.who.int/mediacentre/factsheets/fs297/en/; [Accessed 15 May 2018].

47. World Cancer Report 2014, https://www.who.int/cancer/publications/WRC_2014/en/; [Accessed 15 May 2018].

48. Myakishev-Rempel M, Stadler I, Brondon P, Axe DR, Friedman M, Nardia FB, Lanzafame R. A Preliminary Study of the Safety of Red Light Phototherapy of Tissues Harboring Cancer. Photomedicine and Laser Surgery 2012; 30(9): 551–558.

49. Jadaud E, Bensadoun R. Low-level laser therapy: a standard of supportive care for cancer therapy-induced oral mucositis in head and neck cancer patients? Laser Therapy 2012; 21(4):297–303.

50. McDowell FH. Neurorehabilitation. Western Journal of Medicine. 1994; 161(3): 323–327.

51. What are neurological disorders? http://www.who.int/features/qa/55/en/, [Accessed 1 June 2018].

52. Lampl Y, Zivin JA, Fisher M. Infrared laser therapy for ischemic stroke: a new treatment strategy: results of the NeuroThera Effectiveness and Safety Trial-1 (NEST-1). Stroke 2007; 38:1843–1849.

53. Hashmi JT, Huang Y-Y, Osmani BZ, Sharma SK, Naeser MA, Hamblin MR. Role of Low-Level Laser Therapy in Neurorehabilitation. PM & R: the journal of injury, function, and rehabilitation. 2010; 2(12 Suppl 2):S292-S305.

54. Hamblin MR. Shining light on the head: Photobiomodulation for brain disorders. BBA Clinical 2016; 6:113–124.

55. Wikramanayake TC, Rodriguez R, Choudhary S, Mauro LM, Nouri K, Schachner LA, Jimenez JJ. Effects of the Lexington LaserComb on hair regrowth in the C3H/HeJ mouse model of alopecia areata. Lasers in Medical Science 2012; 27(2):431–436.

56. Shukla S, Sahu K, Verma Y, Rao KD, Dube A, Gupta PK. Effect of helium-neon laser irradiation on hair follicle growth cycle of Swiss albino mice. Skin Pharmacology and Physiology 2010; 23(2):79–85.

57. Kim SS, Park MW, Lee CJ. Phototherapy of androgenetic alopecia with low level narrow band 655-nm red light and 780-nm infrared light. Journal of the American Academy of Dermatology; American Academy of Dermatology 65th Annual Meeting. 2007; AB112.

58. Satino JL, Markou M. Hair regrowth and increased hair tensile strength using the HairMax LaserComb for Low-Level Laser Therapy. International Journal of Cosmetic Surgery and Aesthetic Dermatology 2003; 5:113–117.

59. Leavitt M, Charles G, Heyman E, Michaels D. HairMax LaserComb laser phototherapy device in the treatment of male androgenetic alopecia: A randomized, double-blind, sham device-controlled, multicentre trial. Clinical Drug Investigation 2009; 29(5):283–292.

60. Sadick NS. Handheld LED array device in the treatment of acne vulgaris. Journal of Drugs in Dermatology 2008; 7(4):347–350.

61. Weiss RA, McDaniel DH, Geronemus RG. Clinical experience with light-emitting diode (LED) photomodulation. Dermatologic Surgery 2005; 31(9 Pt 2):1199–1205.

62. Dierickx CC, Anderson RR. Visible light treatment of photoaging. Dermatologic Therapy 2005; 18(3):191–208.

63. Weiss RA, McDaniel DH, Geronemus RG, Weiss MA. Clinical trial of a novel nonthermal LED array for reversal of photoaging: clinical, histologic, and surface profilometric results. Lasers in Surgey and Medicine 2005; 36(2):85–91.
64. Russell BA, Kellett N, Reilly LR. A study to determine the efficacy of combination LED light therapy (633 nm and 830 nm) in facial skin rejuvenation. Journal of Cosmetic & Laser Therapy 2005; 7(3–4):196–200.
65. Ablon G. Combination 830-nm and 633-nm light-emitting diode phototherapy shows promise in the treatment of recalcitrant psoriasis: preliminary findings. Photomedicine and Laser Surgery 2010; 28(1):141–146.
66. Okuni I, et al. Low level laser therapy (lllt) for chronic joint pain of the elbow, wrist and fingers. Laser Therapy 2012; 21(1):15–24.
67. Alghadir A, Omar MT, Al-Askar AB, Al-Muteri NK. Effect of low-level laser therapy in patients with chronic knee osteoarthritis: a single-blinded randomized clinical study. Lasers in Medical Science 2014; 29(2):749–755.
68. Bjordal JM, Johnson MI, Lopes-Martins RA, Bogen B, Chow R, Ljunggren. Short-term efficacy of physical interventions in osteoarthritic knee pain. A systematic review and meta-analysis of randomised placebo controlled trials. BMC Musculoskeletal Disorders 2007; 8:51.
69. Chow RT, Johnson MI, Lopes-Martins RA, Bjordal JM. Efficacy of low-level laser therapy in the management of neck pain: a systematic review and meta-analysis of randomized placebo or active-treatment controlled trials. Lancet 2009; 374(9705):1897–1908.
70. Lopes-Martins RA. Tendinitis, an open avenue for low-level laser therapy. Photomedicine and Laser Surgery 2014; 32(7):369–370.

71. Konstantinovic LM, Cutovic MR, Milovanovic AN, Jovic SJ, Dragin AS, et al. Low-level laser therapy for acute neck pain with radiculopathy: a double-blind placebo-controlled randomized study. Pain Medicine 2010; 11(8):1169–1178.

72. Jain TK, Sharma NK. The effectiveness of physiotherapeutic interventions in treatment of frozen shoulder/adhesive capsulitis: a systematic review. Journal of Back and Musculoskeletal Rehabilitation 2014; 27(3):247–273.

73. Lim HM, Lew KK, Tay DK. A clinical investigation of the efficacy of low level laser therapy in reducing orthodontic postadjustment pain. American Journal of Orthodontics and Dentofacial Orthopedics 1995; 108(6):614-622.

74. Leal-Junior EC, Johnson DS, Saltmarche A, Demchak T. Adjunctive use of combination of super-pulsed laser and light-emitting diodes phototherapy on nonspecific knee pain: double-blinded randomized placebo-controlled trial. Lasers in Medical Science 2014; 29(6):1839–1847.

75. Krishnan V. Orthodontic pain: from causes to management—a review. European Journal of Orthodontics 2007; 29(2):170–179.

76. Bergius M, Kiliaridis S, Berggren U. Pain in orthodontics. Journal of Orofacial Orthopedics 2000; 61(2):125–137.

77. National Department of Health and South African National AIDS Council. South African HIV and TB investment case – summary report phase 1. 2016. http://sanac.org.za/wp-content/uploads/2016/03/1603-Investment-Case-Report-LowRes-18-Mar.pdf; [Accessed 30 May 2018].

78. .Venter, W F et al. Cutting the cost of South African antiretroviral therapy using newer, safer drugs. South African Medical Journal, 2016; 107(1):28-30.

79. South African National AIDS Council (SANAC) ‘Let our actions count: National Strategic Plan 2017-2022'[pdf]. https://sanac.org.za/wp-content/uploads/2017/06/NSP_FullDocument_FINAL.pdf; [Accessed 30 May 2018].

80. Tamar Kahn, UNAIDS deal will make state-of-the-art HIV drug affordable in SA:https://businesslive.co.za/bd/national/health/; [Accessed 30 May 2018].

81. John Cohen, new single-day pill for HIV treatment promises more bang for less buck: http//sciencemag.org/news/2017/09/new-single-day-pill-for-hiv-treatment-promise; [Accessed 30 May 2018].

82. Cipla’s new triple combination antiretroviral drug approved, https://www.cipla.co.za/cipla-news/ciplas-new-triple-combination-antiretroviral-drug-approved/; [Accessed 22 March 2019].

83. Mylan launches first fixed-dose combination TLD for People Living with HIV in South Africa, http://www.mylansa.co.za/en-za/news/2018/mylan-launches-first-fixed-dose-combination-tld; [Accessed 22 March 2019].

84. Jubault V, Burgard M, Le Corfec E, Costagliola D, Rouzioux C, Viard JP. High rebound of plasma and cellular HIV load after discontinuation of triple combination therapy. Aids. 1998; 12(17): 2358–2359.

85. Ruiz L, Martinez-Picado J, Romeu J, Paredes R, Zayat MK, Marfil S, Negredo E, Sirera G, Tural C, Clotet B. Structured treatment interruption in chronically HIV-1 infected patients after long-term viral suppression. Aids 2000; 14(4):397–403.

86. Preston BD, Poiesz BJ, Loeb LA. Fidelity of HIV-1 reverse transcriptase. Science 1988; 242(4882):1168-1171.

87. HIV Treatment Overview, https://www.hiv.gov/hiv-basics/staying-in-hiv-care/hiv-treatment/hiv-treatment-overview); [Accessed 19 March 2018].

88. HIV treatment and an undetectable viral load to prevent HIV transmission, http://www.catie.ca/en/fact-sheets/transmission/hiv-viral-load-hiv-treatment-and-sexual-hiv-transmission; [Accessed March 19 2018].

89. Efavirenz, https://medlineplus.gov/druginfo/meds/a699004.html; [Accessed 19 March 2018].

90. Sluis-Cremer N, Tachedjian G. Mechanism of inhibition of HIV replication by non-nucleoside reverse transcriptase inhibitors. Virus Research 2008; 134:147-156.

91. Chun TW, Carruth L, Finzi D, Shen X, DiGiuseppe JA, Taylor H, Hermankova M, Chadwick K, Margolick J, Quinn TC, Kuo YH, Brookmeyer R, Zeiger MA, Barditch-Crovo P, Siliciano RF. T.W. Quantification of latent tissue reservoirs and total body viral load in HIV-1 infection. Nature 1997; 387:183-188.

92. Montefiori DC. Measuring HIV neutralization in a luciferase reporter gene assay. Methods Molecular Biology 2009; 485:395-405.

93. Platt EJ, Wehrly K, Kuhmann SE, Chesebro B, Kabat D. Effects of CCR5 and CD4 cell surface concentrations on infections by macrophagetropic isolates of human immunodeficiency virus. Journal of Virology 1998; 72(4):2855-64.

94. Maggiolo F. Efavirenz: A decade of clinical experience in the treatment of HIV. Journal of Antimicrobial Agents and Chemotherapy 2009; 64: 910-928.

95. Rakhmanina NY, van der Anker JN. Efavirenz in the therapy of HIV infection. Expert Opinion on Drug Metabolism and Toxicology 2010; 6: 95-103.

96. Staszewski S, Morales-Ramirez J, Tashima KT, Rachlis A, Skiest D, Stanford J, Stryker R, Johnson P, Labriola DF, Farina D, Manion DJ, Ruiz NM. Efavirenz plus zidovudine and lamivudine, in the treatment of HIV-1 infection in adults. New England Journal of Medicine 1999; 341:1865-1873.

97. Troy T, Jekic-McMullen D, Sambucetti L, Rice B. Quantitative comparison of the sensitivity of detection of fluorescent and bioluminescent reporters in animal models. Molecular Imaging 2004; 3:9-23.

98. Baron S. Medical Microbiology (4th ed). TX:University of Texas Medical Branch at Galveston, 1996.

99. Basso FG, Oliveira CF, Kurachi C, Hebling J, Costa CA. Biostimulatory effect of low-level laser therapy on keratinocytes *in vitro*. Lasers Medical Science 2013; 28: 367-374.

100. Apostolova N, Gomez-Sucerquia LJ, Alegre F, Funes HA, Victor VM, Barrachina MD, Blas-Garcia A, Esplugues JV. ER stress in human hepatic cells treated with Efavirenz: Mitochondria again. Journal of Hepatology 2013; 59: 780-789.

101. Weiβ M, Kost B, Renner-Müller I, Wolf E, Mylonas I, Brüning A. Efavirenz causes oxidative stress, endoplasmic reticulum stress, and autophagy in endothelial cells. Cardiovascular Toxicology 2016; 16: 90-99.

102. Ogawa M, Takemoto Y, Sumi S, Inoue D, Kishimoto N, Takamune N, Shoji S, Suzu S, Misumi S. ATP generation in a host cell in early-phase infection is increased by upregulation of cytochrome c oxidase activity via the p2 peptide from human immunodeficiency virus type 1 Gag. Retrovirology 2015; 12:97.

103. Engelberg-Kulka H. Bacterial Programmed Cell Death and Multicellular Behavior in Bacteria. PLoS Genetics 2006; 2(10): 1518-1526.

104. Bolton DL, Hahn BI, Park EA, Lehnhoff LL, Hornung F, Lenardo MJ. Death of CD4+ cell lines by human immunodeficiency virus type 1 does not depend on caspases or apoptosis. Journal of virology 2002; 76(10): 5094-5107.

105. Papadopulos-Eleopulos E. Reappraisal of AIDS--is the oxidation induced by the risk factors the primary cause. Medical Hypotheses 1988; 25(3): 151–162.

Chapter 3

Optical trapping and transmission spectroscopy for HIV-1 detection in TZM-bl cells

Introduction

In this chapter, a short outline on various optical trapping modes such as counter propagating beam trap, levitation trap and single beam trap is given. That is then followed by a section in which forces responsible for optical trapping are explained. In addition to that, mechanisms used to trap Rayleigh and Mie particles are clarified, followed by a detailed description on how optical trapping efficiency is determined using the Q value method. Next, general principles to be considered in the construction of an optical trapping system using a Gaussian beam are outlined. As the chapter winds up, the construction of the optical trapping system and its use to trap TZM-bl cells is reported, followed by both the description and the discussion of HIV-1 infection detection in TZM-bl cells using optical trapping coupled to transmission spectroscopy.

3.1 Optical traps

3.1.1 Outline of the various optical trapping modes

Optical trapping is a powerful and versatile method that uses laser light to manipulate microscopic particles using devices that are commonly known as optical tweezers or optical traps [1].

Since light (in the form of a photon) carries momentum that is proportional to its energy, when light is reflected, refracted or absorbed by a particle it undergoes a change in momentum. In turn, the particle also experiences a similar change in momentum due to the force exerted on it [2, 3]. Therefore, the optical trap is based on the momentum transfer associated with the redirection of light as it interacts with a dielectric particle. The redirection or refraction results in a force that holds the particle in a three-dimensional (3D) manner [1]. Since optical traps exert very small forces (in the order of picoNewton, 10^{-12} N), their use is effective and sufficient for the non-invasive manipulation of microscopic particles [4]. For successful trapping of the particles, the refractive index of the particle ought to be higher than that of the surrounding medium [2]. Another important factor, for optical trapping to take place, a laser beam should be tightly focused through a high numerical aperture microscope objective for the generation of gradient forces counteracting the scattering forces in the propagation direction [5].

The first three trapping geometries were demonstrated by Arthur Ashkin as revealed in figure 3.1. Ashkin first demonstrated the trapping system using two counter propagating beams to form a dual beam trap in 1970 as depicted in figure 3.1A. Later on a stable single beam levitation trap (Figure 3.1B) was demonstrated when manipulating transparent dielectric particles of high refractive index [4].

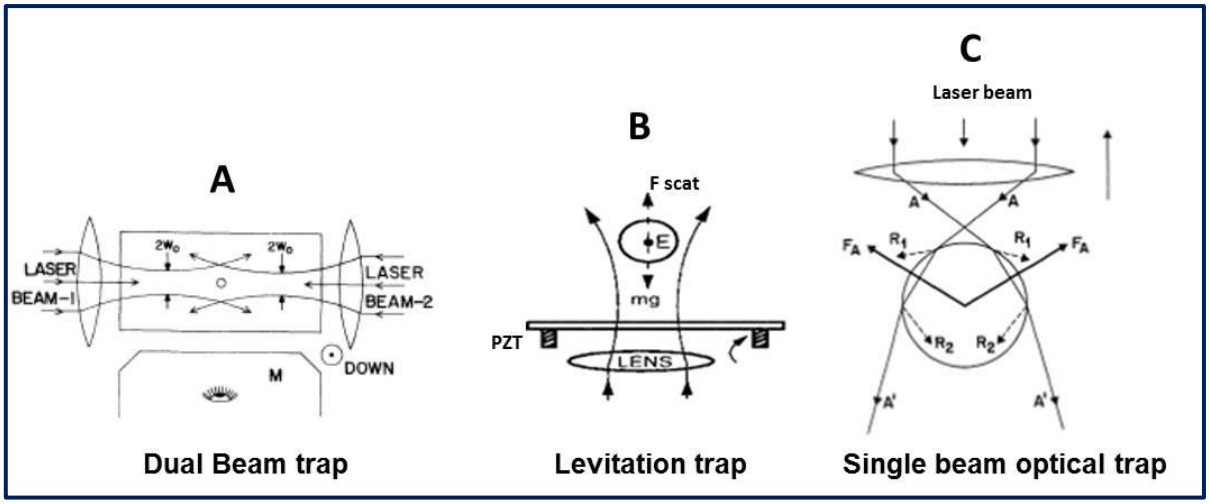

Figure 3.1 Optical trapping geometries: (A) A dual beam trap with lateral confinement controlled by counter-propagating beams. (B) The levitation trap in which the beam intensity spreading provides lateral trapping to form a two dimensional trap in which the scattering force dominates. Presented in picture (C) is a single beam optical trap or a gradient force trap in which the optical gradient forces overcome the scattering forces resulting in a three dimensional trap [1, 4].

The earlier optical traps were dependent on laser radiation pressure force to stably hold spheres in the axial plane against gravity and the transverse gradient beam held them in the centre of the Gaussian beam. Figure 3.1C shows a trapping system achieved through a single tightly focused laser beam known as optical tweezer [1].

3.2 Forces governing optical traps

3.2.1 Gradient and scattering forces in a three dimensional trap

In optical trapping, when the small particles are exposed to the tightly focused laser beam they experience two types of forces namely gradient and scattering forces. The scattering force is a consequence of light having momentum and is produced by the photons as they come into contact with the particle. It acts in the beam propagation direction and is dependent on light intensity, the laser beam wavelength, the particle size and its refractive index contrast against the medium in which they are immersed.

On the other hand, the gradient force is the one that pushes towards the laser focus in the region of highest light intensity. It is linearly dependent on the spatial variation of the intensity of the light field and on the dielectric contrast of the particle relative to the surrounding media [6].

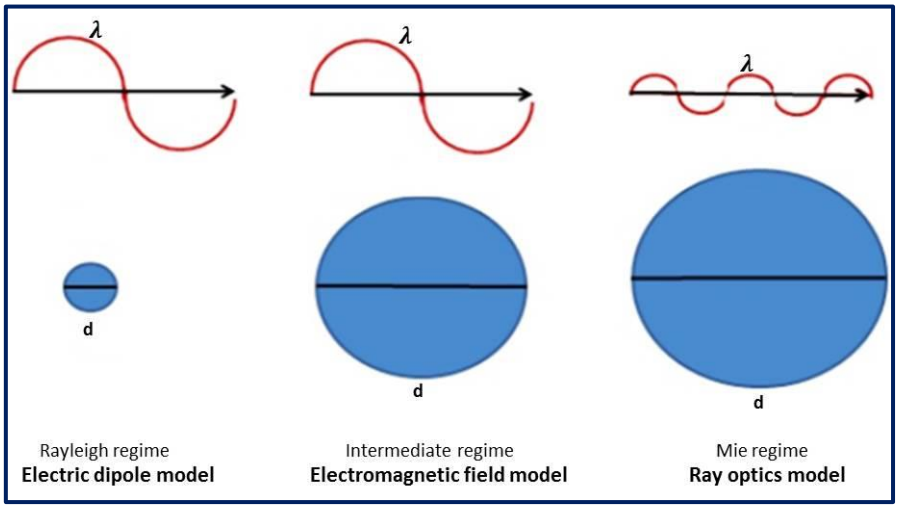

Figure 3.2 Three optical trapping approaches based on the beam wavelength and particle size [7,8].

Based on the laser beam wavelength (λ) and the size of the particle (r) and forces involved, there are three proposed approaches as shown in Figure 3.2: one based on electric field associated with the light Rayleigh where the particle size is smaller than the wavelength ($r < \lambda$), the next one is based on ray optics for particles in the Mie regime in which the particle size is greater than the wavelength of the trapping beam ($r > \lambda$) and the last one based on electromagnetic field model for particles in the intermediate regime in which the particle size is almost equal to the beam wavelength in size ($r \sim \lambda$) [7, 8].

3.2.2 Mie regime explained

In this regime, the wavelength of the laser beam is smaller than the diameter of the trapped particle and it uses the Ray Optics approach or the conservation of momentum model [3].

The effect of a laser beam on a microscopic particle with a bigger diameter can be modelled with a bundle of rays, with each ray weighted according to its light intensity. A photon of wavelength λ has momentum:

$$\boldsymbol{p = h/\lambda} \tag{3.1}$$

(or $\hbar k$) where h is Plank's constant, $\hbar$ is h/2π, and k is wave number. When a particle causes light to change its direction through refraction or reflection, the change of momentum is experienced from individual light rays and an equal but opposite momentum change is generated. When using the ray optics approach, if a transparent microscopic particle is situated within a gradient of light, the refraction of rays of differing intensity (due to the gradient) through the particle results in a change in total momentum of the exiting laser beam and hence a corresponding reaction force on the particle, which draws the particle into the region of highest light intensity of the beam as depicted in Figure 3.3A. An equilibrium position is reached and the particle is held in the beam centre as the rays of light passing through and exiting the particle are balanced with no overall change in momentum of the beam.

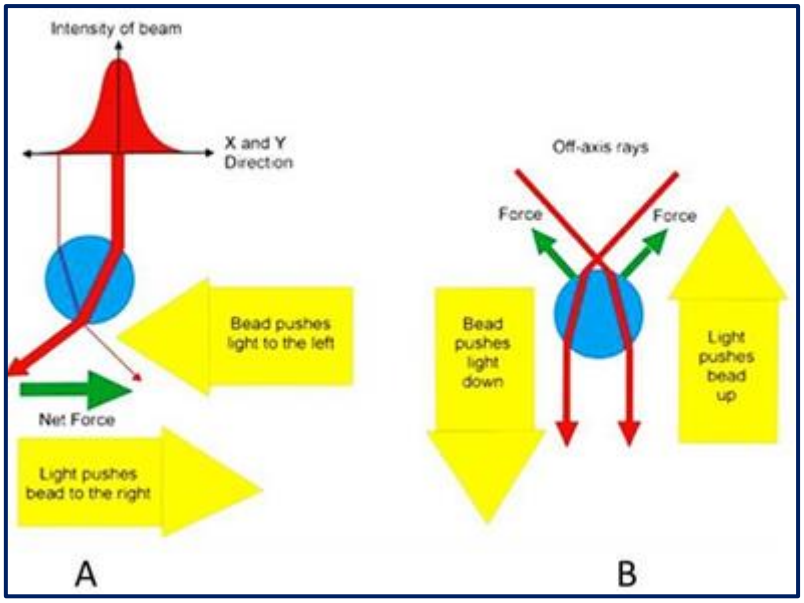

Figure 3.3 The ray optics of the lateral and axial trapping force within optical tweezers. Shown in (A), when a bead with a refractive index higher than the surrounding medium is positioned to the left of the beam's region of highest intensity; more rays get refracted from the right to the left as they go through the bead. The net force then transfers momentum towards the left and the particle encounters an equal but opposite force drawing it towards the beam centre. In (B), off axis rays lead to axial trapping as they get refracted in the direction of beam propagation and a force of equal size but opposite direction is exerted on the bead causing the change in the momentum of light [10, 11].

This trapping force is due to the transverse gradient force which is a result of the Gaussian intensity distribution of the laser mode; however an axial gradient is also required in order to lift the particle and manipulate it in three dimensions [7, 9]. For axial trapping in the z (vertical plane) direction, off axis rays come in at an angle towards the particle and gain momentum in the beam propagation direction. This momentum change results in a force that pushes the particles upwards against the beam propagation direction towards the beam focal region, thereby generating a trapping force in the z-direction, hence the three dimensional trap. The point of equilibrium is obtained when the scattering force and gravity (both push the bead downward) is balanced by the axial gradient force (which pushes the bead in an upward direction) (Figure 3.3B).

3.2.3 Interaction of light with Rayleigh particles

In this regime, particles are much smaller than the laser beam wavelength and therefore trapping them considers the force in terms of the electric field in the region of the trapped particles. When a polarisable particle is situated in the electric field it experiences an electric dipole moment as it responds to the electric field of the laser beam and is attracted to intensity gradients in the electric field towards the focus (if the refractive index is greater than 1). When the particle moves to where the electric field is highest (which is the focus), the energy of the system will be at a minimum [12].

3.2.4 Trapping intermediate regime

In this regime, the particle size is comparable to the trapping laser beam wavelength, and therefore neither the electric field approach nor the ray optics approach is suitable to determine the forces that are responsible for trapping. However, the electromagnetic theories are applicable for intermediate size range [13]. In this work both the beads and cells trapped lie in the Mie regime, since the laser beam wavelength used was 1064 nm and the beads used had a 2 μm diameter and TZM-bl cells ranged anything between 12 and 25 μm in diameter.

3.2.5 Optical trap efficiency

The capability of the optical tweezing system to trap or hold particles of interest is determined by making use of the Q value method. This method works by measuring the velocity at which the particle escapes from the trap when it is dragged through the sample medium. It is obtained by translating the motorized sample stage which holds the sample chamber at a known velocity and calculating the velocity at which the particle escapes from the trap. With the stage motion controller the sample stage can be manoeuvred at a constant velocity.

The sample is usually a microscopic particle suspended in liquid and the sample chamber with a well is normally made up of a bottom coverslip and a top coverslip separated by a vinyl spacer (~100 μm depth, 12 mm in diameter). The well of the sample chamber is the vinyl spacer opening as illustrated in Figure 3.4.

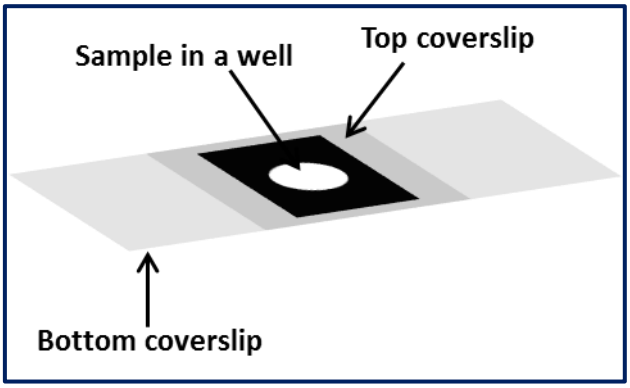

Figure 3.4 The figure shows the sample chamber made of two coverslips and a well where the sample is loaded in between the coverslips.

The Stokes drag force (F_{drag}) which is present during the dragging process is equal to the forces exerted on the particle (F_{trap}). The dragging denotes the horizontal pulling of the particle through the sample chamber as depicted in Figure 3.5.

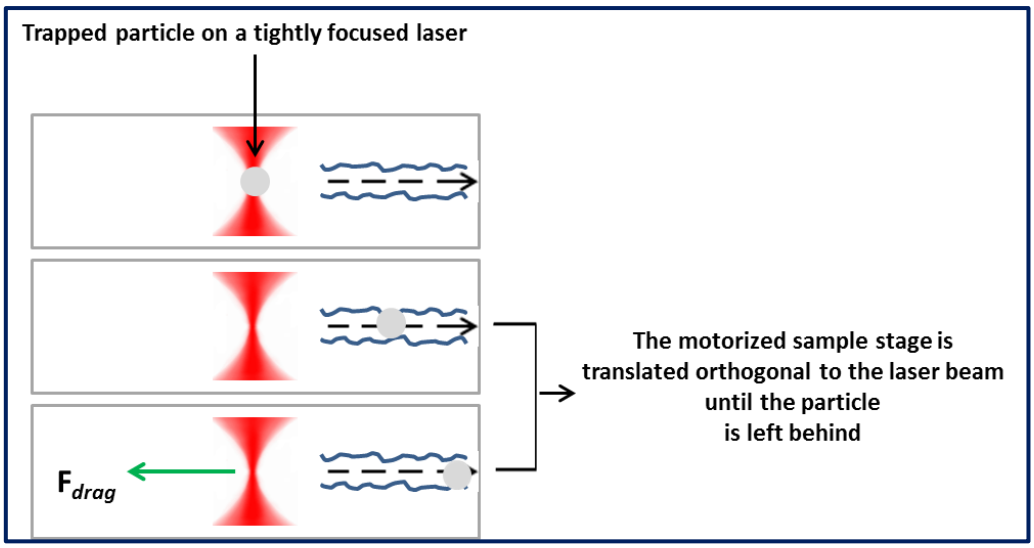

Figure 3.5 The drag force opposes the relative motion of a particle through a fluid, acting in the direction opposite to the oncoming flow velocity and depends on the velocity [14]

The Stokes drag force determined by using equation 3.2:

$$\boldsymbol{F_{drag} = 6\pi\eta v r} \tag{3.2}$$

where η is the fluid viscosity, r is the particle radius and v is the particle velocity with respect to the fluid [15].

The drag force varies with the particle dragging velocity and it is zero when the particles are stationary. This is the maximum force that can be exerted by the optical trap at a given laser power and it is usually in picoNewton order. The critical velocity for the particle escape from the trap scales linearly with laser power. The trapping efficiency of any optical tweezer configuration is usually described in terms of a dimensionless parameter Q, the fraction momentum transferred to the trapping force from the trapping laser beam, which is related to the force on the particle, F_{trap}, the laser power P, c for the speed of light, and the surrounding medium refractive index n_m through the equation:

$$F_{trap} = Q\frac{n_{md}P}{c} \quad \ldots \quad (3.3)$$

Since the Stokes drag force is equal to the optical force exerted on the particle;

$$F_{drag} = F_{trap} \quad (3.4)$$

therefore,

$$6\pi\eta v_c r = Q\frac{n_{md}P}{c} \quad (3.5)$$

and,

$$Q = \frac{6\pi\eta v_c r}{n_m P} \quad (3.6)$$

According to Felgner et al 1995 reported that both the lateral and axial trapping efficiencies of microparticles are used to measure the force at which the particles are effectively trapped [16]. The Q values of the optical forces acting on small dielectric particles tend to be in the range of 0.03 to 0.1 [17].

3.2.6 Optical trapping via a Gaussian beam

Optical trapping uses a highly focused (non-diverging) Gaussian beam to trap and manipulate microparticles. The most preferred lasers for optical traps are continuous wave lasers as pulsed lasers would damage specimens due to their high energy in space and time [18]. Construction of a home built optical trapping system can be achieved by using off the shelf optical components, as long as special emphasis is put on optical arrangement and alignment [19]. The arrangement of optical components must be done such that the beam is expanded, reflected and delivered to the back aperture of a microscope objective via sets of lenses and mirrors set on

the beam path. Furthermore, a laser wavelength and its quality must be considered, as well as other aspects as discussed below.

The laser should deliver a single mode output (Gaussian TEM_{00} mode). The Gaussian beam irradiance is exponentially reduced towards the edges of the beam thereby providing the transverse optical gradient needed to trap particles in a three dimensional optical trap. In addition, a few essential properties that one should consider when selecting a good trapping laser include the laser wavelength and the M^2 factor of the laser [20]. The laser beam quality is assessed by M^2, which signifies how closely a beam matches the ideal Gaussian beam. The M^2 value of a beam that matches a perfect Gaussian beam profile is 1, and such a beam would have no transverse aberration when focused to a diffracted limited spot [21]. A good-quality optical trap is achieved when the M^2 of a laser beam focused with a high numerical aperture microscope objective is less than 1.1 [22].

The chosen laser beam should have a wavelength that lies out of the absorption region of the trapped particle and the medium it is immersed in [18]. When the laser wavelength is close to the absorption band of the trapped particle, undesirable thermal effects are created. These undesirable effects have a potential to damage the trapped particle, thereby causing the destabilization of the trap [7]. Hence lasers within the infrared region (~750 to 1200 nm) of the electromagnetic spectrum are the most preferred when trapping biological materials as most cells display good transparency in this region [9]. Shorter wavelengths below 800 nm can cause damage to the cells as this is the region in which the majority of cellular molecules absorb light [23, 24, 25]. Water as one of the cellular molecules has a very complex absorption spectrum due to its various phases and transitions, which causes it to absorb light at different regions of the electromagnetic spectrum [26, 27].

In order to reduce the heating effects generated when using the usual water, heavy water (D_2O) is used because it absorbs less within the infrared region [28]. In addition to water, cells also contain carbohydrates, nucleic acids and proteins, which also have their various light absorbing characteristics [29].

A stable three dimensional trapping is established when the gradient force is greater than the scattering force [7]. It is attained by using a high numerical aperture (NA $\geq$ 1.2) microscope objective, which produces steep gradients due to the angle which the off axis rays come into the sample [9]. The numerical aperture is a dimensionless value that represents the ability of the microscope objective to gather light and defines the smallest region that light can be focused at its focal point. It is defined by NA = $n\sin\theta$, where n is the refractive of index of the medium and θ is the half angle of the cone of light that enters or leaves the microscope objective. The use of infinity corrected microscope objectives is common in the construction of optical trapping systems, as they offer the highest flexibility.

Furthermore, a good quality optical trapping system is produced by overfilling the back aperture of the microscope objective with a laser beam, so as to obtain a diffracted limited spot and also generate a considerable gradient in the focused beam [20]. The overfilling of the back aperture is gained by expanding and collimating the laser beam with a telescope. Before the beam enters the back aperture of the microscope objective, it goes through a simple 1:1 telescope arrangement (beam steering) in order to allow conjugate images to be formed between the beam steering mirror and the back focal plane of the microscope objective. The beam steering ensures that the beam does not travel off its position. During the steering, the beam overfilling the back aperture needs to be centred upon the back aperture [30].

By means of a dichroic mirror placed at 45º, the beam is directed into the microscope objective, but allows white light from the Koehler illumination to pass through and an image is formed on the camera which can be viewed on the monitor.

3.2.7 Gaussian beam propagation

Gaussian beams have single maximum centred along the beam propagation direction and diverging at an angle away from beam waist w_0. The diverging angle θ can be described by equation 3.7 [31].

$$\boldsymbol{\theta = \frac{\lambda}{\pi w_0}} \tag{3.7}$$

where λ is the wavelength of the laser light. The Rayleigh length (Z_R) of a laser beam as described by the following equation,

$$\boldsymbol{Z_R = \frac{\pi w_0^2}{\lambda}} \tag{3.8}$$

is the distance along the beam propagation direction (z axis) where the cross section of the beam waist is doubled as illustrated in Figure 3.6 [32].

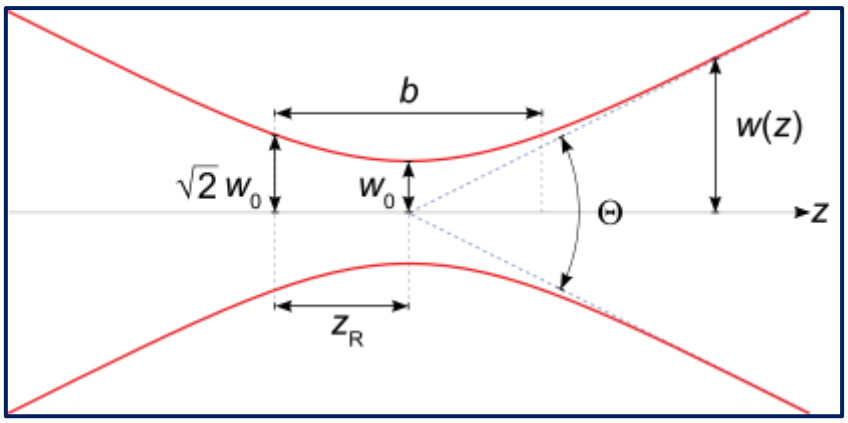

Figure 3.6 The Rayleigh length Z*R* of a Gaussian beam and the beam waist w_0 are shown. The Gaussian beam width *w(z)* is set as a function of the axial distance, with b being the depth of beam focus and as the total angular spread [33].

The beam divergence as described in equation 3.7 shows that the smaller the radius of the waist and the longer the wavelength, the sturdier is the beam divergence from the waist [34]. In its propagation the Gaussian beam keeps the Gaussian intensity profile along its entire beam axis; with only a variation in the beam radius. In addition, Gaussian beams stay Gaussian even after passing simple optical elements such a lenses and mirrors with no aberrations [35].

3.3 Typical optical trapping setup

3.3.1 Assembling an optical trapping system

The MIL-S-1064 nm diode laser with a beam spot of 1 mm was used in this work. Since the back aperture of the microscope objective used was 8 mm, the beam size had to be magnified to slightly overfill it. The beam size was expanded with a simple two bi-convex lens telescope L1 and L2 (f = 25.4 mm and f = 300 mm respectively) to ~8.3 mm. The newly expanded beam was directed to the microscope objective through the beam path by being reflected with mirrors M1 and M2 in Figure 3.7.

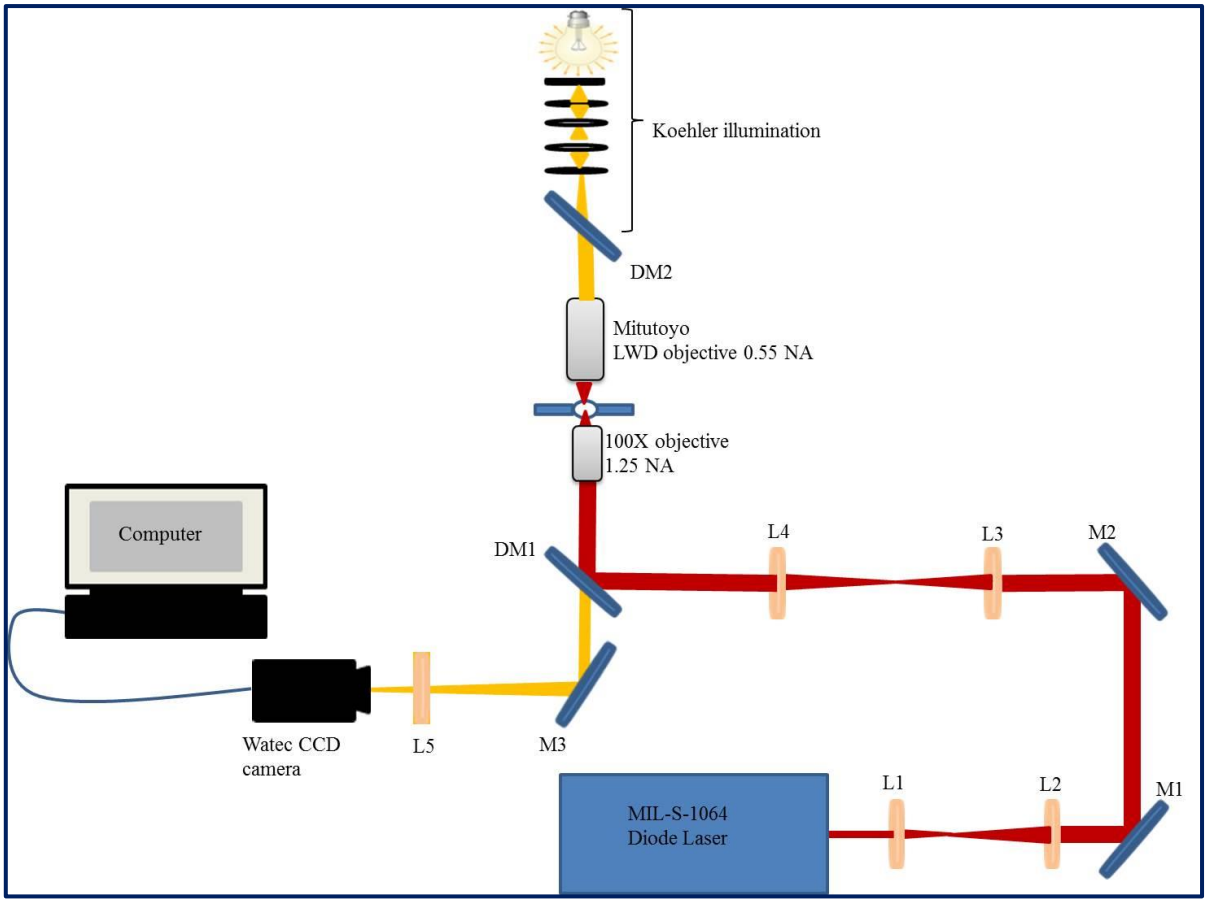

Figure 3.7 A presentation of a basic optical trapping system constructed using a 1064 nm diode laser with maximum output power of 1.5 W. This setup is useful for biological trapping as it consists of an infrared laser.

Mirror M2 then reflected the beam to the 1:1 telescope arrangement for the steering of the beam at the back aperture of the microscope objective. The beam steering comprised of two identical plano-convex lenses, L3 and L4 (f = 100 mm each), which were separated by the sum of their focal lengths, so that the incident parallel beam produces a parallel output of the same beam diameter [17]. The flat surfaces of the lenses face each other; as such the spherical aberration is minimized [36]. A dichroic mirror positioned at 45° was placed after L4 to reflect the laser beam into the 100X oil immersion microscope objective with a high numerical aperture of 1.25, but also to allow the white light from the Koehler illumination to pass through for the formation of the image on the charge coupled device (CCD) camera which can be viewed on a computer monitor.

The 100X objective focused the laser beam to a 1.08 μm diffraction limited spot. The white light was directed to the CCD camera by M3 and reduced using lens L5 in order to fill the detection area in the camera. The xyz translation stage on which the sample was placed was situated just above the microscope objective. By translating the stage, the sample could be moved to different directions. Above the sample stage was a Koehler illumination setup which provided an even illumination across the sample.

3.3.2 Optical trapping of microspheres and TZM-bl cells

Having built and aligned the setup illustrated in Figure 3.7, its efficiency was assessed by trapping 2 μm polystyrene microspheres. The spheres were successfully trapped using 97 mW laser power output on the sample stage as shown in Figure 3.8.

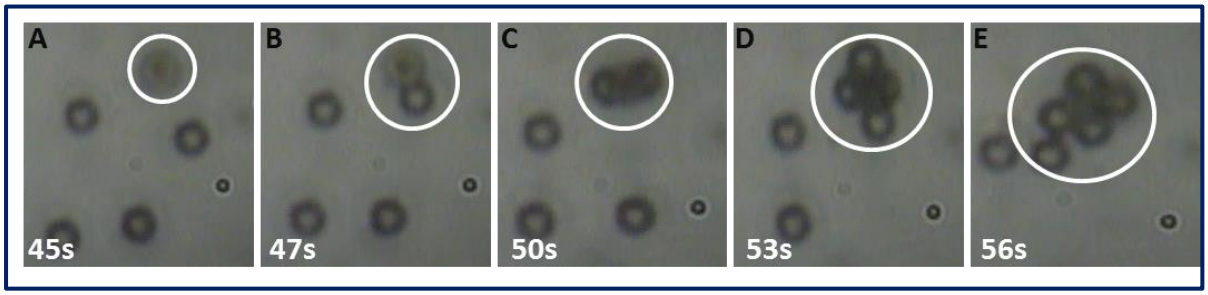

Figure 3.8 Pictures from a CCD camera displaying the trapping of 2 μm polystyrene beads using the optical trapping system illustrated in Figure 3.7 at 97 mW. The particles are trapped by the laser, and the beam position on the slide is depicted by the white circle. The images were taken at different time points after the sample (slide containing beads suspended in detrium oxide) was exposed to the beam on the trapping system (A) After 45 seconds (s), (B) 47s, (C) 50s, (D) 53s and (E) 56s.

In Figure 3.8 the spot where the beam is focused is shown by a white circle, with Figure 3.8A illustrating an already trapped bead and four nearby beads that are not yet trapped, but floating in solution. In Figure 3.8B; at 47 seconds one of the beads that were floating in A has been trapped, and the same is observed in C and D as the clump (highlighted by a white circle) of

beads grew. Figure 3.8E shows that more beads had been trapped including the ones that were floating in Figure 3.8A.

Following the successful trapping of microspheres, the optical trapping system was further assessed in order to determine its capacity to trap cells. TZM-bl cells were trapped after exposing them to the laser beam on the sample stage of the same trapping system. The TZM-bl cells were used as they are a cell line widely used in HIV-1 related research studies, mainly the ones looking into finding HIV treatment. This cell line has CD4 and CCR5 molecules on the cell surface to enable HIV-1 entry. Since they are permissive to HIV-1 infection, they were used in the current study instead of using blood samples that would require human study participants. TZM-bl cells are 25 μm in size and 12 times bigger than the polystyrene beads trapped in Figure 3.8. The trapping of the cells was observed from 47 mW with a weak trap that falls out at the slightest move (40 μm/s) of the sample stage. However, as the power increases the trap becomes more stable, with 185 mW being the maximum power of the laser on the sample stage. After trapping the cell at 185 mW average power the sample stage was moved to different directions, in order to assess and determine the conditions that would cause the cell to fall out of the trap. Figure 3.9 shows a trapped cell at 155 mW with the sample stage moving at 160 μm/s to the right.

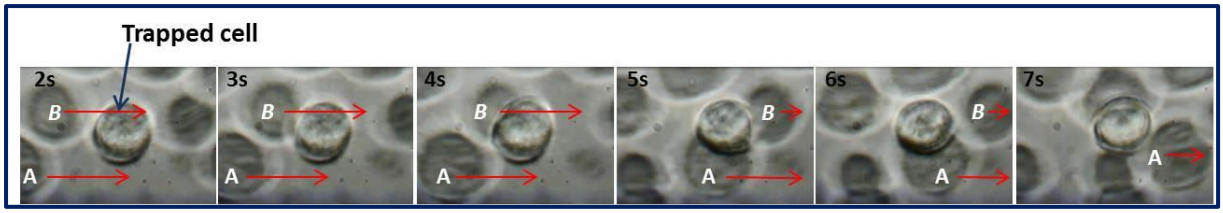

Figure 3.9 Pictures from a CCD camera displaying the trapping of TZM-bl cells using the optical trapping system illustrated in Figure 3.7. The sample stage is moved towards the right and the untrapped cells (such as cell A and B) also flow to the right, while the trapped cell remains unmoved. At different time points it is visible that the untrapped are shifting from their original positions as indicated by the red arrows.

Once the cell was trapped and the stage moved, the trapped cell remained at the same spot while the nearby cells moved across it as shown at the different time points of Figure 3.9. In Figure 3.9, at 2 and 3 seconds, cells A and B are moving towards the right in the direction of the trapped. At 4 seconds cell B is passing behind the trapped cell and at 5 seconds cell B has partially gone past the trapped cell while cell A is still passing the trapped one. At 6 seconds cell B has far gone past the trapped cell. At 7 seconds cell B has gone past area visible to the camera and cell B is about to disappear too. Being able to trap the TZM-bl cells led to the next step of trapping both HIV-1 infected and uninfected in order to examine them and differentiate between HIV-1 infected and uninfected cells using transmission spectroscopy, which would be discussed in the next section.

3.4 Detection of HIV-1 infection in TZM-bl cells using optical trapping in conjunction with transmission spectroscopy

3.4.1 Transmission spectroscopy overview

The interaction of light with matter can result into light being transmitted, absorbed or reflected. Since this section deals with transmission spectroscopy, the focus will be on the transmission of light instead of the other mechanisms that occur as a result of light and matter

interaction. Transmission of light occurs when electromagnetic radiation passes through a material without being absorbed and therefore the transmittance of any given material is the amount of the incident light that travels all the way through to the other side of a particular barrier. This then implies that transmission spectroscopy is the measurement (analysis) of the emission of energy as electromagnetic radiation as a function of wavelength that has been passed through a sample [37]. It is a non-invasive and real time optical detection technique that has found wide applications in pharmaceutical industry as well as in biological and medical fields [38, 39, 40, 41, 42]. This technique's detection ability is based on distinguishing samples based on size, shape and sample concentration, it is highly sensitive with pico-molecular ranges detection limits [42].

Transmission spectroscopy has been successfully used for the diagnosis of dengue viral infection. According to Firdous *et al* 2012 it was done by recording transmission spectra of both the dengue infected blood samples and the uninfected ones [43]. The infected blood spectra showed a band with a more convincing band from 400 to 600 nm [43]. Dengue viral infection may be diagnosed by processes such as nucleic acid detection by polymerase chain reaction (PCR), virus isolation in cell cultures and virus specific antibodies. However, the latter two techniques are the most sensitive, but they are not routinely used due to high costs associated with them. Therefore, the availability of a fast screening, cost effective and easy to use method could reduce the cost related burden in the diagnosis of dengue fever [43].

In another study conducted by Mahon *et al* 2013 transmission spectroscopy was used in marine ecosystems and freshwater for the detection of invasive species with adverse impact on the economy and biodiversity.

It was used for the early detection of undesirable species for effective biocontrol to alleviate possible ecological and economical destruction [44]. They tested to check if transmission spectroscopy would be able to detect the presence of the invading species within a sample with mixed species, they also investigated if concentration of the target species could be determined and tested for differences between amplified DNA and unamplified. In the study they were able to screen samples obtained directly from nature (with no modification) without the necessity for prior PCR amplification. Due to its user friendliness and short detection times, transmission spectroscopy is an attractive technique in environmental monitoring studies where it can easily be taken and used at the point of sample collection without getting to the laboratory. This makes it a useful tool for field application [44].

Literature has shown that near infrared transmission spectroscopy technique can allow the determination of the mean paracetamol content of intact tablets by looking at the spectra pattern [38]. In addition, transmission spectroscopy is often applied to determine the tissue properties. It has been used to quantify for instance tissue chromophore concentration [39]. Furthermore, the analysis of transmission spectra patterns has led to the differentiation of red from white human blood cells, as well as cancerous from non-cancerous cell species and the investigation of the influence of wavelength on red blood cell aggregation [41, 42, 45]. However, when examining the experimental makeup of the transmission spectroscopy, there are some parameters that affect recorded spectra. These parameters include sample thickness and sample unevenness that causes severe loss of the transmitted signal; therefore during sample preparation care must be taken on sample thickness and homogeneity [38, 42]. The transmission measurements are often done on immobilized cells using substrate or aqueous cells suspension.

In both cases samples are not uniformly distributed, therefore unevenness would generate spectral artefacts [41]. These artefacts generally alter the peak intensity that cause false interpretation of results obtained [39].

The coupling of transmission spectroscopy with optical trapping provides an attractive method that allows for the manipulation of single cells instead of only focusing on cells in suspension or a layer of cells that might be uneven. In essence, optical trapping helps to overcome the limitation imposed by transmission spectroscopy of the ensemble measurement and sample thickness [46].

3.4.2 Coupling of the optical trapping system with transmission spectroscopy

The trapping system demonstrated in Figure 3.7 was slightly modified by integrating the transmission detection system and the newly formed trapping/transmission system is exhibited in Figure 3.10. The laser beam was used for both optical trapping and laser transmission spectroscopy. A long working distance objective (distance focal of 200 mm) was utilized to collect the transmitted laser light from the sample and also coupled the Koehler illumination to the sample plane. The collected transmitted laser beam was focused into a single mode fibre by a 40 mm distance focal lens in order to guide the light onto the entrance slit of the Andor spectrometer (Shamrock 303i) and the transmittance spectra were detected by the Andor iStar 734 series CCD camera. The iStar camera was air cooled to -200ºC in order to reduce the effect of dark current, which increases the amount of fixed pattern noise [47]. The image trapped cells were viewed through video camera (Watec, W96N15832 CCD camera) illuminated by the Koehler illumination system.

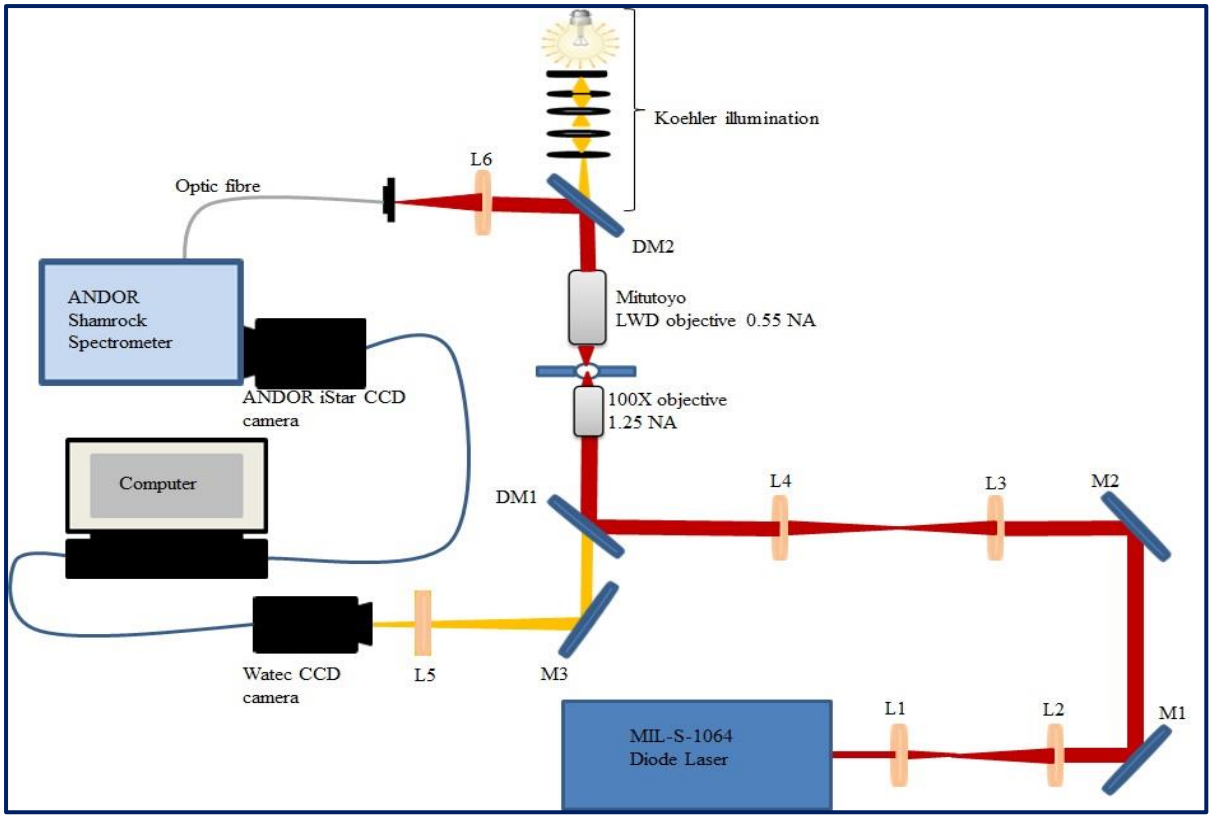

Figure 3.10 Optical trapping coupled to the transmission spectroscopy experimental system used to determine the transmittance spectra of TZM-bl infected and uninfected single cells. L1-L6 refers to lenses used, M1-M2 are the infrared mirrors, M3 is the highly reflective silver mirror and DM is the dichroic mirror.

3.4.3 Optical trapping and transmission spectroscopy measurements on HIV-1 infected TZM-bl cells

In two separate 35 mm glass bottom petri dishes 500 µl suspension of infected and uninfected cells were added and these samples were covered with glass coverslips prior to observation on the optical setup. For the purpose of transmittance experiments, background subtractions and normalization were first conducted by subtracting the background light from the signal and have a laser intensity reference and thereafter the samples were analyzed. The transmission spectra of HIV-1 infected and uninfected TZM-bl cells were captured using the Andor solis software. The intensity of transmission was expressed in terms of photon count which is a number of light photons transmitted through a trapped cell.

Preceding the optical trapping transmission experiment, the background and reference intensities were recorded and Figure 3.11 outlines how the procedure was performed.

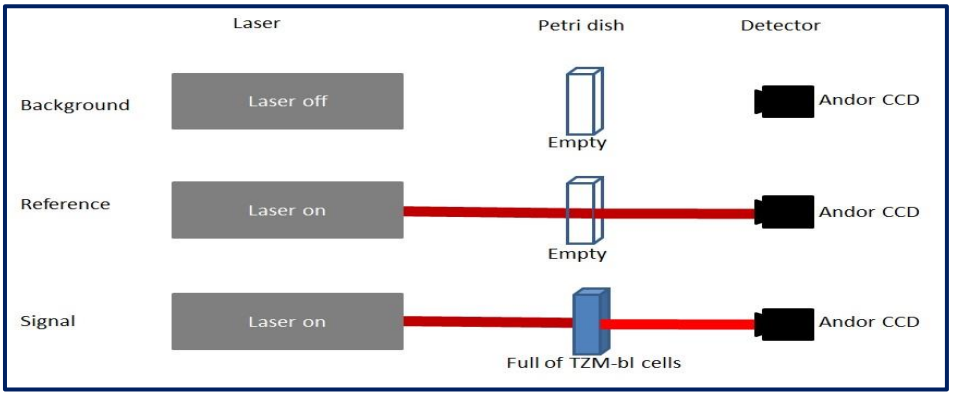

Figure 3.11 A schematic representation of a procedure used to record the background, reference and transmitted signal.

The intensity background was acquired by recording a dark signal when the laser was off and the petri dish was empty. On the other hand, the reference intensity was captured with laser on and an empty petri dish. However, the sample signal was measured with laser on and petri dish containing TZM-bl cells in suspension, with one cell trapped. In data processing, the transmission spectra are shown in transmittance percentage given by the following equation:

$$I_T\,(\%) = 100 * \left(\frac{I_S - I_B}{I_0} \right) \qquad (3.9)$$

With I_T being the transmittance percentage intensity, I_S the signal intensity, I_B background intensity, I_0 reference intensity. It is worth noting that the reference intensity is the background corrected incident intensity.

The initial form of transmission investigation done was to study the influence of the virus on the transmittance intensity signal by measuring the transmittance intensity of media only and then the media with virus (media and virus on Figure 3.12). Figure 3.12 shows transmittance intensity of cell growth media only and that of media with virus. The two transmission spectra appear relatively similar with a transmittance percentage of 20%.

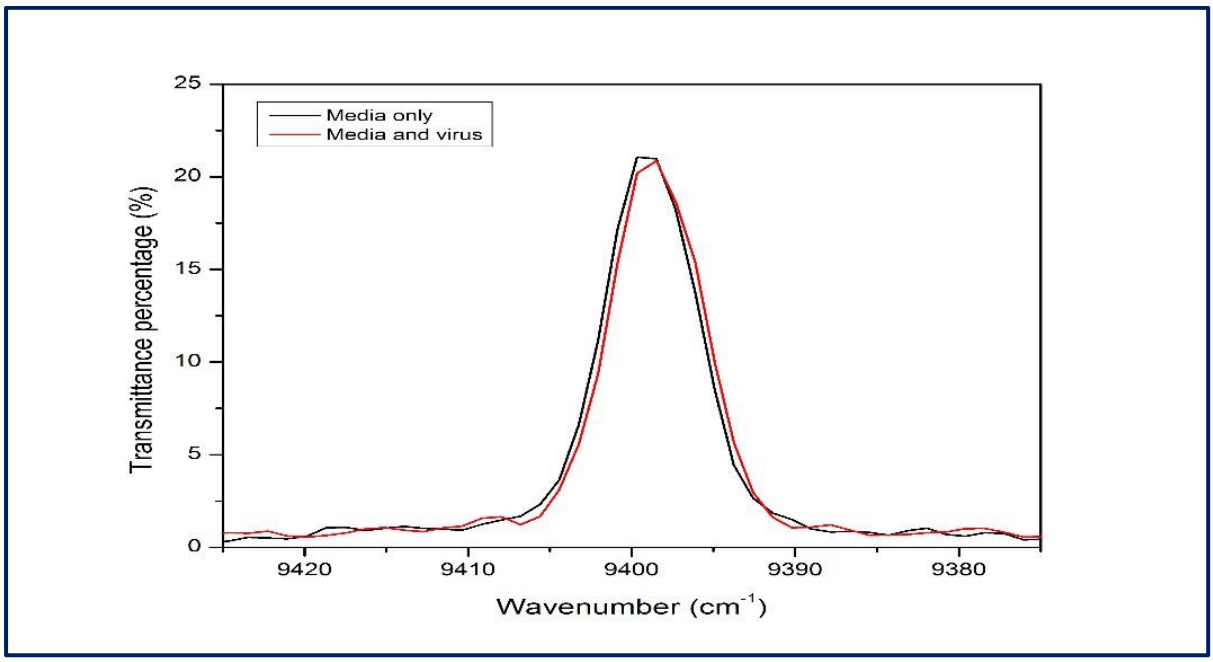

Figure 3.12 Transmission spectra of cell growth media (black) and pseudo-virus & media (red) recorded between 9425 cm^{-1} and 9375 cm^{-1}.

For each trapped cell 50 signal spectra were recorded and an averaged spectrum was calculated and automatically distributed from the Andor solis software. The exposure time to capture each spectrum was 3.4 seconds, making the total average acquisition time for 50 spectra 3 minutes as shown in Figure 3.13. The final spectrum obtained was exported into Origin-Pro 8 for data analysis. The transmission spectra of both uninfected and infected cells have peaks at 9398 cm^{-1} even though they show slight variation in the peak amplitude as depicted by the transmittance percentage.

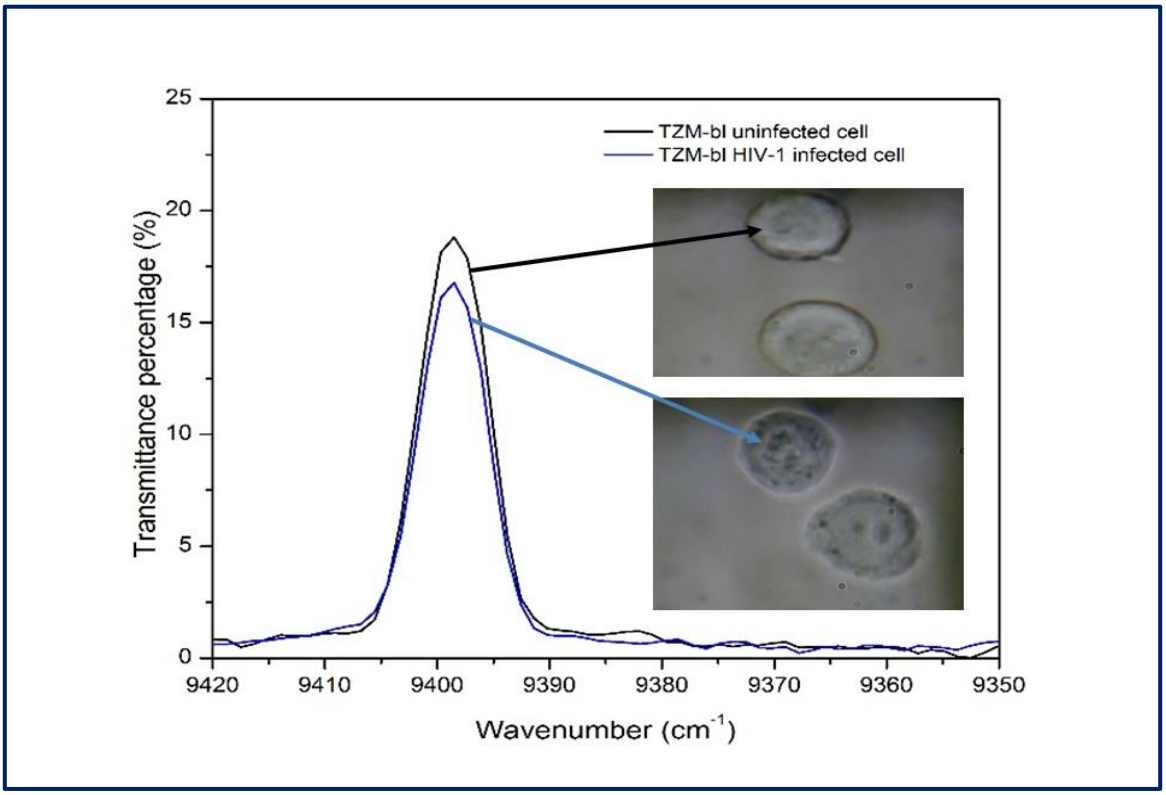

Figure 3.13 Transmission spectra for individually trapped HIV-1 infected and uninfected cells suspended in cell growth media in the region from 9420 cm^{-1} to 9350 cm^{-1}. Each spectrum represents the average of 50 spectra of trapped cells. The inserted pictures show trapped uninfected and HIV-1infected TZM-bl cells with HIV infected (indicated by a blue line) cells appearing more granular than uninfected cells (indicated by a black line).

To confirm consistency and reproducibility, the measurements were repeated on ten infected and uninfected cells. Figure 3.14 shows the transmittance peak intensities of HIV-1 infected (in red) and uninfected (in black) TZM-bl cells. The overall average of the ten transmittance intensity percentages for HIV-1 infected and uninfected was found to be 15.95±0.79 and 19.73±0.98, respectively. The results revealed that transmittance percentage of uninfected TZM-bl trapped cells remain greater than the one for HIV-1 infected trapped cells.

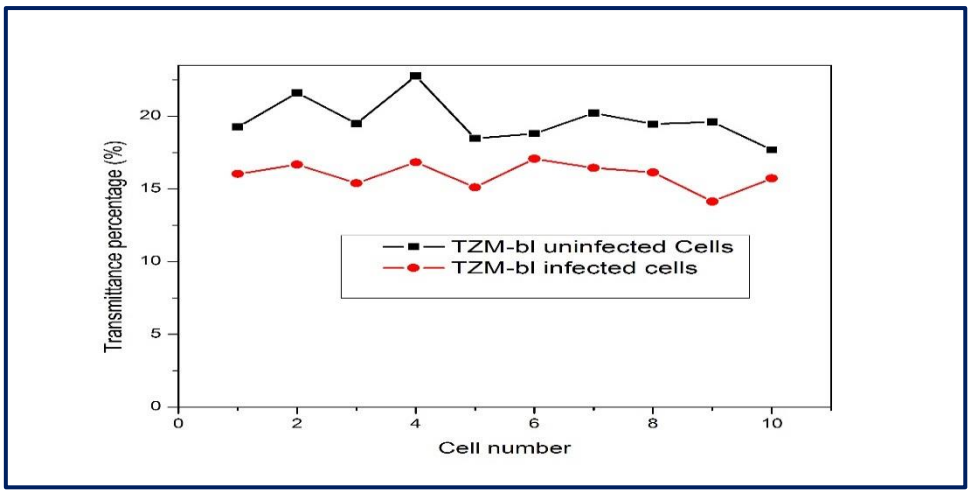

Figure 3.14 Transmittance spectra peaks values of 10 infected cells compared to those of 10 uninfected cells.

In addition to transmittance percentages data of HIV-1 infected and uninfected cells, areas under their spectral peaks were integrated.

Table 3.1: Values of area under the spectral peaks of ten HIV-1 infected and uninfected TZM-bl cells in nm^2

Cell	1	2	3	4	5	6	7	8	9	10
Uninfected	69.76	71.44	72.23	73.55	70.67	70.50	71.64	71.73	70.83	69.94
Infected	64.50	67.35	66.89	67.35	68.53	69.10	69.19	68.90	68.20	67.14

The values of the areas beneath the graphs attained for ten cells are presented in table 3.1. The results show that areas under the spectral peaks of infected cells are less than those of uninfected cells. These findings confirm the trend seen in the transmittance percentages data.

3.5 Discussion

In this study optical trapping was used to hold both microspheres and cells; with the intention of analysing cells so as to differentiate between HIV-1 infected and uninfected TZM-bl cells using transmission spectroscopy. As shown in Figure 3.8 and 3.9 the 1064 nm laser used successfully trapped both the microspheres and the cells.

Both cells and microspheres have diameters greater than the wavelength of the trapping beam and they both used the ray optics trapping approach as outlined in Figure 3.3. However, it was easier to trap microspheres than cells, so much that when trapping microspheres clumps (Figure 3.8) were formed as many microspheres were drawn to the beam centre and this was not observed when trapping cells (Figure 3.9). The differences in trapping microspheres and the cells could be primarily attributed to the differences in sizes. The cells were 25 μm in diameter while the microspheres were only 2 μm. Since the beam centre has the highest intensity compared to the edges, it was easier to tightly trap smaller particles even into clumps than holding 25 μm cells. In addition to the differences in sizes, the polystyrene beads had a higher refractive index of 1.5 compared to the cells with a refractive index of 1.37 [48, 49].

In trapping, particles with higher refractive index are easier to trap compared to those of lower refractive index [2]. During the trapping experiments, it was also observed that a tight trap in cells occurs at higher powers compared to microspheres as reported in Figures 3.8 and 3.9, where powers of 97 mW and 155 mW were used for microspheres and cells respectively. In the system used the minimum power at which the laser's trapping abilities were observed was 30 mW for microspheres, but 47 mW for cells. At these low powers the particles would be pulled towards the beam centre even though it would not last for long or when the stage is moved the particle would leave the trap. In some instances, the particle would just leave the trap when another particle in Brownian motion comes into contact with the trapped particle.

After coupling the trapping system with transmission spectroscopy and assessing the transmission patterns of the background, reference and the sample as shown in Figure 3.11, transmittance intensities between the plain media and the media containing the virus were measured (Figure 3.12). There were similarities in transmittance intensities and these similarities were not alarming because pseudo-viruses are generally stored in growth medium.

Pseudo-viruses are produced using HEK293T cells and at harvest the medium in which the virus is contained is filtered to remove any traces of cells that could be in the medium and the filtered medium (the pseudo-virus) is stored at -80°C. During cell infection with a pseudo-virus, a small volume of the medium containing the virus is added to cells, hence there are no significant differences in the spectra measurements obtained when assessing transmittance intensities of media only and that of media with virus as demonstrated in Figure 3.12. Transmission spectra are strongly influenced by the biochemical composition of a sample, its homogeneity and sample thickness [39-41].

The absence of differences between the media only and the media with virus samples was an indication that the virus in cell growth media does not influence the transmission measurements. These results correlate well with what was previously reported that differences between two different samples can be detected by even a slight difference in the intensity; especially if the samples are very similar or highly related [41, 42]. Infected and uninfected TZM-bl cells present a transmittance peak intensity percentage around 16.77% and 18.80 %, respectively. These differences in transmittance spectrum are attributed to parameters such as sample thickness, cell consistency, refractive index and sample thickness (path length of the light). Seeing that cells in suspension are approximately spherical, the path length of the near infrared light in the cell will be equal to the diameter of the cell.

The Zeiss axiocam (ERc 5s) CCD camera combined with the Olympus CKX41 microscope (with 60X objective lens) were used to estimate the average diameter of the HIV-1 infected and uninfected cells by measuring cell sizes and calculating the average diameter. The average diameters obtained for HIV-1 infected and uninfected was 17.04 ±1.10 µm and 18.77±2.39 µm, respectively.

This transmittance percentage difference observed could be hypothetically attributed to the differences in refractive index of the two cell groups. The cell images in Figure 3.13 show visible morphological differences between infected and uninfected cells, with the infected cells showing granularity. Numerous lines of evidence show that HIV-1 infection can generate a wide range of reactions in the host cell, hence the granularity in infected cells [50-52]. These reactions include the processing of viral protein into peptides molecules that change the biochemical composition of cells. As a result, the scattering coefficient will be altered due to change in the refractive index. It has been reported that light experiences deflection because of the internal cellular structures (organelles) [53]. The granularity and potential light scattering in the HIV-1 infected could be the second factor that induced low transmission of the near infrared light. This study demonstrated the great potential that optical trapping has in disease diagnosis when coupled with spectroscopy for analysis.

These findings have been encouraging, as such other spectroscopy techniques with more specificity such as Raman spectroscopy will be used to further analyze the trapped cells so as to pinpoint the differences between HIV-1 infected and uninfected cells. Additionally, super resolution imaging techniques will be coupled to the trapping system in order to visually observe the molecular differences between infected and uninfected cells.

References

1. Ashkin A, Dziedzic J, Bjorkholm J, Chu S. Observation of a single-beam gradient force optical trap for dielectric particles. Optics Letters 1986; 11:288–290.
2. Ashkin A. Acceleration and Trapping of Particles by Radiation Pressure. Physical Review Letters 1970; 24:156-159.

3. Ashkin A. Optical trapping and manipulation of neutral particles using lasers. Proceedings of the National Academy of Sciences of USA 1997; 94:4853-4860.
4. Ashkin A, Dziedzic JM. Stability of Optical Levitation by Radiation Pressure. Applied Physics Letters 1974; 24:586-588.
5. Wördemann M. Structured Light Fields: Applications in optical trapping, manipulation and organisation. Springer, 2012.
6. Rohrbach A, Stelzer EHK. Trapping forces, force constants, and potential depths for dielectric spheres in the presence of spherical aberrations. Applied Optics 2002; 41(13):2494-2507.
7. Ashkin A, Dziedzic JM. Optical trapping and manipulation of viruses and bacteria. Science 1987; 235(4795):1517–1520.
8. Ashkin,A. Optical trapping and manipulation of neutral particles using lasers: a reprint volume with commentaries. World Scientific Publishing Company, 2006.
9. Svoboda K, Block S. Biological applications of optical forces. Annual Review of Biophysics and Biomolecular Structure 1994; 23:247-285.
10. Optical tweezwers: merging physics, forces and a bit of fantasy 30 April 2015, https://insights.globalspec.com/article/905/optical-tweezers-merging-physics-force-and-a-bit-of-fantasy, [Accessed 5 June 2018].
11. Dholakia K, Spalding G, MacDonald M. Optical tweezers: the next generation. Physics World. 2002; 15(10):31.
12. Ashkin A. Forces of a single-beam gradient laser trap on a dielectric sphere in the ray optics regime. Biophys Journal 1992; 61(2):569–582.
13. Nieminen TA, Loke VLY, Stilgoe AB, Knöner G, Brańczyk AM, Heckenberg NR, Rubinsztein-Dunlop H. Optical tweezers computational toolbox. Journal of Optics A: Pure and Applied Optics 2007; 9: S196–S203.

14. Mthunzi, P. (2010). Optical Sorting and Photo-transfection of Mammalian Cells (Doctoral thesis), University of St Andrews, St Andrews.
15. Zhang H, Liu K-K. Optical tweezers for single cells. Journal of the Royal Society Interface 2008; 5:671–690.
16. Felgner H, Muller O, Schliwa M. Calibration of Light Forces in Optical Tweezers. Applied Optics 1995; 34:977-982.
17. Molloy JE, Padgett MJ. Lights, action: Optical tweezers. Contemporary Physics 2002; 43(4): 241-258.
18. Neuman KC, Chadd EH, Liou GF, Bergman K, Block SM. Characterization of photodamage to Escherichia coli in optical traps. Biophysical Journal 1999; 77: 2856-2863.
19. Block SM. in Constructing Optical Tweezers, Cell Biology: A Laboratory Manual (D. L. Spector, R. Goldman, and L. Leinwand, eds.). Cold Spring Harbor Press, 1998.
20. Neuman KC, Block SM. Optical trapping. The Review of Scientific Instruments. 2004; 75(9):2787–2809.
21. Siegman AE. How to (maybe) measure laser beam quality. in DPSS (Diode Pumped Solid State) Lasers: Applications and Issues , M. Dowley, ed., Vol. 17 of OSA Trends in Optics and Photonics (Optical Society of America, 1998), paper MQ1.
22. Lee WM, Reece PJ, Marchington RF, Metzer NK, Dholakia K. Construction and calibration of an optical trap on a fluorescence optical microscope. Nature Protocols. 2007; 2(12):3226-3238.
23. Konig K, Liang H, Berns MW, Tromberg BJ. Cell damage in near-infrared multimode optical traps as a result of multiphoton absorption. Optics Letters 1996a; 21:1090–1092.

24. Konig K, Tadir Y, Patrizio P, Berns MW, Tromberg BJ. Effects of ultraviolet exposure and near-infrared laser tweezers on human spermatozoa. Human Reproduction 1996b; 11:2162–2164.
25. Leitz G, Fallman E, Tuck S, Axner O. Stress response in Caenorhabditis elegans caused by optical tweezers: wavelength, power, and time dependence. Biophysical Journal 2002; 82:2224–2231.
26. Bernath, PF. The spectroscopy of water vapour: Experiment, theory and applications. Physical Chemistry Chemical Physics 2002; 4:1501-1509.
27. Tennyson J et al. IUPAC critical evaluation of the rotational-vibrational spectra of water vapor. Part I. Energy levels and transition wavenumbers for $H2^{17}O$, and $H2^{18}O$. Journal of Quant. Spectroscopy Radiat Transfer 2009; 110:573-596.
28. Dholakia K, Reece P. Optical micromanipulation takes hold. Nanotoday 2006; 1:18–27.
29. Cooper GM. The Cell: A Molecular Approach. The Molecular Composition of Cells. 2nd edition. Sunderland (MA): Sinauer Associates; 2000.
30. Moothoo DN. et al. Beth's experiement using optical tweezers. American Journal of Physics 2001; 69: 271-276.
31. Paschotta R. article on 'beam divergence' in the Encyclopedia of Laser Physics and Technology, https://www.rp-photonics.com/beam_divergence.html, [Accessed on 8 June 2018].
32. Siegman, Anthony. Lasers. University Science Books, 1986.
33. Rayleigh length, https://en.wikipedia.org/wiki/Rayleigh_length, [Accessed 7 June 2018].
34. Gaussian beam, https://www.rp-photonics.com/gaussian_beams.html, [Accessed 10 July 2019].

35. Gaussian Beam Propagation, https://www.edmundoptics.com/resources/application-notes/lasers/gaussian-beam-propagation/, [Accessed 10 July 2019].
36. Block SM. Nanometres and picoNewtons: the macromolecular mechanics of kinesin. Trends in Cell Biology 195; 5:169–175.
37. Binetti VR, Schiffman JD, Leaffer OD, Spanier JE, Schauer CL. The natural transparency and piezoelectric response of the Greta oto butterfly wing. Integrative Biology 2009; 1:324-329.
38. Eustaquio A, Blanco M, Jee RD, Moffat AC. Determination of paracetamol in intact tablets by use of near infrared transmittance spectroscopy. Analytica Chimica Acta 1999; 383:283-290.
39. Matcher SJ, Cope M, Delpy DT. Use of the water absorption spectrum to quantify tissue chromophore concentration changes in near-infrared spectroscopy. Physics in Medicine and Biology 1993; 38:177-196.
40. Miller LM, Dumas P. Chemical imaging of biological tissue with synchrotron infrared light. Biochimica et Biophysica 2006; 1758:846-857.
41. Mourant JR, Gibson RR, Johnson TM, Carpenter S, Short KW, Yamada YR, Freyer JP. Methods for measuring the infrared spectra of biological cells. Physics in Medicine and Biology 2003; 48:243-257.
42. Shao H, Kumar D, Lear L. Single cell detection capability of an optofluidic spectroscopy biosensor. Institute of Electrical and Electronics Engineers 2005; 3(5):183-186.
43. Firdous S, Ahmed M, Rehman A, Nawaz M, Murtaza S. Transmission spectroscopy of dengue viral infection. Laser Physics Letters 2012; 9(4):317-321.

44. Mahon AR, Barnes MA, Li F, Egan SP, Tanner CE, Ruggiero ST, Feder JL, Lodge DM. DNA-based species detection capabilities using laser transmission spectroscopy. Journal of the Royal Society Interface 2013; 10:0120637
45. Uyuklu M, Canpolat M, Meiselman HJ, Baskurt OK. Wavelength selection in measuring red blood cell aggregation based on light transmittance. Journal of Biomedical Optics 2011; 16(11):117006.
46. Wakamoto Y, Inoue I, Moriguchi H, Yasuda K. Analysis of single-cell differences by use of an on-chip microculture system and optical trapping. Fresenius' Journal of Analytical Chemistry 2001; 371:276-281.
47. Bettonvil F. Digital all-sky cameras III: Effect of Peltier cooling on fixed pattern noise. Proceedings of the IMC, Roden 2006; 138-140.
48. Polybeads microspheres, https://www.polysciences.com/skin/frontend/default/polysciences/pdf/TDS%20238.pdf, [Accessed June 2018].
49. Lue N, Choi W, Popescu G. Live cell refractometry using Hilbert phase microscopy and confocal reflectance microscopy. Journal of Physical Chemistry A. 2009;113(47):13327–13330.
50. Mekouar K, Mouscadet JF, Desmaele D, Subra F, Leh H, Savoure D, Auclair C, d'Angelo J. Styrylquinoline derivatives: A new class of potent HIV-1 integrase inhibitors that block HIV-1 replication in CEM cells. Journal of Medicinal Chemistry 1998; 41:2846-2857.
51. Volotskova O, Dubrovsky L, Keidar M, Bukrinsky M. Cold Atmospheric plasma inhibits HIV-1 replication in Macrophages by targeting both the virus and the cells. Plos one 2016; 0165322.

52. Trotard M, Tsopoulidis N, Tibroni N, Willemsen J, Blinder M, Ruggieri A, Fackler OT. Sensing of HIV-1 infection in TZM-bl cells with reconstituted expression of STING. Journal of virology 2016; 90(4):2064-2076.
53. Eckstein DA, Sherman MP, Penn ML, Chin PS, De Noronha CMC, Greene WC, Goldsmith MA. HIV-1 vpr enhances viral burden by facilitating infection of tissue macrophages but not nondividing CD4+ T Cells. Journal of Experimental Medicine 2001: 194:1407-1419.

Chapter 4

Label-free detection of HIV-1 infection in TZM-bl cells using luminescence spectroscopy

Introduction

In chapter 3 the focus was on optical trapping and transmission spectroscopy measurements for HIV-1 infected and uninfected cells, summarising the history, mechanisms and applications thereof, in medical and biological research. The current chapter focuses on luminescence based label-free detection of HIV-1 infection in TZM-bl cells. The first section gives an overview on luminescence and how it occurs through absorption and emission of radiation, as well as a detailed description on how bioluminescence takes place and its applications. This is followed by a detailed overview on luminescence spectroscopy and the major components of such systems. Also, both the quantitative and qualitative analysis of samples using luminescence based techniques is reviewed. Next, the use of luminescence spectroscopy is demonstrated for the first time in the detection of HIV-1 infection in TZM-bl cells. Finally, the findings of the study are discussed.

4.1 Luminescence mechanisms

4.1.1 General introduction on luminescence

Luminescence is the emission of electromagnetic radiation (light) by a substance following the absorption of energy [1].

This emission takes place when the materials emitting light are reasonably cold, unlike light emitted from incandescent figures such as burning coal, metal iron and electric current heated wire. Therefore, luminescence is an umbrella term that includes all forms of light emission that are not a consequence of high temperatures. Luminescent substances are known as phosphors and have wide applications in TV screens, modern LEDs, cell phone screens, biological imaging, emergency route signage, etc. Luminescence is also seen in organic substances such as luminols or the luciferins in fireflies and glow worms as well as in some pigments used in outdoor advertising. The real value of phosphors lies in their capacity to transform invisible forms of energy into visible light [2]. Luminescence can be categorized according to the energy used to excite the phosphor and produce light (luminescence) and the classes are: photoluminescence which occurs when excitation is by a photon (normally uses UV radiation), chemi-luminescence occurs when the material is excited by the energy of chemical reaction, cathode-luminescence is due to excitation by means of energetic electrons, electroluminescence is due to excitation by an electric voltage and triboluminescence is produced by mechanical energy such as grinding [3]. The focus of the current study is bio-luminescence as the luminescence is produced due to the reaction that takes place between the luciferase enzyme expressed by the TZM-bl cells after HIV-1 infection had taken place. The cellular luciferase enzyme then reacts with the luciferase reagent added to the infected cells 48 hours post infection.

4.1.2 Absorption and production of luminescence

In general, luminescence covers two processes, which are absorption or excitation and emission. During absorption a photon of energy passes some of its energy to excite electrons from low energy levels to higher energy levels.

The absorption of energy leading to luminescence takes place by either the host lattice (as shown in Figure 4.1) or by intentionally doped impurities. The emission usually happens on the impurity ions which are called activator ions when they generate the desired emission. When the activator ions show weak absorption, a second impurity ion called the sensitizer is added, which absorbs the energy and then transfer the energy to the activators. So, in the host lattice, the activator becomes excited by the absorbed energy; the electron on it absorbs the energy and is raised to an excited state.

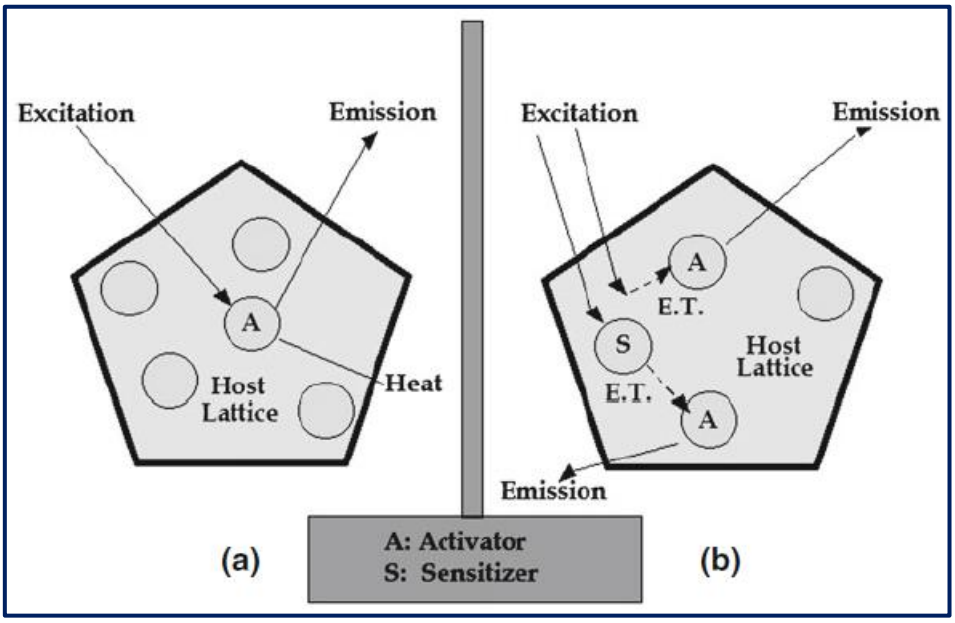

Figure 4.1 Schematic representation illustrating (a) direct excitation of the activator and (b) indirect excitation followed by energy transfer from the sensitizer or host to the activator [4].

The excited state then returns to the ground state by photon emission [3]. The observed emission from a luminescent centre is a process of returning to the ground state radioactively. Competing with luminescence are non-radiative processes, and in order to design an efficient phosphor, the non-radiative process must be suppressed.

The basic luminescence mechanism is demonstrated in Figure 4.1. Excitation by absorbance of some form of energy leads to two technically important classes of luminescent species, which are fluorescence and phosphorescence. Their production is illustrated in Figure 4.2. These two terms are based on both the persistence of luminescence and the way in which the luminescence is produced. When an electron is excited to a singlet state with a lifetime of nanoseconds, it then returns to its ground state emitting a photon in the form of fluorescence. On the other hand, an electron may be lifted to a higher energy state known as the excited triplet state. For quantum mechanical reasons, transitions from triplet states to singlet states are forbidden, thereby causing the lifetime of triplet states to be considerably longer than the singlet ones.

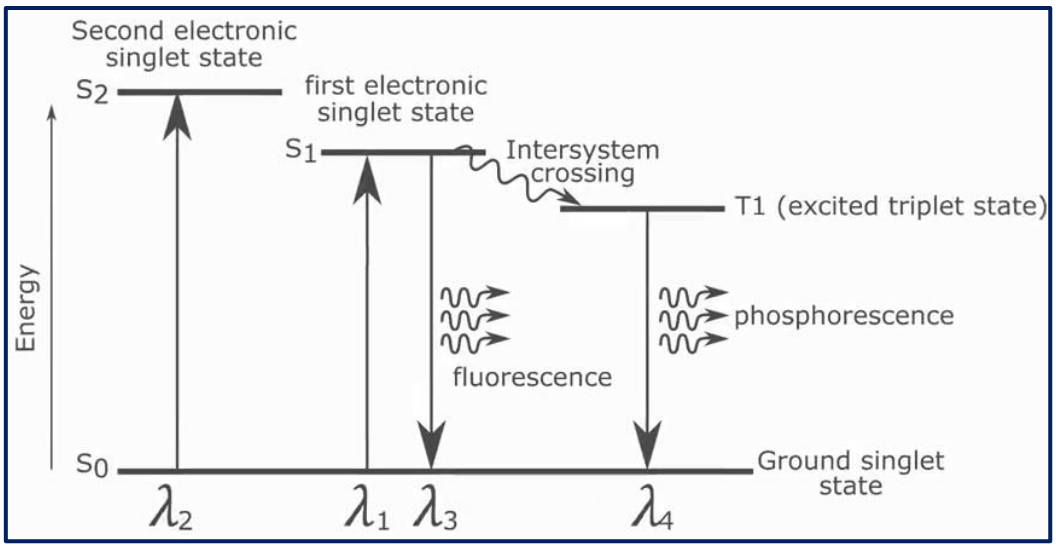

Figure 4.2 Energy diagram showing absorption of light and the processes involved in the emission of light as fluorescence and phosphorescence [5].

Therefore, luminescence from triplet energy states has longer duration than those originating from the singlet states and phosphorescence is observed [4].

In this study we observed bioluminescence in the form of phosphorescence as the luminescence stayed for a longer period and this was observed in the decay curve as shown later in the chapter (Figure 4.7C).

4.1.3 Bioluminescence

The emission of light by living organisms or laboratory biochemical systems developed from organisms is known as bioluminescence. It occurs occasionally in a broad range of organisms such as bacteria and fungi, insects, fish and marine invertebrates. However, there is no knowledge of its natural existence in mammals, birds, plants amphibians and reptiles. Bioluminescence is as a result of a chemical reaction (chemi-luminescence) whereby the conversion of chemical energy to radiant energy produces very little heat to no heat at all, hence the process is also referred to as cold light [6,7]. In the majority of bioluminescent organisms, the essential light-emitting elements are the oxidizable organic molecules luciferin and the enzyme luciferase. The luciferin-luciferase reaction is an enzyme-substrate reaction in which luciferin the substrate is oxidized by molecular oxygen and the reaction is catalyzed by the enzyme luciferase, resulting to light emission as summarized in Figure 4.3. The emission of light goes on until all the luciferin is completely oxidized.

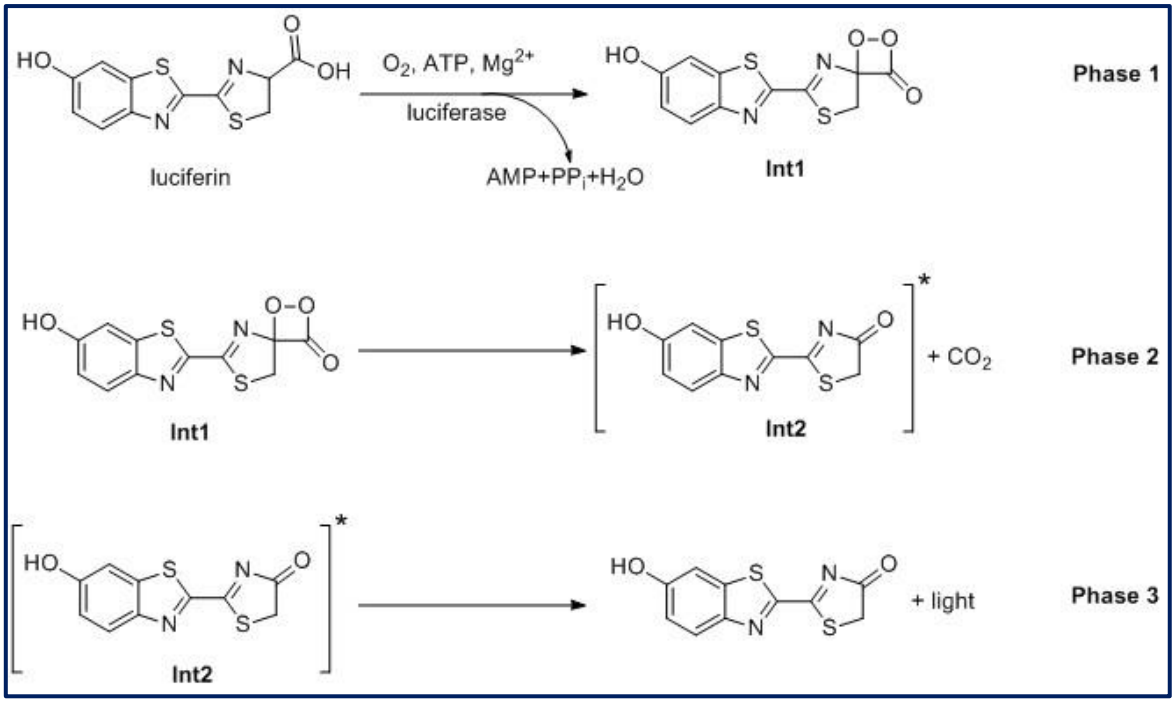

Figure 4.3 Mechanism of luciferin bioluminescence: In phase 1, luciferin reacts with oxygen under ATP consumption, Mg^{2+} assistance and luciferase catalysis to yield a reactive, highly unstable intermediate Int1. This intermediate is decomposing in the second stage into carbon dioxide and intermediate Int2 in excited state (Phase 2). Int2 undergoes de-excitation by emission of a photon with a characteristic wavelength (Phase 3). In case of luciferin, the emission maximum is at 550-570 nm [6].

Unlike with photoluminescence whereby a shorter wavelength excites the molecule and then emit at a longer wavelength, in bioluminescence emission is due to a reaction that takes place within a biological system. In firefly luminescence, which is what the current study is focusing on, adenosine triphosphate (ATP) primarily reacts with firefly luciferase, ionic magnesium, and firefly luciferin to form a complex (luciferase-luciferyl-adenylate) and pyrophosphate. The complex then reacts with molecular oxygen to emit light. Sufficient energy is liberated in the last step to transform the electronic configuration of the luciferase-luciferyl-adenylate complex from the ground state to excited state. The high-energy complex then misplaces energy by radiating a photon of visible light and goes back to the ground state [7]. Generally,

bioluminescence and chemi-luminescence based techniques are extensively used in biology and biochemistry such as in the detection of low ATP concentrations using bioluminescence as ATP is required for luciferin oxidation [7].

Developments in the field of molecular biology have presented biotechnological means that make use of low background signal, detectability and swiftness of these luminescence based systems. They offer a great platform to *in vitro* and *in vivo* constant monitoring of biological processes such as disease progression, interaction of proteins and gene expression, as well drug discovery, diagnostic and clinical applications. The combination of luminescent enzymes with specific recognition features has given rise to the existence of selective and sensitive tools such as nucleic acid hybridization assays, immunoassays, microscopy or imaging and recombinant whole-cell biosensors. The popularity of these luminescence based analytical techniques has been intensified by their high detectability, which also makes them suitable for use in miniaturized analytical tools such as high density well microtiter plates, microarrays and microfluidic devices for the screening of proteins and genes in small sample sizes [4]. Bioluminescence has been applied in various immunoassays for either direct marking of antibodies and antigens with luminescent molecules or labeling with enzymes detectable luminescent substrates. Luminescent based reactions have gained much popularity due to their sensitivity for measuring enzyme labels [8]. Bioluminescence immunoassays resulted from using photo-proteins such as recombinant aequorin or a firefly luciferase coding DNA fragments as tags [9, 10]. Luminescence based assays have an influence on all forms of DNA diagnostic methods. The detection of viral DNAs is commonly achieved by using gene probe hybridization assays in combination with digoxigenin-anti-digoxigenin and biotin-streptavidin tagging systems.

Multiplex PCR methods can achieve detection limits in the range of 1-10 femtograms of DNA and they have been used in the detection of various diseases causing agents in urine specimens [11]. The value of bioluminescent based techniques was demonstrated in a study where it was compared to magnetic resonance imaging to confirm the therapeutic effect of 1,3-bis(2-chloroethyl)-1-nitrosourea (BCNU) treatment in orthotopic rat brain tumors. These tumors resulted from 9L gliosarcoma cells genetically engineered to stably express firefly luciferase. The bioluminescence imaging results obtained were similar to those of magnetic resonance imaging, proving that it can also be effectively used in monitoring therapeutic effects of various compounds in living organisms [12]. According to Rehemtulla et al 2002, bioluminescence can be employed to assess the potential of therapeutic compounds for various diseases [12]. In another study conducted by Bernau human neural progenitor cells (stem cells) expressing luciferase were introduced into a rat in order to track these cells *in vivo* [13]. The cells were successfully tracked in the rat striatum for up to 12 weeks using bioluminescence imaging. This outcome was an indication that stem cells have a great potential in the development of cell based treatment for neurodegenerative disorders [13]. Bioluminescent labelled microRNAs have been employed for the detection of cancer.

MicroRNA, miR21 was used as it is found in high levels in various cancers such as those of breast, liver, ovarian, pancreatic and brain when assessed with corresponding normal tissues. The luciferase labelled miR21 expression levels were high in human breast adenocarcinoma MCF-7 cancer cells compared to non-tumorogenic MCF-10A cells. The detection of miR21 was enabled by using the bioluminescence based hybridization assay [14]. This section summarized various bioluminescence based techniques used in the field of biological and medical sciences. However, since this chapter is focusing on the use of luminescence spectroscopy, the next section will give an overview on luminescence spectroscopy.

4.2 Overview of luminescence spectroscopy

4.2.1 Principles of luminescence spectroscopy

As it has already been alluded to in section 4.1.2, luminescence or emission of light is a consequence of the interaction of light with matter. Emission is therefore a response to some form of acquired energy. This input energy causes molecules to get excited. As stated by quantum mechanics, molecules are permitted to be in certain distinct forms with definite amounts of internal energy (the quantum mechanically permitted states). A molecule can alter its state in between legitimate states if the difference in the energy between the two states is provided by an external source. In addition, the interaction of light with molecules can be divided into contributions equivalent to nuclear vibrational and rotational motion, electron transitions and spin interactions. Nonetheless, for luminescence spectroscopy, the occurrence of absorption and emission can easily be defined in terms of transitions of electrons between defined states [15, 16]. This transition between two molecular states can be seen as a switch of an electron from one molecular orbital to another. An excited molecule is rapidly reduced to the lowest vibrational level of the excited electronic state, which occurs in the time range of femto seconds to pico seconds.

Luminescence arises as a result of decay from higher energy state to a permissible vibrational level in the electronic lower state as displayed in Figure 4.2 [4, 16]. Therefore, luminescence spectroscopy is the measurement of the manner in which molecules or systems emit radiation. Spectroscopic records are often denoted by an emission spectrum, a plot of the response of interest as a function of wavelength [17]. The emission spectrum is the emitted light comprising of phosphorescence, delayed fluorescence and fluorescence thus yielding three types of emission spectra.

Figure 4.4 shows absorption, excitation and emission spectra of a typical flourophore, as the fluorescence emission spectrum indicates almost mirror-like symmetry with its absorption spectrum.

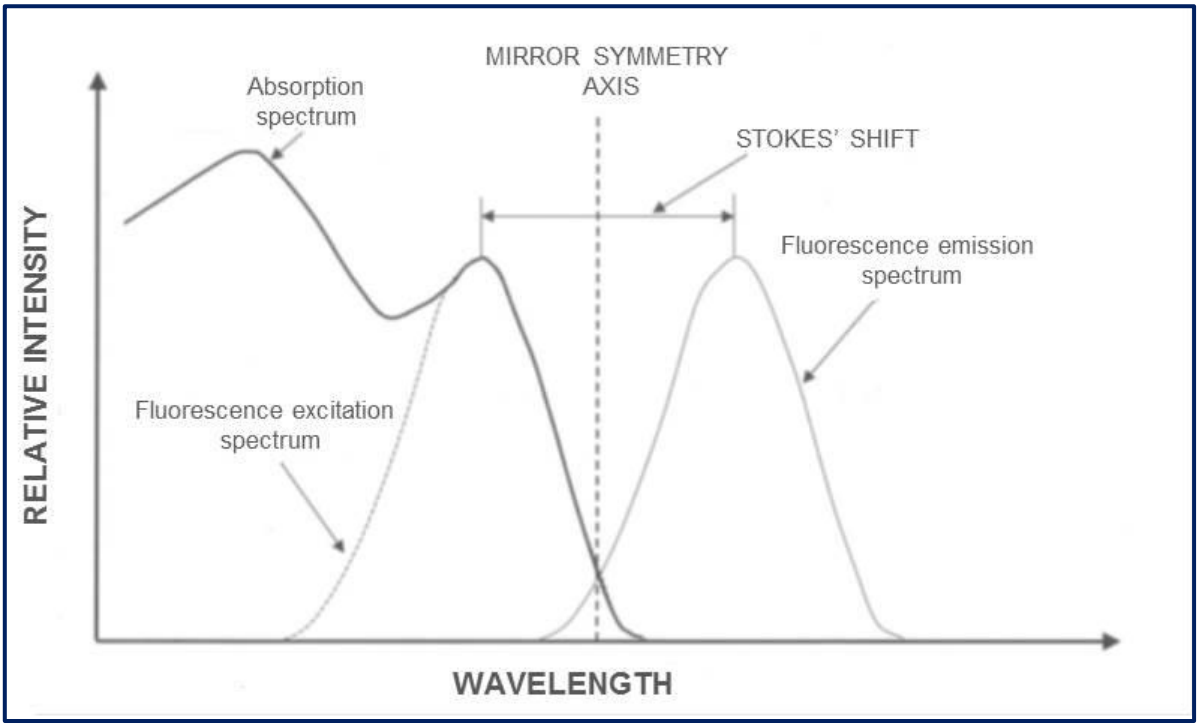

Figure 4.4: Absorption, excitation and emission spectra of a typical molecule [16].

The fluorescence is spectrally the same as the delayed fluorescence, on the other hand the phosphorescence spectrum while similar in shape is red shifted as a whole. The unconventionality of the shape of the fluorescence emission spectrum from the wavelength of the exciting light stems from the fact that emission always occurs from the lowest excited. If the shape of the emission spectrum is altered with changing wavelengths of the exciting light, then the existence of more than one fluorescent compound should be considered [16].

4.2.2 Essential elements in luminescence spectroscopy systems

A typical luminescence spectroscopy system needs a radiation source for excitation, a monochromator to choose the required wavelength for excitation, a sample holder, a detector a signal output display where the measurement is displayed (normally a computer screen) [18]. In the majority of commercial devices, the emitted radiation is generally detected at right angles to the incident beam; as such configuration presents the lowest background from incident light. Figure 4.5 below, illustrates the essential components of a spectrometer, moreover, frontal and straight through geometries are also employed mainly in instruments used to read microplates [16, 18].

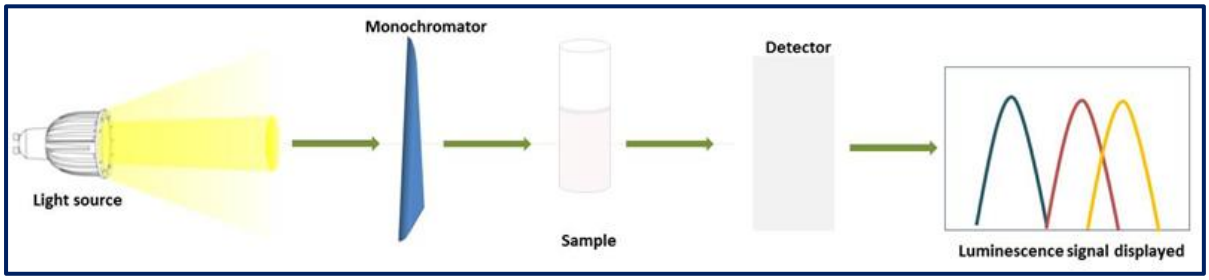

Figure 4.5 A schematic representation of essential elements in a spectroscopy system. The light source supplies radiation which goes through the monochromator for the selection of a single wavelength. The light then goes through the sample and the emitted light is transmitted and strikes the detector. The amount of emitted light is displayed through a luminescence spectrum [16,18].

Radiation sources for excitation include arc lamps for example xenon, tungsten, halogen, hydrogen, mercury deuterium lasers and synchrotrons. The light from the lamp is collected by an elliptical mirror and focused to the entrance slit of the monochromator. Then, the gratings in the monochromator can disperse radiation from 200 to 900 nm. On the other hand, entrance and exit slits of the monochromator regulate both the light intensity and wavelength spread.

Both the excitation and emission slit widths should generally be the same. The excitation monochromator selectively provides a narrow band of wavelengths of excitation that hit the sample. A fraction of the incident light is taken up by the sample, and some of the molecules in the sample fluoresce. There is no flawless monochromator; therefore some stray light (light with other wavelength other than the one of interest) will always be transmitted. The emitted light is transmitted in a narrow range centred about the specified emission wavelength and exits through the adjustable slits, and ultimately striking the detector. Then signal is enlarged and causes a voltage proportional to the measured emitted intensity [16, 18]. A luminescence spectrum of a sample is recorded by scanning the emission monochromator for a constant wavelength of the excitation light. Since the source light has different intensities at all wavelengths, it may vary during each experiment, causing distortion of the spectrum. This irregularity is corrected using an additional reference photodiode that each instrument should be equipped with. The reference photodiode measures a fraction of source light separated using a beam splitter after the exit slit of excitation monochromator before it enters the sample holder. By rationing the luminescence signal to the reference signal, correction is made for variation in excitation light intensity as function of wavelength [18].

Of note, a detector should meet four basic requirements, which form critical parts of the spectrometer. A good detector must be able to detect a signal over several orders of magnitude of intensity from a few photons per second to multi-millions of photons per second. In addition to that, the rate of response of the detector must be faster than of the reaction in the case of luminescence and the signal output should be directly related to the light intensity arriving at it. Furthermore, it must be sensitive over wide spectral range; at the least it must cover from 400-600 nm and ideally it should cover the whole visible spectrum. The detector that covers the spectral range from the ultraviolet region to the infrared region would be the best choice

[19]. As already mentioned in the previous section, this study used bioluminescence which did not require a sample to be excited by light, however, the emission was due to reaction between luciferin and luciferase enzyme, which produced light.

4.2.3 Quantitative and qualitative analysis of samples

Generally, luminescence based analytical techniques are used for both quantitative and qualitatitive analysis. In some techniques it is used for qualitative analysis only (such is common in disease diagnosis) and in most instances the systems or methods that can do quantitative analysis also do qualitative analysis. Laser induced fluorescence spectroscopy has been used in the diagnosis of cancer in human tissues as a qualitative mechanism. Luminescence cancer diagnosis is done through the introduction of a drug such as hematoporphyrin derivative which is selectively retained by the tumour. When excited with light of appropriate wavelength, the drug localized in the tumour fluoresces. This fluorescence is used for the detection of the tumor and also enables its imaging. Luminescence spectroscopy is also utilized for accurate determination of glucose which is an essential component in biological systems and blood glucose levels are an indicator of one's health status. Out of range glucose levels provide important information of diseases such as diabetes. Glucose levels in the serum can be determined using a sensor based on fluorescence quenching method [20]. This sensor is a luminescent qualitative analytical method. Luminescence is also utilized as a quantitative tool in measuring ATP in mammalian cells. This is an energy carrying molecule found in cells of all living things, which captures chemical energy obtained from the breakdown of food molecules and supplies energy for other cellular processes [21].

Since ATP is present in all metabolically active cells, it is therefore a cell viability marker. ATP concentrations are significantly reduced when cells undergo death via various pathways;

therefore, monitoring its levels provides a platform to assess cytostatic and proliferative effects in the environment. The amount ATP, determined by the relative luminescence units is directly proportional to the number of metabolically active cells in a given culture. Such assays rely on the properties of a thermostable recombinant luciferase, which generates a stable luminescent signal [22, 23].

The study of marine petroleum pollutants utilizes luminescence spectroscopy as a qualitative analytical technique to detect slicks of oil on the water surface, determination of petroleum contaminants in seawater and for monitoring petroleum derivative compounds as well as finding sources of water pollution. Hydrocarbons are major oil components and only a few of these fluoresce and petroleum strongly absorbs ultraviolet and blue light. Despite this luminescence is a phenomenon used in oil testing as oil luminescence covers a spectral region of ultraviolet and visible light (270-400 nm) [18].

In the current study luminescence spesctroscopy was used for both qualitative and quantitative analysis to detect HIV-1 infection in TZM-bl cells and also measure luminescence intensity which is equivalent to virus concentration within infected cells. The results were interpreted as, the higher the virus concentration, the higher the luminescence intensity in cells. TZM-bl cells are HeLa cells engineered to express the luciferase enzyme gene when HIV-1 infection has taken place. Therefore, when the infected cells are lyzed with a luciferase reagent, the luciferase enzyme expressed in the cells reacts with the reagent and generate luminescence. The luminescence produced is equivalent to the number of infected cells.

4.3 Label-free detection of HIV-1 infection in TZM-bl cells

This section focuses on the two techniques used in this study to assess and measure HIV-1 infection in TZM-bl cells. Sub-section 4.3.1 covers the use and the results obtained from conventional method of assessing HIV-1 infection in TZM-bl, which is the luciferase assay using a luminometer (GloMax® Discover System). The following sub-section 4.3.2 reports on the detection of HIV-1 infection using the Horiba Jobin Yvon Fluorolog 3 photoluminescence spectrometer system, which was used for the first time in the detection of HIV infection. For both methods, the sample preparation was the same as TZM-bl cells were infected with 4 different virus volumes i.e. concentrations: 50, 100, 150 and 200 µl. After 48 hours of incubating cells with the virus, the cells were divided into two sets so that they could be analyzed with the two different techniques discussed in sub-sections 4.3.1 and 4.3.2.

4.3.1 GloMax® Discover System used for the detection of HIV-1 infection in TZM-bl cells

This experiment was done in order to compare the results obtained from this established method with those obtained when using the Horiba detection method investigated in sub-section 4.3.2, which is being used for the first time in the detection of HIV-1 infection. Cell suspensions infected with different concentrations of the pseudovirus were mixed with equal volume of the luciferase reagent from the Bright-Glo™ luciferase assay system (E2610, Promega, Anatech) in a 96 well black plate and incubated for 2 minutes at room temperature in the dark to allow for cell lysis.

Before loading the plate for reading in the GloMax® Discover System for luminescence measurements, the contents of the plate were mixed by pipetting up and down. Figure 4.6 shows the results acquired from the assay.

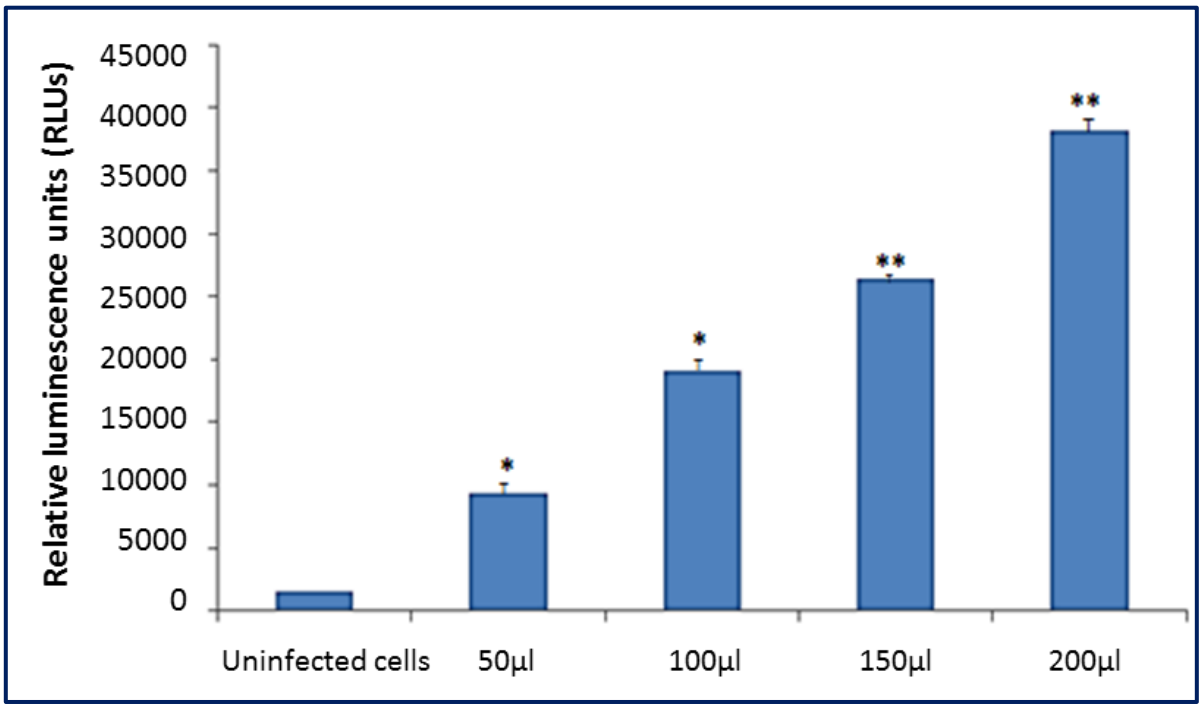

Figure 4.6 The luciferase assay used for the detection of HIV-1 infection in TZM-bl cells and quantification of luminescence intensities at different viral concentrations ranging from 50 µl to 200 µl. The cells infected with 200 µl showing the highest intensity, while the uninfected cells exhibited the least luminescence levels. Significant differences between the infected and uninfected cells are represented on the bar columns as (*) = $P < 0.05$ and (**) = $P < 0.01$. Error bars represent the standard error of the mean when n =3.

As expected, uninfected cells showed no luminescence, while infected cells displayed the presence of luminescence. The luminescence intensity in infected cells increased with the increase in virus concentration added in cells. According to the results obtained, cells infected with 50 µl had the lowest luminescence intensity, followed by the cells infected with 100 and 150 µl, the ones infected with 200 µl had the highest luminescence intensity as shown in Figure 4.6.

4.3.2 Horiba Jobin Yvon Fluorolog 3 photoluminescence spectrometer system used for the detection of HIV-1 infection in TZM-bl cells

Similarly to the sample preparation used for the Glomax system in 4.3.1, cell suspensions in cuvettes were mixed with equal volumes of the luciferase reagent, incubated for 2 minutes in the dark and mixed by pipetting before loading cuvettes in the instrument for measurements. Figure 4.7 shows luminescence intensity plotted against a range of wavelengths (400 nm to 800 nm) in order to assess the intensity at different viral concentrations and also determine a wavelength at which the luminescence in TZM-bl cells is best detected.

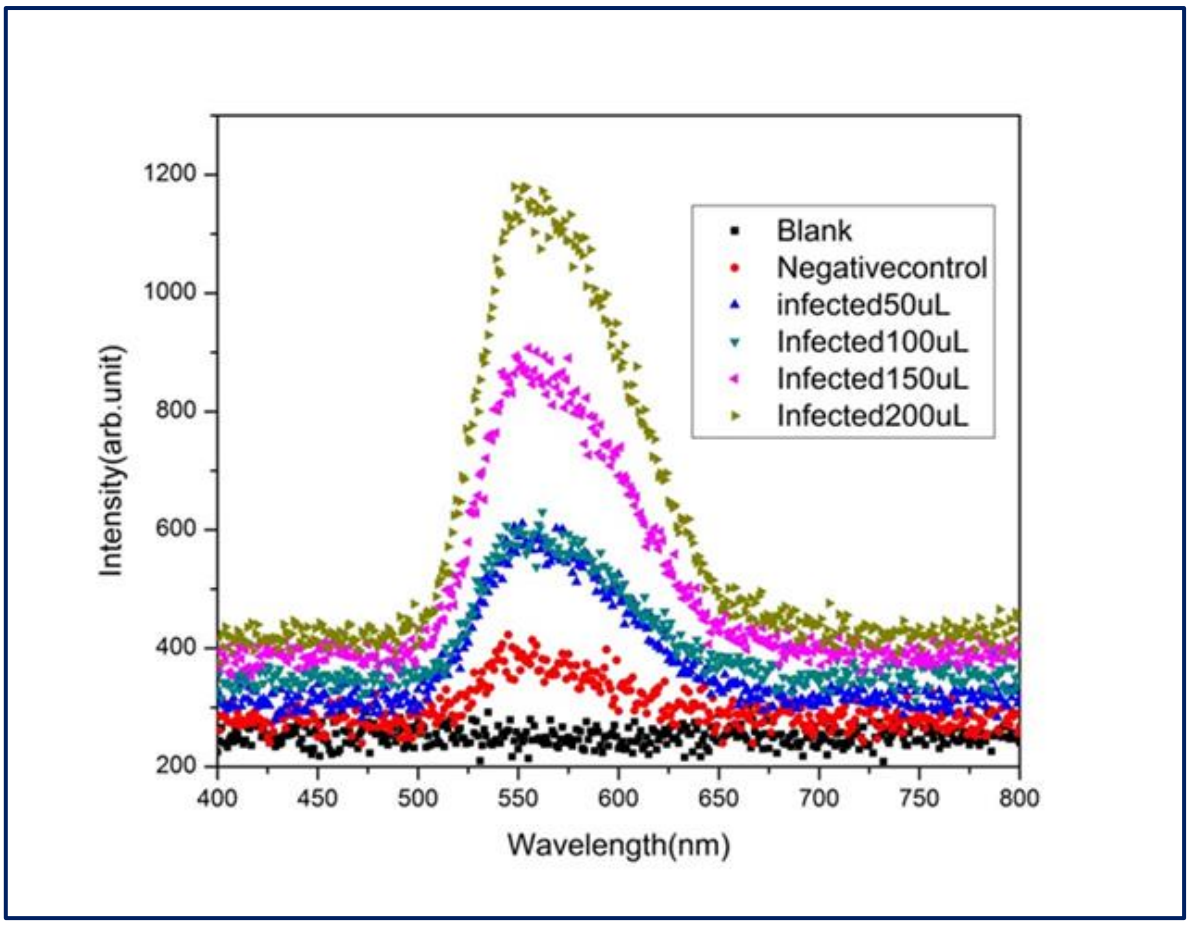

Figure 4.7 Luminescence spectroscopy used to detect HIV-1 infection and measurements of luminescence intensities. at various concentrations (50, 100, 150 and 200 µl) of the ZM35 pseudovirus are detected around 555 nm.

As represented in Figure 4.7, luminescence was observed around 555 nm, however according to some reports firefly bioluminescence is also observed at 620 nm [24]. Moreover, Figure 4.7 indicates that infection in TZM-bl cells was detected and there were differences in luminescence intensities at different virus concentrations. With 200 µl of the virus volume displaying the highest intensity, followed by 150 µl, while there were no significant differences observed between 100 µl and 50 µl. The blank which was made of the luciferase reagent and the cell medium showed no luminescence (no visible peak around 555 nm), whereas the negative control (uninfected cells) exhibited negligible luciferase activity. Figure 4.7 also exhibits that 555 nm was the best wavelength for the detection of luminescence in TZM-bl cells in this study.

The lifetime of luminescence in infected TZM-bl cells was assessed with Horiba Jobin Yvon Fluorolog 3 photoluminescence spectrometer system. The steady state luminescence emission spectra resulting from the expression of the luciferase gene in TZM-bl cells were recorded with a Photomultiplier tube detector. The luminescence spectra decay was recorded over a long period by integrating the recorded spectra time and each spectrum was recorded at fixed time intervals of 1.4 minutes. The luminescence data obtained was analyzed by importing it into an analysis software; Microcal Origin Pro 8. This software uses the default import setting to import the data file to construct luminescence intensity spectra as shown in Figure 4.8.

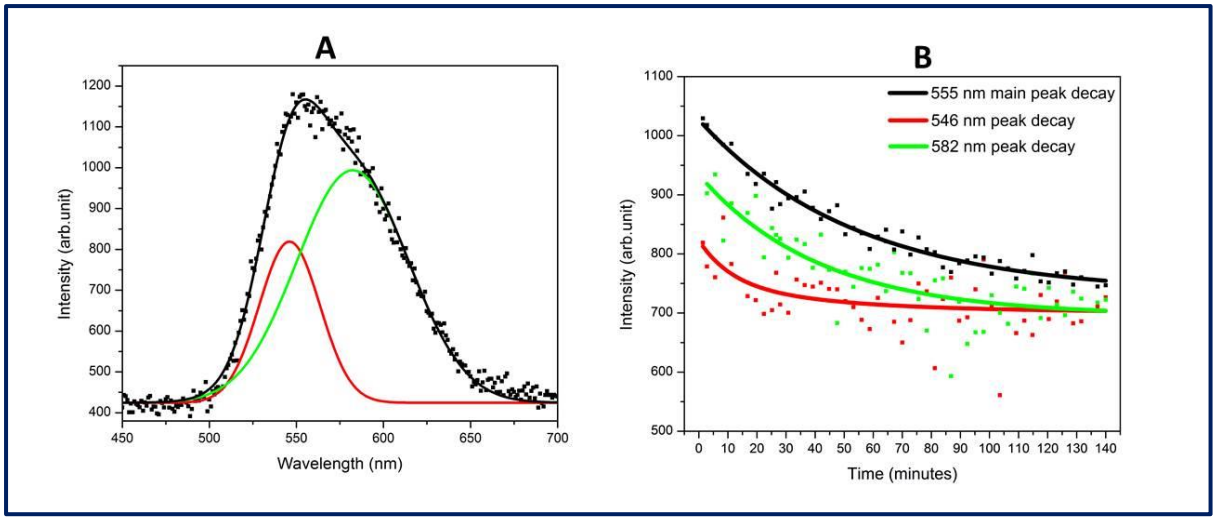

Figure 4.8 Luminescence intensity spectra in TZM-bl cells. (**A**) Gaussian fit of HIV-1 infected luminescence spectrum between 450 nm and 700 nm. (B) Luminescence exponential decay fits of 546 nm, 555 nm and 580 nm peaks.

A second order exponential decay fit was done for each of the spectrum at 546 nm, 555 nm and 582 nm and table 4.1 summarizes the decay times at each of the three wavelengths.

Table 4.1: Summary of decay times for each wavelength as displayed in Figure 4.8B.

Peak wavelength	**Time in minutes (T1)**	**Time in minutes (T2)**	**Standard deviation (minutes)**
546	44.29	11.05	±4.9
555	53.96	53.96	±5.20
582	41.68	41.68	±4.17

Once the spectrum was plotted, a Gaussian function curve fitting was performed on the peaks of the spectrum. The red and green curves exhibited in Figure 4.8A represent the two Gaussian

fits; making a summation of the two Gaussian spectral peaks to one that fits the whole recorded spectrum. The black curve in Figure 4.8A indicates the result of the fitting. The Gaussian spectral function for the curves fitting was done in the region between 450 nm and 700 nm. Figures 4.8A and B demonstrate that luminescence was detected at lower intensities at wavelengths 546 and 582 nm compared to the intensity of the main peak at 555 nm. Finally, Figure 4.8B displays three luminescence spectra decay recorded at 546 nm, 555 nm (main peak) and 582 nm and the luminescence intensity at all three wavelengths decreased with time.

4.4 Discussion

Disease diagnosis involves the detection and quantification of several molecules and bio-particles; examples include viruses, bacteria, proteins, DNA and RNA. These are analyzed using established methods such as biological assays (like ELISA), PCR, gel electrophoresis and flow cytometry [25, 26]. However, these techniques necessitate the use of labels that increase diagnosis costs and complexity by dependence on expensive equipment. Owing to this, alternative label-free methods have been developed [27]. The rise of label-free methods is enhanced by the growing need and interest to have medical diagnostics for tailored medicine and early disease detection, as well as the need for techniques that can be used in resource limited settings. As a result, a significant shift and/or transformation in diagnostic techniques has been observed. This transformation has given rise to easy to use, label-free, simple, sensitive, portable and cheaper means of detection [27, 28, 29].

Because of the high need of using label-free systems in disease detection, the current study then looked into the use of luminescence detection based on the intrinsic properties of cells. When focusing on inherent properties there is normally no need to use labelling.

A similar approach is used in the viability assay for quantification of ATP, ATP reacts with luciferase, luciferin and oxygen; as such, at high ATP levels, the luminescence will also increase [22, 23]. In this study the TZM-bl cell line was used, which is a widely used cell line in HIV-1 research. This cell line is engineered to express the luciferase enzyme gene when HIV-1 infection has taken place [30], so the presence of the luciferase gene in these cells is seen as an intrinsic property. Therefore, when the infected cells are lyzed with the luciferase reagent, the luciferase enzyme expressed in the cells reacts with the luciferase reagent and generates luminescence.

The detection of HIV-1 infection in TZM-bl cells using the GloMax® Discover System and Horiba Jobin Yvon Fluorolog 3 photoluminescence spectrometer system yielded satisfactory outcomes. For both techniques, in the absence of HIV-1 infection there were insignificant luminescence levels detected as demonstrated in figures 4.6 and 4.7. The low luminescence levels identified in uninfected cells are as a result of endogenous bioluminescence (autoluminescence) which exists in most mammalian cells at low levels [31]. Furthermore, luminescence intensity increased with the increase in virus concentration, which signifies that more cells were infected with the virus as the virus concentration increased. The luminescence produced is presented as relative luminescence units (RLUs) and is equivalent to the number of infected cells. The obtained RLUs are directly proportional to the number of infectious virus particles present in the initial inoculum [32]. However, this occurrence is different from what happens in the infected individual. In an infected individual one viral particle multiplies within the host cells and therefore the viral load increases as the time progresses. On the other hand, when infecting with a pseudovirus; one viral particle that infects a cell does not multiply, consequently the number of viral particles that were present in the initial inoculum will not change after 48 hours of incubation.

When detecting luminescence with the Glomax Discover, no wavelength was selected as that system has an in-built option to measure luminescence without choosing a wavelength. However, when detecting luminescence with the Horiba Jobin Yvon Fluorolog 3 photoluminescence spectrometer, it was measured over a range of wavelengths (400 nm and 800 nm) because of the differences in luminescence wavelengths as reported in various sources in literature [33,34]. As such, there was a need to assess luminescence at a wider range of wavelengths instead of only choosing one. This was to ensure that even if it is detected at more than one wavelength, the wavelength where it is best emitted can be identified in this study. In literature, some report that 560 nm is the best wavelength to detect firefly luminescence, which is the luciferase present in the TZM-bl cells [24,33,35]. While others report that firefly luciferase can be detected between 560 nm and 570 nm. This is very close to what was observed in TZM-bl cells in this study. This observation is in line with various literature sources that mention different wavelengths and wavelength ranges at which the firefly luciferase luminescence is detected [24,33,34,35]. Figure 4.7 indicates that luminescence emission occurred around 555 nm. In addition to 555 nm, Figures 4.8A and B illustrate that luminescence was also detected at 548 nm and 580 nm. In both Figures 4.7 and 4.8, 555 nm is the wavelength with the highest luminescence intensities detected.

Also, the use of Horiba Jobin Yvon Fluorolog 3 photoluminescence spectrometer offered a platform to assess luminescence lifetime in TZM-bl cells with ease. The luminescence decay was monitored for over time by setting the instrument to automatically continue with measurements over that period, which was unattainable when using the Glomax Discover system. By doing the exponential decay fit I was able to determine the luminescence lifetime in HIV infected TZM-bl cells.

Furthermore, knowing the luminescence lifetime in TZM-bl cells was necessary in order to have an idea of how long it would take for a signal to diminish when a similar system is used in label free diagnostic devices.

For the purposes of developing luminescence based smart diagnostic devices for HIV-1 diagnosis, TZM-bl cells are the most ideal choice of cells because they already have the luciferase gene. Therefore, detection and quantification of HIV-1 infection in TZM-bl cells shows that when doing thorough studies on cellular molecules affected during HIV-1 infetion (or any other infection/diseases) it is possible to come up with luminescence based label-free disease detection systems, which would add value and reduce costs associated with disease diagnosis. For the first time, in this study I showed that HIV-1 infection in TZM-bl cells can be detected using the Horiba Jobin Yvon Fluorolog 3 photoluminescence spectrometer. Such findings are encouraging and have also highlighted that there is possibility of using luminescence not only for HIV detection, but also for detection and analysis of other biological metabolites. As such our future research studies will focus in the development of luminescence based analytical systems for various metabolites.

References

1. Shinde KN, Dhoble SJ, Swart HC, Park K. Phosphate Phosphors for Solid state lighting. Springer-Verlag Berlin Heidelberg, 2012.
2. Gundermann, K.D. Luminescence, https://www.britannica.com/science/luminescence, [Accessed 15 March 2018].
3. Bamfield, Peter. Chromic Phenomena Technological Applications of Colour Chemistry, The Royal Society of Chemistry, 2010.

4. Ronda C. Luminescence From Theory to Applications. Wiley-VCH, New York, 2008.
5. Basics and principle of Fluorescence & Phosphorescence measurement, https://www.youtube.com/watch?v=CcN8NnGGPhs; [Accessed 10 July 2018].
6. Bioluminescence, http://www.chemistryandlight.eu/index.php/bioluminescence/. 2018; [Accessed 12 July 2018].
7. Bioluminescence, https://www.britannica.com/science/bioluminescence, [Accessed 12 July 2018].
8. Ito K, Nakagawa K, Murakami S, Arakawa H, Maeda M. Highly sensitive simultaneous bioluminescent measurement of acetate kinase and pyruvate phosphate dikinase activities using a firefly luciferase-luciferin reaction and its application to a tandem bioluminescent enzyme immunoassay. Analytical Sciences 2003; 19(1):105-109.
9. Mirasoli M, Deo SK, Lewis JC, Roda A, Daunert S. Bioluminescence immunoassay for cortisol using recombinant aequorin as a label. Analytical Biochemistry 2002; 306(2):204-211.
10. Chiu NH, Christopoulos TK. Two-Site Expression Immunoassay Using a Firefly Luciferase-coding DNA Label. Clinical Chemistry. 1999; 45(10): 1954–1959.
11. Mahony JB, Jang D, Chong S, Luinstra K, Sellors J, Tyndall M, Chernesky M. Detection of Chlamydia trachomatis, Neisseria gonorrhoeae, Ureaplasma urealyticum, and Mycoplasma genitalium in First-void Urine Specimens by Multiplex Polymerase Chain Reaction. Molecular Diagnosis 1997; 2(3):161-168.
12. Rehemtulla A, et al. Molecular imaging of gene expression and efficacy following adenoviral-mediated brain tumor gene therapy. Molecular Imaging 2002; 1:43–55.
13. Bernau K, Lewis CM, Petelinsek AM, Benink HA. *In vivo* tracking of human neural progenitor cells in the rat brain using bioluminescence imaging. Journal of neuroscience Methods 2014; 228:67-78.

14. Cissell KA, Rahimi Y, Shrestha S, Hunt EA, Deo SK. Bioluminescence-Based Detection of MicroRNA, miR21 in Breast Cancer Cells. Analytical Chemistry 2008; 80(7):2319-2325.
15. Lamola, Angelo. Creation and Detection of the Excited States. Marcel Dekker, 1971.
16. Deshpande SS. Principles and Applications of Luminescence Spectroscopy. Critical Reviews in Food Science and Nutrition. 2001; 41(3):155-224.
17. Spectroscopy, https://en.wikipedia.org/wiki/Spectroscopy, [Accesses 16 July 2018].
18. Naresh K. Applications of fluorescence spectroscopy. Journal of Chemical and Pharmaceutical Sciences 2014; 5(Special Issue):18–21.
19. Fereja TH, Hymete A, Gunasekaran T. A recent review on chemiluminescence reaction, principle and application on pharmaceutical analysis. ISRN Spectroscopy 2013.
20. Hussain AM, Sarangi SN, Kesarwani JA, Sahu SN. Au-nanocluster emission based glucose sensing. Biosensors and Bioelectronics 2011; 29(1):60-65.
21. Adenosine triphosphate coenzyme, https://www.britannica.com/science/adenosine-triphosphate; [Accessed 22 July 2018].
22. Crouch SPM, Kozlowski R, Slater KJ, Fletcher J. The use of ATP bioluminescence as a measure of cell proliferation and cytotoxicity. Journal of Immunological Methods 1993; 160(1):81-88.
23. CellTiter-Glo® Luminescent Cell Viability Assay Technical Bulletin, https://worldwide.promega.com/resources/protocols/technical-bulletins/0/celltiter-glo-luminescent-cell-viability-assay-protocol/; [Accessed 22 July 2018].
24. Ugarova NN. Luciferase of Luciola mingrelica fireflies. Kinetics and regulation mechanism. Journal of Bioluminescence and Chemiluminescence 1989; 4(1):406–418.
25. Witwer KW, Buzás EI, Bemis LT, Bora A, Lässer C, Lötvall J, Nolte-'t Hoen EN, Piper MG, Sivaraman S, Skog J, Théry C, Wauben MH, Hochberg F. Standardization of

sample collection, isolation and analysis methods in extracellular vesicle research. Journal of Extracellular Vesicles 2013; 2:20360.

26. Shen J, Li Y, Gu H, Xia F, Zuo X. Recent development of sandwich assay based on the nanobiotechnologies for proteins, nucleic acids, small molecules, and ions. Chemical Reviews 2014; 114:7631–7677.
27. Zeming KK, Salafi T, Shikha S, ZhangY. Fluorescent label-free quantitative detection of nano-sized bioparticles using a pillar array. Nature Communications 2018; 9:1254.
28. Lavrik NV, Sepaniak M J, Datskos P G. Cantilever transducers as a platform for chemical and biological sensors. Review of Scientific Instruments 2004; 75:2229-2253.
29. Waggoner PS, Craighead HG. Micro- and nanomechanical sensors for environmental, chemical, and biological detection. Lab Chip 2007; 7:1238-1255.
30. Wei X, Decker JM, Liu H, Zhang Z, Arani RB, Kilby JM, Saag MS, Wu X, Shaw GM, Kappes JC. Emergence of resistant human immunodeficiency virus type 1 in patients receiving fusion inhibitor (T-20) monotherapy. Antimicrobial Agents and Chemotherapy 2002; 46(6): 896–1905.
31. Troy T, Jekic-McMullen D, Sambucetti L, Rice B. Quantitative comparison of the sensitivity of detection of fluorescent and bioluminescent reporters in animal models. Molecular Imaging 2004, 3(1):9-23.
32. Montefiori, David. Evaluating neutralizing antibodies against HIV, SIV and SHIV in luciferase reporter gene assays. Current Protocols in Immunology, John Wiley & Sons. 2004:
33. Thorne N, Inglese J, Auld DS. Illuminating insights into firefly luciferase and other bioluminescent reporters used in chemical biology. Chemistry & Biology 2010;17(6):646–657.

34. Baldwin TO. Firefly luciferase: the structure is known, but the mystery remains. Structure 1996; 4(3):223-228.
35. Sadikot RT, Blackwell TS. Bioluminescence imaging. Proceedings of the American Thoracic Society 2005; 2(6):537–512.

Chapter 5

Single molecule analysis in HIV-1 infected cells using structured illumination microscopy (SIM)

Introduction

The main focus of chapter 5 is the detection of HIV infection in TZM-bl cells using structured illumination microscopy (SIM). Section 5.1 gives an overview on super resolution microscopy (SRM) by briefly summarizing microscopy history in 5.1.1 which led to the development of SRM. The development of SRM is followed by describing how the different SRM techniques pass diffraction limit for the observation of nanometer molecules. Sub-section 5.1.3 reports on how SRM has been previously applied through giving a brief literature review. Then, sections 5.2, deals with the mechanisms of SIM, which give this technique the capability to go beyond diffraction limit. Further in 5.2, the generation of Moire patterns, which is an essential characteristic of the SIM is described. Following that, in section 5.3, reports on various studies that have been conducted using SIM. Of note, section 5.3 is followed by section 5.4 which discusses HIV molecules detected in this study. The following section; section 5.5 reports on what the current study focused on, which is the use of SIM for the detection of HIV infection in TZM-bl cells. The results obtained in section 5.5 are discussed in section 5.6.

5.1 Overview of super resolution microscopy

5.1.1 Development of super resolution microscopy

Microscopy uses visible light and well-arranged lenses to both detect and magnify small (microscopic) objects that are difficult to resolve with a naked eye [1]. Light microscopy has been extensively used in medical and biological fields for its ability to visualize and investigate organs, tissues, cells and microorganisms. Therefore, light microscopy led to many discoveries (or acquiring of new knowledge) with magnification playing a significant role as it enlarges invisible substances and makes them look bigger and visible [2]. However, simple light microscopy even with high magnification is not adequate to visualize cellular molecules and processes because of a limit in optical resolution caused by the diffraction of visible light when it passes through a round aperture at the back focal plane of an objective [3]. Our environment has various organisms and structures of different sizes; ranging from metres (m) to nanometres (nm) (Figure 5.1) and there is no single imaging technique to visualize all organisms.

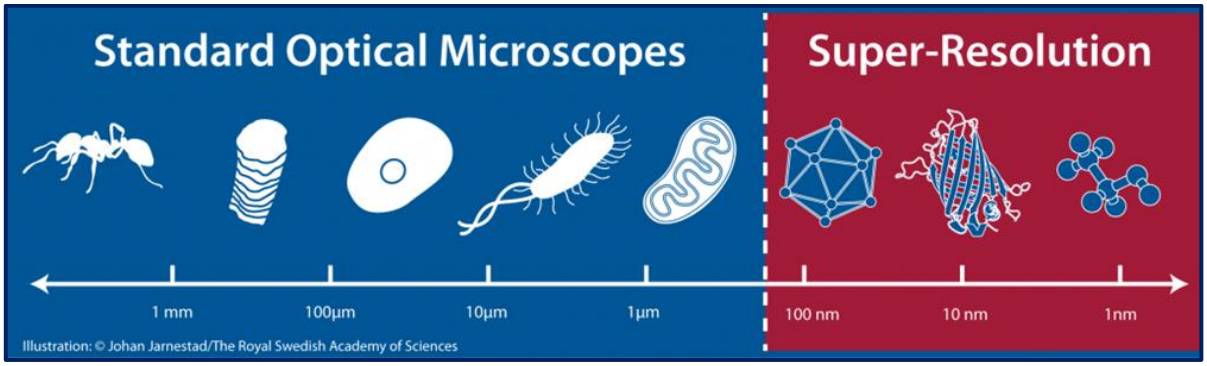

Figure 5.1 Various sizes of organisms and molecules that are visualized with different techniques. The blue shaded region shows organisms in the millimetre (mm) and micrometre (µm) size range that can be visualized with either a naked eye or standard optical microscopy. The red shaded region shows organisms and molecules in the nm size range that cannot be visualized using standard light microscopy, but require super resolution microscopy [4].

Organisms in the millimetre range and above are visible in the human eye, those in micrometre range can only be visualized using standard optical microscopes and those in the nanometre range (below 200 nm) can be visualized with super resolution imaging systems. The limit in optical resolution led to the generation of fluorescence microscopy. In fluorescence microscopy, cellular and subcellular configurations and components could be observed through molecule specific labelling independent of nearby molecules and due to high contrast of fluorophores to a dark background [5]. Despite these improvements, conventional fluorescence microscopy is restricted in its ability to differentiate between tiny and closely-spaced items as separate objects. Diffraction limit hinders the resolution of structures below 200 nm as it was first described by Abbe 1873 [6,7]. Owing to the wave nature of light, a point source of light in the sample plane of the microscope cannot be re-focused to a single point in an image, but the light is diffracted to form an intensity distribution known as the point spread function (PSF), with a size defined as $d \approx \frac{\lambda}{2NA}$ in the lateral plane and defined as $d \approx \frac{2\lambda n}{NA^2}$ in the optical axis.

Thus, the resolution of conventional fluorescence microscopy is limited to a diameter of about 200 nm in the lateral plane; and >450-700 nm in the optical axis; wherein λ is the wavelength of light and NA is the numerical aperture of the objective and *n* the refractive index [8]. The PSF is the stable size of the spread of a single point of light that is diffracted through a microscope and an object that can be resolved by a microscope. Objects of smaller size seem to be the same size as the PSF and those closer than the width of the PSF are not seen as separate objects. Thus, if two small objects are positioned within the width of a PSF, they become indistinguishable [5,9,10]. Even so, the recent years have seen a rise in unprecedented technical innovations of super resolution microscopy which have altered the limits of optical resolution from around 250 nm to about 10 nm [11].

Thus, super resolution microscopy was developed to overcome the resolution limit of conventional fluorescence microscopy. The next sub-section 5.1.2 describes how resolution is enhanced beyond the diffraction limit thereby enabling the observation of nanometre structures.

5.1.2 Observation of nanometre structures by passing the diffraction limit of light

In response to the shortcomings of conventional fluorescence microscopy, several imaging systems such as confocal microscopy and multiphoton fluorescence microscopy have gone beyond the diffraction limit of light microscopy [12]. In confocal microscopy, the resolution of the image is generally determined by the size of the focused light spot typified by the PSF. When the excitation PSF is smaller, the image would be more precise. Two closely located objects can be well resolved when using confocal microscopy if they are parted by at least 180-300 nm [13]. Confocal microscopy provides some advantages over conventional fluorescence microscopy as it reduces background information from the focal plane and also controls depth of field (Figure 5.2). It uses spatial filtering techniques to remove out of focus glare in samples with thickness greater than the closest plane of focus [14].

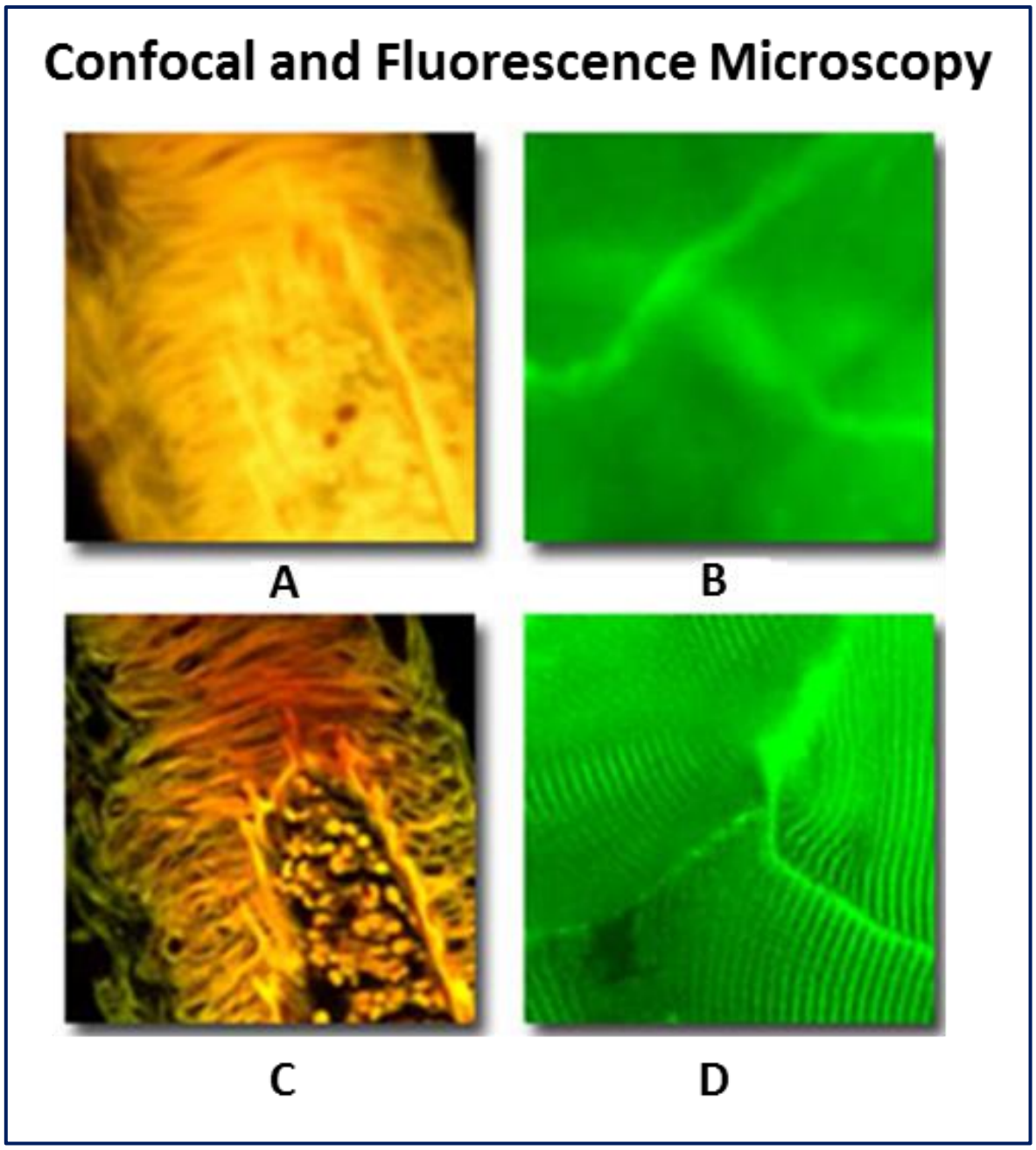

Figure 5.2 Images that compare standard fluorescence microscopy and confocal fluorescence microscopy. In (A), a fluorescently stained human medulla with standard microscope exhibiting intense glare, (C) imaged with laser scanning confocal microscope fluorescent revealing a significant structural detail of the medulla. (B) A standard fluorescence microscopy blurred image of whole rabbit muscle fibres stained with fluorescein and (D) a more resolved whole rabbit muscle fibre imaged with confocal microscopy [14].

Despite this significant improvement, these systems are still limited by diffraction [15]. In order to achieve spatial resolution and overcome the diffraction limit, a number of super resolution fluorescence microscopy methods such as stimulated emission depletion (STED) microscopy, reversible saturable optically linear fluorescence transitions (RESOLFTs), structured-illumination microscopy (SIM), stochastic optical reconstruction microscopy (STORM), photoactivated localization microscopy (PALM), fluorescence photoactivation localization microscopy (FPALM) and saturated excitation (SAX) have been developed. In these new systems developed to beat the diffraction barrier, the key aspect is to make use of fluorescent molecules. This can be achieved by using various means such as stimulated emission, structured illumination, photoactivation, cis-trans isomerization, triplet pumping, saturated excitation. To this point, almost all super resolution microscopy applications are dependent on the excitation and emission properties of fluorescent tags to solve the diffraction limit [2]. These systems offer a spatial resolution of 10 to 100 nm and the most recent developments have reported that 1 nm resolution is achievable [16].

In general, all these methods generate diffraction unlimited images by using the physical characteristics of fluorescent tags to distinguish emissions from two adjacent molecules within a diffraction limited section. The systems fall into two classes; the first class uses patterned illumination to spatially modulate the fluorescence behaviour of molecules within a diffraction limited area, such that they do not illuminate at the same time, thereby achieving sub-diffraction limit resolution. Systems in this class are STED, RESOLT and SSIM [17,18,19,20,21]. The second category uses single molecule imaging, which uses photo-switching or other means to randomly activate separate molecules within the diffraction limited region at different times. Images with sub-diffraction limit resolution are then reconstructed from the measured positions of individual fluorophores.

This class includes systems such as STORM, PALM and FPALM [22,23,24]. Now that I have described how super resolution microscopy beats diffraction limit, the next sub-section 5.1.3 discusses the applications of SRM in biological systems to demonstrate its efficiency.

5.1.3 Super resolution microscopy applications in biological systems

Super resolution microscopy (SRM) has been widely applied in many biology fields and it is expanding to other fields. In this section, I will summarise a few examples including some uses of SRM thus far. Super resolution microscopy has aided the studying of numerous subcellular components and much knowledge has been generated. Because of it, abnormalities or diseases in living organisms can be detected at molecular level. At the early stages of SRM techniques, various subcellular structures (such as microtubules, focal adhesion complexes, endoplasmic reticulum, actin and mitochondria) with well-characterized features were often used as proof of concept model systems [25,26,27]. Such studies demonstrated both the systems' capabilities to visualize molecular structures and synergies in the cellular environment [6].

Super resolution microscopy has provided a platform to understand plasma membrane. In general, plasma membranes are mostly made up of lipids and proteins; and their compositions vary among organisms and organelles [28]. The composition of molecules on the cell membranes has not been fully studied because of diffraction limit as these molecules are nano-scale structures that could not be visualized with conventional imaging systems [29]. The molecules on the cell membrane have various functions, including those involved in the immune systems and disease development in various organisms, such as the use of CD4 receptor and CCR5 co-receptor for HIV infection [30].

The configuration of immune receptors has been comprehensively studied by super resolution systems. Using STED, the interaction between parasites and the plasma membrane; for example, maturation-induced clustering of HIV Env proteins that depends on the Gag interacting env tail has been shown [31]. In a similar fashion, PALM and STORM has been used to understand the interaction between the host and the virus [32,33].

In another study they showed that the Bax protein organises as ring like structures in apoptotic cells [34]. Bax protein is situated on the mitochondrial membrane of apoptotic cells and plays a major role in apoptosis. Its build-up and oligomerisation leads to the release of cytochrome c and ultimately cell death. This observation shed more light on how the abundance of Bax protein contributes to cell death via apoptosis [34,35]. The mitochondrial inner membrane system is suggested to be essential in the protein network that regulates mitochondrial function and structure. The clusters of this system and their distribution in the mitochondria have been illustrated by STED [36]. In the same manner, cytochrome c oxidase subunit 2 in the mitochondria was spotted by STED [37].

Through SRM, we are gaining more understanding of the molecules contained within the nucleus [6]. The analysis of highly compact DNA packaging and its interaction with proteins within the nucleus can only be achieved using super resolution imaging [6]. For instance, studies with 3D SIM showed morphological fluctuations of chromosomes and nuclear lamin during early mitosis [38]. In another study, STORM exhibited a great potential in resolving chromatin fibers [39]. Backer and team created a method of examining the structure of individual DNA strands, and also characterizing DNA-dye interactions [40].

The ability to obtain such crucial information is essential in detecting diseases due to abnormalities at molecular level.

Super resolution microscopy has massively contributed to the understanding of HIV-1 replication, which would have been difficult to achieve with conventional microscopy as HIV is between 120 and 140 nm in diameter [41]. Furthermore, the understanding of HIV-1 replication has contributed in the discovery of anti-HIV treatment. Therefore, SRM is among the technologies/techniques that have significantly contributed towards achieving the great successes obtained thus far in the field of HIV-1 research. Using STORM, it was demonstrated that Gag assembly at the surface of infected cells regulates both *env* mobility and distribution in an *env* cytoplasmic tail manner [32]. Such a process secures *env* incorporation into newly produced viral particles and also prevents the premature activation of *env* fusogenecity, thereby avoiding syncytia formation [32]. This understanding is essential as it is has a potential to lead to the development of an anti-HIV drug that would interfere with this process, thereby producing non-infectious viral particles.

In another study they successfully imaged the HIV integrase enzyme (IN) at approximately 30 nm using FlAsH-PALM [42]. The obtained resolution permitted them to characterize the spreading of integrase within the virions and to distinguish diverse HIV structural populations according to their morphology [42]. Using direct STORM, the changes in the molecular distribution of viral proteins during the infection have been visualized [43]. Mentioned here are only few examples illustrating the significance of various SRM techniques used in biological sciences. The next section will focus on the mechanisms of structured illumination microscopy (SIM), which is the technique used in this thesis.

5.2 Mechanisms of structured illumination microscopy

SIM is a structured illumination technique which uses structured illumination and computational reconstruction to attain up to two times better resolution than the diffraction limit. The grating structured excitation light is shed on the fluorescence distribution of the sample to generate Moiré fringes (Figure 5.3) that have spatial beat frequency from between the structured excitation light and the fluorescing sample [44]. Under normal illumination with no striped pattern (homogeneous illumination), the point spread function of the objective makes it difficult to distinguish between objects separated by a distance bigger than 200 nm. This is because the high spatial frequency information of the sample missing in conventional microscopy can be identified by imaging the Moiré patterns, which have a lower spatial frequency than the sample. Yet with structured illumination, the overlap between the high frequency arrangement of entities within the sample and the high frequency of the illumination lines form a design of lower frequency permitting to make a distinction between two objects parted by 200 nm [44].

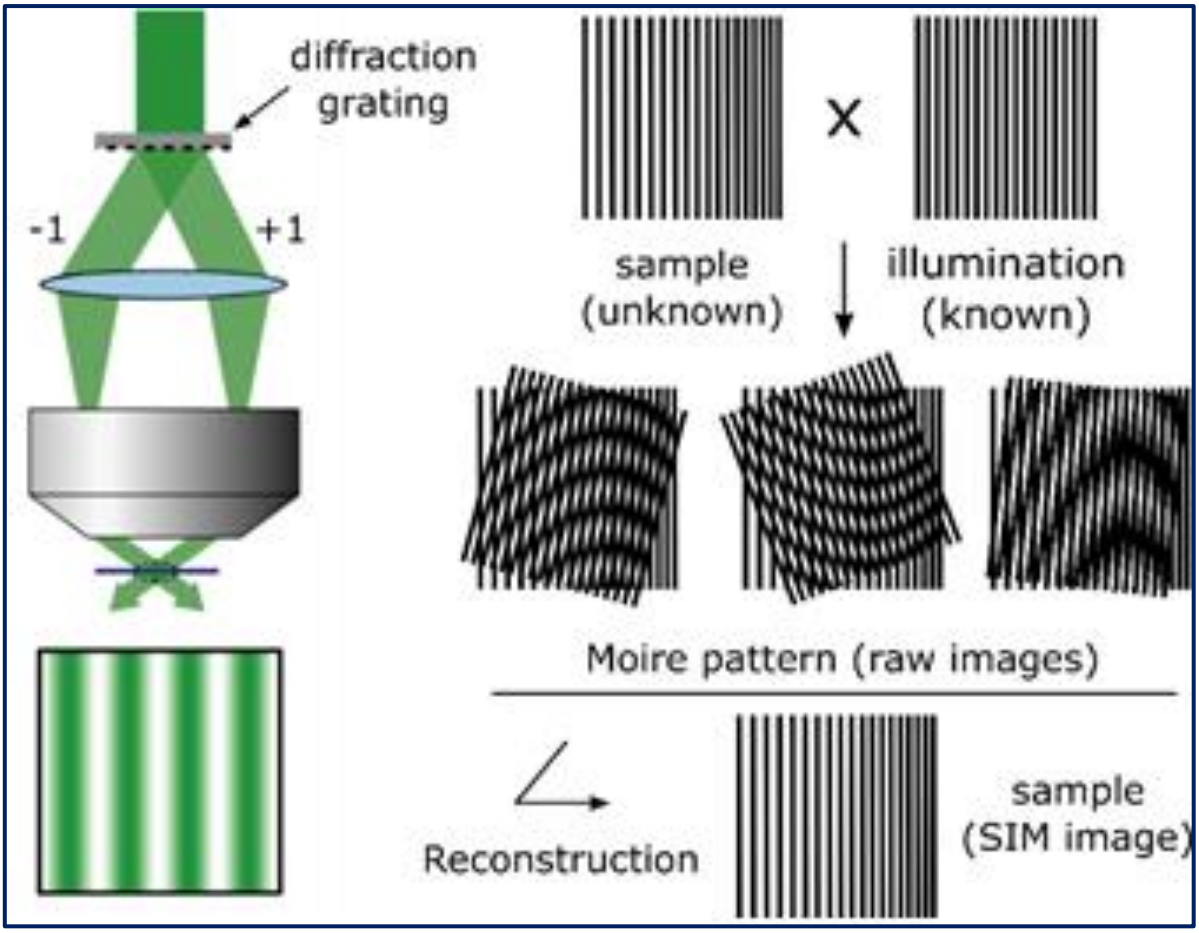

Figure 5.3 Diagram explaining Moiré effect and the SR-SIM principle. A sample with an unknown pattern is illuminated with a known grating pattern on the microscope objective. When the two un-identical patterns are superposed generate moiré fringes with an unresolved image. The unresolved image formed is reconstructed to give rise to the final resolvable image [44,45].

Finally, to produce a highly resolved image, sub-diffractive information is extracted and numerous unprocessed images must be put together, each being attained at different angles of the structured illumination. This is achieved by shifting the diffraction grating (rotation and translation); therefore high resolution is acquired by scanning the sample from different angles in the presence of the Moiré pattern. SIM images can be acquired either in a three dimensional (3D) format or two dimensional format depending on the number of times the diffraction grating shifting takes place.

To obtain a 3D image, 15 images are to be acquired using 3 rotations and 5 translations, whereas the 2D image is obtained with 9 unprocessed images with 3 rotations and 3 translations [46].

Structured illumination microscopy has a spatial resolution that increases by two over the conventional wide-field microscopy and it uses standard dye which makes it less expensive [44]. Furthermore, SIM can use up to four wavelengths; making it a useful method to access multiple resolved information inside cells and suitable for live cell imaging, with high imaging speed while its sample preparation is not complicated [47,48]. Despite its attractive features, it also has a few limitations, such as sensitivity to out of focus light and difficult to focus in thick and densely labelled samples as well the possible generation of artefacts during the image reconstruction, which can ruin the quality of images [49,50].

5.3 Applications of structured illumination microscopy

Commercial forms of SIM are widely used for imaging either extensions or replacements of conventional fluorescence microscopes such as scanning confocal microscopes. Thus far, the use of these systems is mostly observed in structural biology studies using fixed cells. However, live cell imaging is gradually emerging in time lapsed studies. Besides applications in cell biology, SIM has been used in studying bacterial processes and analysis of viral structures. The slow movement of SIM in live cell imaging is due to the speed with which the illumination pattern is produced and moved through the specimen, as well as not yet fully optimized image acquisition time in some systems. Despite the slow progress in SIM live cell imaging, a lot has been done in as far as structural biology studies.

In one study 3D-SIM was used for structural analysis of the dissemination of chromatin in mammalian cells nuclei [51]. Here, up to three different colour channels were concurrently used to visualize chromatin in fixed C2C12 myoblast cells. This was done along with the nuclear pore complex and nuclear lamina. In that study they were able to resolve single nuclear pore complexes which co-localized with channels in nuclear lamina [51]. The three dimensional imaging depth of SIM and specificity of fluorescently stained antibodies has made it possible to co-localize structural proteins in all dimensions. Due to this ability, the visualisation of replication foci down to single replicons has been demonstrated [52]. In another study, Regev-Rudzki supplemented biochemical analysis techniques with SIM to reveal that *Plasmodium falciparum* infected red blood cells use exosome like vesicle for communication between parasites [53]. In a similar study they investigated how the parasite exports proteins and remodels red blood cell structures to ensure that parasites inside infected cells survive [54].

Besides cell biology applications, SIM has also been employed in microbiology in which it has opened a platform for many new possibilities. Several studies in microbiology have studied the distribution and the structure of FtsZ, which is a bacterial homologue of eukaryotic cell tubulin, which assembles into so called Z ring leading up to bacterial cell division. In *Staphylococcus aureus*, *Escherichia coli* and *Bacillus subtilis* SIM demonstrated that Z rings are patchy and discontinuous rather than forming a continuous structure [55,56]. Time lapse imaging enabled them to show that the localization of FtsZ with the Z ring is dynamic and remains heterogeneous throughout the cell division process. These illustrate how efficient this technique is to get to such nano-scale detail. In another study they used SIM to follow the development of the repair of DNA double stranded breaks in living bacterial cells [55].

They were also able to determine the sequence and stoichiometry at which non-identical bacterial enzymes have to assemble at the site of DNA double stranded breaks in order to

identify and repair the local damage. They found that enzyme RecA, which is a repair enzyme, forms packages to regulate the search for damage sites [56]. The use of SIM has shed some light on the position of enzymes involved in bacterial cell division. They used pulse labelling of diving bacteria with fluorescent amino acids and observed that the peptidoglycan septum is continuously made from the cell surface inward and the synthesis takes place at separate locations that circle around the division level. These studies are clear demonstrations that enhancing resolution has brought about new biological insights [57].

In the utilisation of SIM for the analysis of viral structures, individual vaccinia virus particles were imaged to track virus morphogenesis and maturation by using a fluorescent viral clone [58]. Due to the 3D nature of the system, they were able to determine the viral envelope protein B5 as a spherical shape enclosing the virus core, which offers a way of evaluating the degree of maturation of virus particles [58]. A different group used SIM to understand the structure of viral replication complexes of potato virus X [59]. In this chapter SIM is used to check for HIV-1 molecules in infected cells, with the goal to eventually couple the system with optical trapping for diagnostic purposes.

5.4 HIV-1 molecules detected in this study

In chapters 3 and 4 HIV-1 infection was detected by optical trapping coupled with transmission spectroscopy and luminescence spectroscopy, respectively. In chapter 5, I am reporting on how SIM was used for the detection of HIV-1 infection in TZM-bl cells by single molecule analysis, i.e. identifying two HIV-1 molecules; gp41 and p24 in infected cells. For both optical trapping and luminescence spectroscopy, no viral molecules were detected, but HIV infection detection was due to the changes caused by the virus in the cells. In this chapter HIV infection detection

in TZM-bl cells is based on detecting viral molecules in the infected cells. This was done to ascertain that individual molecules of the virus can be detected in infected TZM-bl cells using green fluorescently labelled HIV antibodies and SIM.

HIV and its molecules are less than 200 nm in size and therefore they cannot be clearly imaged or visualized with conventional microscopy, hence this study used SIM. The matured human immunodeficiency virus is around 145 nm in diameter [60]. The virus is roughly 9.8 kilobases in length with nine genes coding for 9 different proteins, which are *Env*, *Pol*, *Gag*, *Rev*, *Tat*, *Nef*, *Vpu*, *Vif* and *Vpr*. The proteins are in three classes, structural, regulatory and accessory proteins [61,62]. However, for the purposes of this work, the focus was on molecules generated from two structural proteins; *Env* and *Gag*, which are gp41 and p24.

The diameter of gp41 according to the electron microscopy analysis was found to be approximately 12.4 nm [63]. The p24 diameter of a matured HIV particle is 55 to 62 nm in diameter on the wide end, and 25 nm in diameter on the narrow end, while the capsid shell is 120 to 130 nm [64]. The differences on the two opposite ends of the capsid (p24) can be seen in Figures 5.4 and 5.5. The capsid protein, p24 (CA) is a 24 kilo-Dalton (kD) protein coded for by the viral Gag structural protein that makes the conical core (as depicted by the navy blue structure in figure 5.4) of viral particles [65].

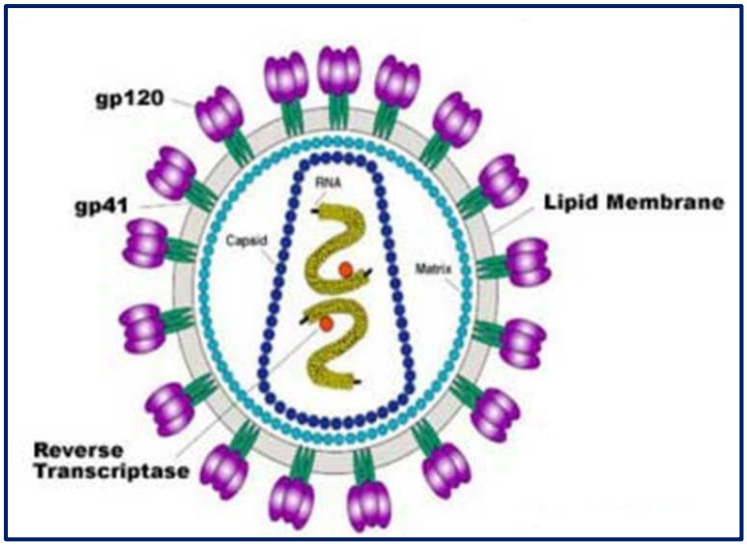

Figure 5.4 Human immunodeficiency virus depicting different virus components. The pink and green trimeric structures on the surface of the virus are gp120 and gp42 envelope proteins, which essential for the entry of the virus into the host cell. They are embedded onto the lipid membrane of the virus. The capsid encloses viral enzymes such as reverse transcriptase and the RNA viral genome and it is the most abundant component of the virus made of thousands copies of the p24 protein [66].

Each viral particle contains approximately 2000 to 4000 p24 molecules (as illustrated in Figure 5.5), making it the most abundant HIV molecule [67].

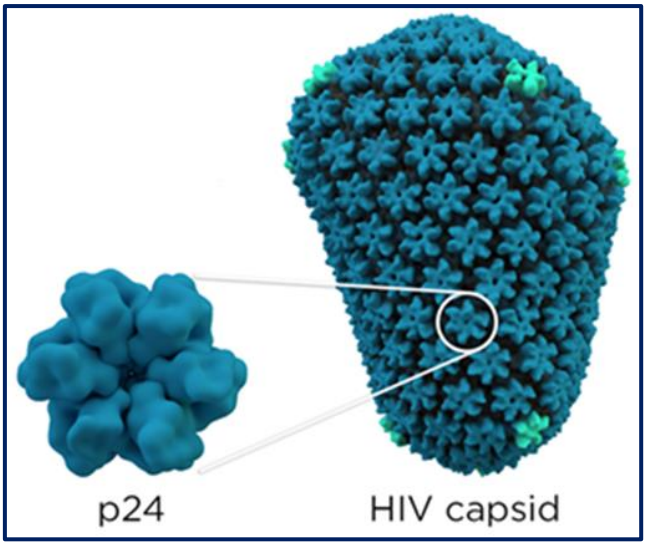

Figure 5.5 The HIV capsid with roughly 2000 copies of the p24 protein. The cone shape of the capsid provides the virus with its conical shape. It is the viral protein that encloses the viral RNA and core proteins of the virus [68].

The p24 antigen emerges within 2 weeks of HIV infection due to the early rapid viral replication resulting to high levels of the virus; with the infected individual being highly infectious [69]. At both early and late HIV infection stages p24 is always at high levels, rendering it a marker of choice for diagnosis [70]. For early diagnosis of HIV infection, p24 protein (antigen) is detected and its early detection has reduced the window period to about 17 days post-infection and enables acute infection identification [71]. The detection of p24 antigen is disrupted by the rise of antibodies, which is most likely due to the development of antigen-antibody complexes in the blood [69]. Since p24 is the most abundant viral molecule, it is the antigen of choice to detect for infant HIV diagnosis as the use of antibody tests could lead to false positive results due to the presence of the mother's antibodies present in the child [69].

The glycoprotein 41 (gp41) is a 41 kD protein which is part of the gp160, a160 kD envelope (Env) structural protein of HIV. Gp 41, an envelope transmembrane protein (the green trimeric

structures in Figure 5.4) coded with gp120, an envelope surface protein (illustrated by the purple trimeric structure in Figure 5.4) [72]. The gp160 envelope protein is the HIV surface protein responsible viral entry into the host cell. While gp120 is mainly responsible for viral attachment as it binds to the CD4 receptor and co-receptor (CCR5 or CXCR4). During attachment conformational changes in both gp120 and gp41 occur, thereby exposing a gp41 region which facilitates fusion of the virus to the host cell membrane [73]. Therefore, gp41 plays a crucial role in HIV infection so much that there is an antiretroviral drug, Enfuvirtide which is a fusion inhibitor [74].

5.5 Detection of HIV infection in TZM-bl cells using structured illumination microscopy

The TZM-bl cells were infected with ZM53 HIV-1 pseudovirus and incubated for 48 hours before being labelled and imaged with Carl Zeiss Confocal LSM 780 Elyra S1 with SR-SIM. The images obtained were analyzed and processed using the Zeiss ZEN lite software in order to obtain clear images of the samples. The results obtained revealed that both gp41 and p24 were well detected in infected TZM-bl cells using confocal microscopy and SIM as illustrated in Figure 5.5.

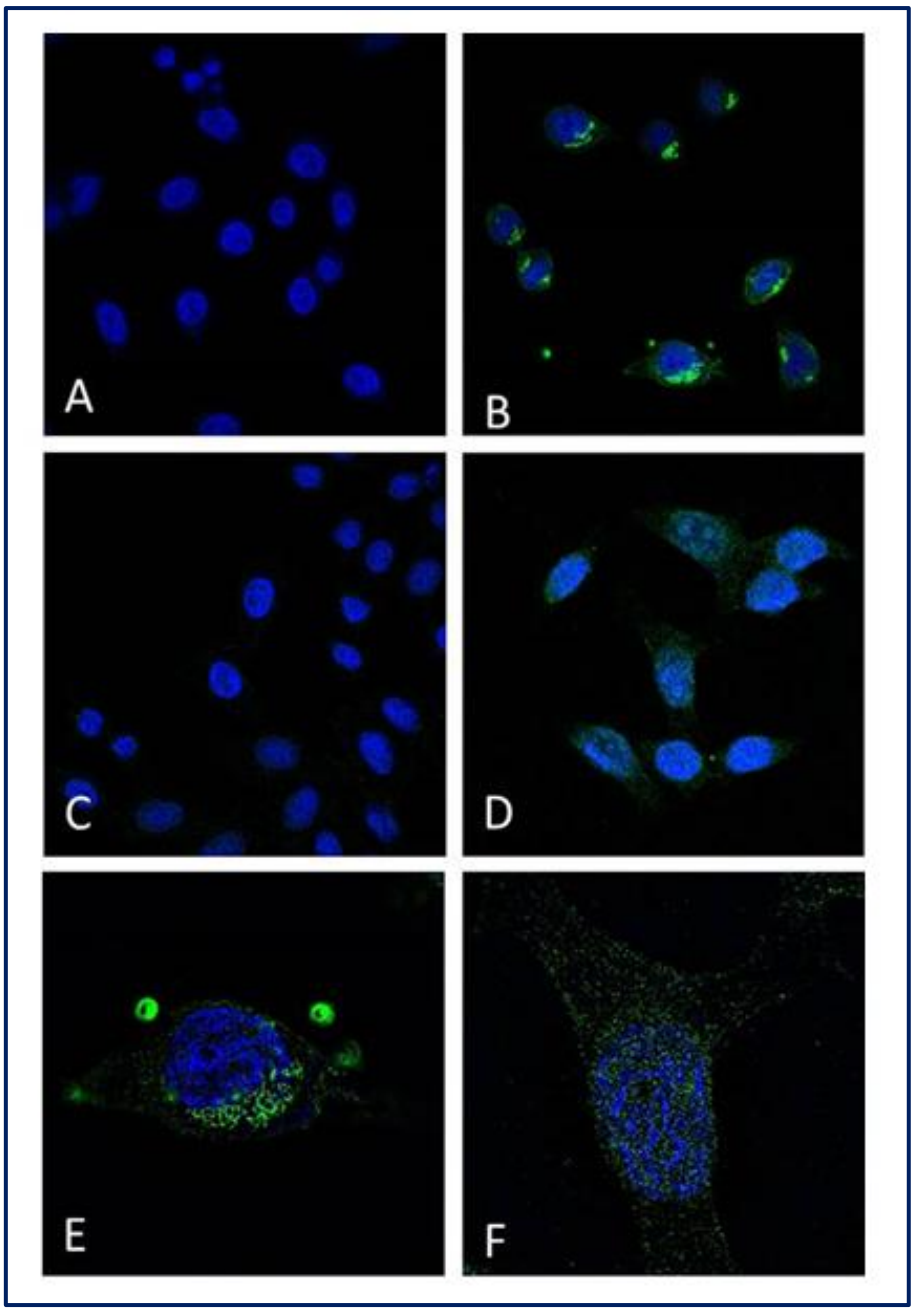

Figure 5.6 Images of labelled TZM-bl cells captured using confocal microscopy and separately SIM showing gp41 and p24 in HIV-1 infected TZM-bl cells. Figure A is an uninfected sample of TZM-bl cells with no green staining, while figure B exhibits HIV-1 infection through green fluorescent gp41 sections on the cells following imaging via confocal microscopy. In figure C a control sample of uninfected cells is compared to infected cells in figure D, where the p24 protein is expressed as green fluorescence after confocal microscopy scanning. The micrograghs in E and F are the 3D snapshots displaying gp41 and p24 respectively in infected cells captured via SIM.

The blue background in images displayed in Figure 5.6 is as a result of staining cells with the Hoescht dye, which stains the cell nucleus and therefore both infected and uninfected cells appeared blue. In addition, the infected cells (Figures 5.6B, D, E and F) also had a green fluorescence because the secondary antibody was attached to a green fluorescent marker, Alexa 488. So the infected cells have green fluorescence which indicates that the viral antibodies used indeed were bound to the viral molecules on the infected cells. Therefore, the presence of the green fluorescence was a confirmation that indeed the cells were infected with HIV. On the other hand, the uninfected cells have no green fluorescence which signifies that no viral molecules were detected in them.

5.6 Discussion

The main aim of the experiments done in this chapter was to confirm what had been revealed by other techniques such as luminescence detection, optical trapping coupled with transmission spectroscopy; that indeed the cells were infected with HIV by visually demonstrating the presence of HIV molecules in the infected cells (Figure 5.6B, D, E and F). The results obtained showed that SIM and confocal microscopy successfully detected HIV infection in TZM-bl cells infected with the ZM53 HIV-1 pseudovirus. This finding confirmed that indeed SIM has better resolution compared to conventional light microscopy, as viral molecules between 12.4 nm and 130 nm were viewed [44, 63, 64]. This correlates well with what has been shown previously, where Hulme *et al* 2015 showed that viral complexes found in the nucleus exhibited a lesser amount of p24 compared to complexes localized at the nuclear membrane and in the cytoplasm [75]. In that study they were able to observe different intensities of p24 at different sites and stages [75]. In another study, the number and localisation of p24 foci post infection was successfully identified and the p24 foci sizes which vary throughout the virus interaction with the cell using SIM were determined [76].

By using confocal microscopy to examine gp41 membrane topology, Liu *et a*l 2010 confirmed that gp41 has a single membrane spanning domain [77]. This was necessary after a different topology model had suggested that gp41 has multiple membrane spanning domains [77].

Furthermore, Figures 5.6A and C which are images of uninfected cells display the specificity of the HIV antibodies used because no fluorescence was detected in uninfected cells despite labelling them in the same way as the infected ones. This demonstrates that the SIM images acquired did not have background noise that would make interpreting results confusing. It further validates the efficiency of the ZEN lite software used for analysis, as it meticulously extracted all the valuable information thus enabling the differentiation of the two cell populations with great ease. The analysis with ZEN lite was necessary as the formation of moire fringes (as described in section 5.2 and illustrated in Figure 5.3) obscure the valuable information in the acquired images which necessitates that the acquired images must be processed in order to attain well resolved images that would display what was in the experimental cells. The images in Figure 6 clearly prove that the ZEN life software effectively processed the images. This is worth noting as one of the limitations of using SIM is that artefacts may be generated during image reconstruction which tends to ruin the quality of images [50]. Therefore, these findings show that there were no artefacts generated.

Additionally, the simplicity of sample preparation and the use of conventional dyes when imaging cell molecules made SIM an attractive imaging option for this study, without compromising the results obtained and using expensive techniques [44]. Being able to successfully use SIM and confocal microscopy for the detection of HIV infection in TZM-bl cells emphasizes the notion that the type of SRM is chosen based on the purpose of the

experiment and the desired goal. In addition, even with confocal microscopy we were able to detect p24 and gp41, however using SIM had an added advantage as the images could be viewed in a 3 dimensional manner as shown in Figures 5.6 E and F. Whereas confocal microscopy images in Figures 5.6 B and D the images could only be viewed from a single dimension.

Successfully imaging and visualising virus molecules in the infected cells, gives the confidence that coupling of the SRM imaging systems with a trapping system would enable the studying of individual cells in order to see the inherent cellular properties thus differentiating between HIV infected and uninfected cells. Such a step would enrich the study as we will be able to study intrinsic properties of cells which would lead to the development of label free detection systems that would fulfil the ultimate goal of developing affordable point of care diagnostic devices for resource limited settings.

References

1. Light microscopy, http://www.ruf.rice.edu/~bioslabs/methods/microscopy/microscopy.html; [Accessed 3 September 2018].
2. Yamanaka M, Smith NI, Fujita K. Introduction to super-resolution microscopy. Microscopy 2014; 63(3):177-192.
3. Patterson GH. Fluorescence microscopy below diffraction limit. Seminars in Cell and Developmental Biology 2009; 20(8):886-893.
4. Abbe's diffraction limit, https://www.kurzweilai.net; [Accessed 3 September 2018].

5. Huang B, Bates M, Zhuang X. Super resolution fluorescence microscopy. Annual Review of Biochemistry 2009; 78:993-1016.
6. Huang B, Babcock H, Zhuang X. Breaking the diffraction barrier: Super-resolution imaging of cells. Cell 2010; 143(7):1047-1058.
7. Abbe E. Beitr€age zur Theorie des Mikroskops und der mikroskopischen Wahrnehmung. Arch Mikrosk Anat 1873; 9:413–418.
8. Born, Max. Principles of Optics. Cambridge University Press, 1999.
9. Thompson RE, Larson DR, Webb WW. Precise nano-meter localization analysis for individual fluorescent probes. Biophysical Journal 2002; 82:2775–2783.
10. Fliegel K. Modeling and Measurement of Image Sensor Characteristics. Radioengineering 2004; 13(4):27-34.
11. Galbraith CG, Galbraith JA. Super resolution microscopy at glance. Journal of Cell Science 2011; 124(10):1607-1611.
12. Zipfel WR, Williams RM, Webb WW. Nonlinear magic: multiphoton microscopy in the biosciences. Nature Biotechnology 2003; 21:1369–1377.
13. Long BR, Robinson DC, Zhong H. Subdiffractive microscopy: techniques, applications, and challenges. Wiley Interdisciplinary Reviews. Systems Biology and Medicine 2014; 6(2):151–168.
14. Confocal microscopy, https://www.olympus-lifescience.com/en/microscope-resource/primer/techniques/confocal/confocalintro/; [Accessed 5 September 2018].
15. Hell SW. Toward fluorescence nanoscopy. Nature Biotechnology 2003; 21:1347–1355.
16. Balzarotti F, et al. Nanometer resolution imaging and tracking of fluorescent molecules with minimal photon fluxes. Science 2017; 355:606–612.

17. Hell SW, Wichmann J. Breaking the diffraction resolution limit by stimulated emission: stimulatedemission-depletion fluorescence microscopy. Optics Letters 1994; 19:780–782.

18. Klar TA, Hell SW. Subdiffraction resolution in far-field fluorescence microscopy. Optics Letters 1999; 24:954–956.

19. Hofmann M, Eggeling C, Jakobs S, Hell SW. Breaking the diffraction barrier in fluorescence microscopy at low light intensities by using reversibly photoswitchable proteins. Proceedings of the National Academy of Sciences of USA. 2005: 102:17565–17569.

20. Gustafsson MGL. Nonlinear structured-illumination microscopy: wide-field fluorescence imaging with theoretically unlimited resolution. Proceedings of the National Academy of Sciences of USA. 2005; 102:13081–13086.

21. Heintzmann R, Jovin TM, Cremer C. Saturated patterned excitation microscopy—a concept for optical resolution improvement. Journal of the Optical Society of America. A 2002; 19:1599–1609.

22. Rust MJ, Bates M, Zhuang XW. Sub-diffraction-limit imaging by stochastic optical reconstruction microscopy (STORM). Nature Methods 2006; 3:793–795.

23. Betzig E, Patterson GH, Sougrat R, Lindwasser OW, Olenych S, Bonifacino JS, Davidson MW, Lippincott-Schwartz J, Hess HF. Imaging intracellular fluorescent proteins at nanometer resolution. Science 2006; 313:1642–1645.

24. Hess ST, Girirajan TPK, Mason MD. Ultra-high resolution imaging by fluorescence photoactivation localization microscopy. Biophysical Journal 2006; 91:4258–4272.

25. Ober RJ, Ram S, Ward ES. Localization Accuracy in Single-Molecule Microscopy. Biophysical Journal 2004; 86:1185–1200.

26. Ben-Tekaya H, Miura K, Pepperkok R, Hauri HP. Live imaging of bidirectional traffic from the ERGIC. Journal of Cell Science 2005; 118:357-367.

27. Jakobs S. High resolution imaging of live mitochondria. Biochimica et Biophysica Acta 2006; 1763(5-6):561–575.

28. Shevchenko A, Simons K. Lipidomics: coming to grips with lipid diversity. Nature Reviews Molecular Cell Biology 2010; 11:593–598.

29. Sezgin E. Super resolution optical microscopy for studying membrane structure and dynamics. Journal of Physics: Condensed Matter 2017; 29:273001.

30. Alkhatib G, Combadiere C, Broder CC, Feng Y, Kennedy PE, Murphy PM, Berger EA. CC CKR5: a RANTES, MIP-1alpha, MIP-1beta receptor as a fusion cofactor for macrophage-tropic HIV-1. Science 1996; 272:1955–1958.

31. Chojnacki J, Staudt T, Glass B, Bingen P, Engelhardt J, Anders M, Schneider J, Müller B, Hell SW, Kräusslich HG. Maturation-dependent HIV-1 surface protein redistribution revealed by fluorescence nanoscopy. Science 2012; 338:524–528.

32. Roy NH, Chan J, Lambele M, Thali M. Clustering and mobility of HIV-1 Env at viral assembly sites predict its propensity to induce cell-cell fusion. Journal of Virology 2013; 87:7516–7525.

33. Muranyi W, Malkusch S, Muller B, Heilemann M, Krausslich HG. Super-resolution microscopy reveals specific recruitment of HIV-1 envelope proteins to viral assembly sites dependent on the envelope C-terminal tail. PLoS Pathogen 2013; 9:e1003198.

34. Salvador-Gallego R, et al. Bax assembly into rings and arcs in apoptotic mitochondria is linked to membrane pores. The EMBO Journal 2016; 35:389–401.

35. Grosse L, Wurm CA, Bruser C, Neumann D, Jans DC, Jakobs S. Bax assembles into large ring-like structures remodeling the mitochondrial outer membrane in apoptosis. The EMBO Journal 2016; 35:402–413.

36. Jans DC, et al. STED super-resolution microscopy reveals an array of MINOS clusters along human mitochondria. Proceedings of the National Academy of Sciences of USA 2013; 110:8936–8941.

37. Singh H, et al. Visualisation and quantification of cardiac mitochondrial protein clusters with STED microscopy. Mitochondrion 2012; 12:230–236.

38. Schermelleh L, Carlton PM, Haase S, Shao L, Winoto L, Kner P, Burke B, Cardoso MC, Agard DA Gustafsson, MGL, et al. Subdiffraction multicolor imaging of the nuclear periphery with 3D structured illumination microscopy. Science 2008; 320:1332–1336.

39. Matsuda A, Shao L, Boulanger J, Kervrann, C, Carlton PM, Kner P, Agard D, Sedat JW. Condensed mitotic chromosome structure at nanometer resolution using PALM and EGFP- histones. PLoS ONE 2010; 5:e12768.

40. Backer AS, Lee MY, Moerner WE. Enhanced DNA imaging using super-resolution microscopy and simultaneous single-molecule orientation measurements. Optica 2016: 3, 659-666.

41. Chojnacki J, Eggeling C. Super-resolution fluorescence microscopy studies of human immunodeficiency virus. Retrovirology 2018; 15:41.

42. Lelek M, Di Nunzio F, Henriques R, Charneau P, Arhel N, Zimmer C. Superresolution imaging of HIV in infected cells with FlAsH-PALM. Proceedings of the National Academy of Sciences of USA 2012; 109(22):8564-8569.

43. Pereira CF, Rossy J, Owen DM, Mak J, Gaus K. HIV taken by STORM: Super-resolution fluorescence microscopy of a viral infection. Virology Journal 2012; 9:84.

44. Gustafsson MG. Surpassing the lateral resolution limit by a factor of two using structured illumination microscopy. Journal of Microscopy 2000; 198:82–87.

45. Moire effect, https://www.cherrybiotech.com; [Accessed 15 September 2018].

46. Carlton PM. Three-dimensional structured illumination microscopy and its application to chromosome structure. Chromosome Research 2008; 16(3):351–365

47. Sydor AM, Czymmek KJ, Puchner EM, Mennella V. Super-Resolution Microscopy: From Single Molecules to Supramolecular Assemblies. Trends Cell Biology 2015; 25:730–748.

48. Wegel E, et al. Imaging cellular structures in super-resolution with SIM, STED and Localisation Microscopy: A practical comparison. Scientific Reports 2016; 6(1):27290.

49. Jost A, Heintzmann R. Superresolution Multidimensional Imaging with Structured Illumination Microscopy. Annual Review of Materials Research 2013;43(1):261–282.

50. Kraus F, et al. Quantitative 3D structured illumination microscopy of nuclear structures. Nature Protocols 2017; 12(5):1011–28.

51. Schermelleh L; et al. Subdiffraction multicolor imaging of the nuclear periphery with 3D structured illumination microscopy. Science 2008; 320(5881):1332−1336.

52. Chagin VO; et al. 4D Visualization of replication foci in mammalian cells corresponding to individual replicons. Nature Communications 2016; 7:11231.

53. Regev-Rudzki N; et al. Cell-cell communication between malaria-infected red blood cells via exosome-like vesicles. Cell 2013; 153(5):1120−1133.

54. Riglar DT; et al. Spatial association with PTEX complexes defines regions for effector export into Plasmodium falciparum-infected erythrocytes. Nature Communications 2013; 4:1415.

55. Strauss MP; Liew AT; Turnbull L; Whitchurch CB, Monahan LG, Harry EJ. 3D-SIM super resolution microscopy reveals a bead-like arrangement for FtsZ and the division machinery: implications for triggering cytokinesis. PLoS Biology 2012; 10 (9):e1001389.

56. Rowlett VW; Margolin W. 3D-SIM super-resolution of FtsZ. and its membrane tethers in *Escherichia coli* cells. Biophysical Journal 2014; 107(8):L17−L20.

57. Bisson-Filho AW; et al. Treadmilling by FtsZ filaments drives peptidoglycan synthesis and bacterial cell division. Science 2017; 355(6326):739−743.

58. Horsington J, Turnbull L, Whitchurch CB, Newsome TP. Sub-viral imaging of vaccinia virus using super-resolution microscopy. Journal of Virological Methods 2012; 186(1−2):132−136.

59. Wanner G, Schroeder-Reiter E, Ma W, Houben A, Schubert V. The ultrastructure of mono- and holocentric plant centromeres: an immunological investigation by structured illumination microscopy and scanning electron microscopy. Chromosoma 2015; 124(4):503−517.

60. Briggs JAG, Wilk T, Welker R, Kräusslich HG, Fuller SD. Structural organization of authentic, mature HIV-1 virions and cores. The EMBO Journal. 2003; 22(7):1707–1715.

61. Muesing MA, et al. Nucleic acid structure and expression of the human AIDS/lymphadenopathy retrovirus. Nature 1985; 313:450-458.

62. Gallo R, et al. HIV/HTLV gene nomenclature. Nature 1988; 333:504.

63. Zhu P, Chertova E, Bess, J, Lifson JD, Arthur LO, Liu J, Roux KH. Electron tomography analysis of envelope glycoprotein trimers on HIV and simian immunodeficiency virus virions. Proceedings of the National Academy of Sciences of USA 2003; 100(26):15812–15817.

64. Gelderblom, Hans, et al. Morphogenesis, maturation and fine structure of lentiviruses. Stockton Press, 1990.

65. Franke EK, Yuan HE, Luban J. Specific incorporation of cyclophilin A into HIV-1 virions. Nature 1994; 372:359-362.

66. Human immunodeficiency virus, https://web.stanford.edu/group/virus/retro/2005gongishmail/HIV.html; [Accessed 15 July 2019].

67. Summers MF, et al. Nucleocapsid zinc fingers detected in retroviruses: EXAFS studies of intact viruses and the solution-state structure of the nucleocapsid protein from HIV-1. Protein Science 1992; 1:563-574.

68. HIV Capsid, https://commons.wikimedia.org/w/index.php?curid=41336993; [Accessed 10 September 2018].

69. Nolan ML, Greenberg AE, Fowler MG. A review of clinical trials to prevent mother-to-child HIV-1 transmission in Africa and inform rational intervention strategies. AIDS 2002; 16:1991–1999.

70. de Wolf F, Lange JM, Houweling JT, Coutinho RA, Schellekens PT, van der Noordaa J, Goudsmit J. Numbers of CD4+ cells and the levels of core antigens of and antibodies to the human immunodeficiency virus as predictors of AIDS among seropositive homosexual men. The Journal of Infectious Diseases 1988; 158:615-622.

71. Fiebig EW, et al. Dynamics of HIV viremia and antibody seroconversion in plasma donors: implications for diagnosis and staging of primary HIV infection. AIDS 2003; 17:1871–1879.

72. Chan DC, Fass D, Berger JM, Kim PS. Core Structure of gp41 from the HIV Envelope Glycoprotein. Cell 1997; 89:263–273.

73. Mao Y, Wang L, Gu C, Herschhorn A, Xiang S, Haim H, Yang X, Sodroski J. Subunit organization of the membrane-bound HIV-1 envelope glycoprotein trimer. Nature Structural & Molecular Biology 2012; 19(9):893–899.

74. Chan DC, Kim PS. HIV entry and its inhibition Cell 1998; 93(5):681–684.

75. Hulme AE, Kelley Z, Foley D, Hope TJ. Complementary Assays Reveal a Low Level of CA Associated with Viral Complexes in the Nuclei of HIV-1-Infected Cells. Journal of Virology 2015; 89(10):5350-5361.

76. Marno K, Al'Zoubi L, Pearson M, Posch M, McKnigh, A, Wheeler AP. The evolution of structured illumination microscopy in studies of HIV. Method. 2015;.88:20-17.

77. Liu S, Kondo N, Long Y, Xiao D, Iwamoto A, Matsuda Z. Membrane topology analysis of HIV-1 envelope glycoprotein gp41. Retrovirology 2010; 7:100.

Chapter 6

Conclusion

This chapter presents a conclusion on the five chapters of this thesis and future work regarding the findings in each of the chapters. In chapter 1, a concise report about HIV, its pathogenesis, various types and subtypes, and other topics associated with it such as treatment challenges and its global distribution are outlined. Furthermore, techniques used in this work such as LLLT for HIV infection control, optical trapping, spectroscopic analysis and single molecule analysis for the detection of HIV-1 infection in TZM-bl cells are summarized before their applications are explored in subsequent chapters. The laser driven systems were used for both the treatment and diagnosis of HIV-1 infection in TZM-bl cells, as lasers have properties that are beneficial in the biological and medical sciences. The outcomes of the study showed that the use of laser based systems for treatment and diagnosis is effective and has a great potential in the field of medicine.

In Chapter 2, a brief history of lasers is given followed by the principles of laser while highlighting the role of each component as well as the two modes of laser output. An overview of laser therapy is outlined by describing the history of light therapy, the mechanisms of LLLT while drawing attention to various cellular components that are necessary in order for a therapy to yield beneficial results. This is then followed by an extensive discussion on the choice of laser wavelength as various wavelengths interact differently with biological material (tissues, cells and organelles) and thereby yielding different results. The interaction of laser with

biological matter according to wavelengths was explained in order to give guidance on the laser choices for various experiments in the field of Biophotonics.

Chapter 2 focused on the use of LLLT towards controlling HIV-1 infection in TZM-bl cells. The results obtained showed a significant reduction in HIV-1 infection in laser irradiated cells. Moreover, as the fluence increased there was further reduction in infection and an increase in undesirable effects on cells was observed. Furthermore, the fluence could not be increased beyond 10 J/cm^2 as that would have increased the exposure time to more than an hour as the power of the laser used was only 30 mW on the sample stage. The fluence is dependent on laser power output, time and the area to be irradiated. When the power is low, the irradiation time would be longer. Nonetheless, the response of cells to irradiation is also dependent on the cell type; it is possible that other cells types would have less undesirable effects compared to the ones observed in TZM-bl cells used in this study. Moreover, the wavelength used also influences how the cells respond to irradiation, with more studies it is possible to find the best wavelength that would successfully reduce HIV-1 infection in TZM-bl cells and also have less undesirable side effects. Of note, in LLLT, there are no standard factors to achieve a desired goal; the efficacy of LLLT based studies are largely influenced by the cell/tissue type and the laser wavelength used, and therefore there are variation between studies.

Additionally, the combination of LLLT and efavirenz further reduced HIV-1 infection in TZM-bl cells and the cells irradiated at 10 J/cm^2 in the presence of efavirenz showed a reduction in infection that was comparable to the uninfected cells. That outcome was a good indication that combining these two unrelated therapies has a great potential.

Such an outcome is promising in the search for an effective HIV treatment as there is a possibility that eventually there could be a way of eradicating HIV infection. Currently, HIV

infected individuals have to be on a lifelong treatment, so far, the available treatment has been unable to get rid of the virus that is lying dormant in the various latent sites within the human body. It is the presence of those latent sites that requires the continuous use of the treatment as the discontinuation of the treatment would lead to the emergence of drug resistant strains of the virus, thereby complicating the disease as there could be unavailability of effective treatment [1]. However, if LLLT would be effective there would be an alternative treatment and also a new form of treatment that has a potential to lead to complete eradication of the infection. Moreover, based on the reports of the use of LLLT in the treatment of other medical conditions, LLLT is reported to have fewer side effects compared to the use of drugs [2]. In the case of HIV treatment, over the years the treatment has improved and the current treatment has lesser side effects compared to the treatment that was used initially [3]. Despite that improvement, which has made the treatment to be tolerable and therefore increased adherence, the treatment is still life long. That is a challenge and therefore an alternative treatment modality which has a potential to eradicate the infection is desirable. Therefore, the next phase of the study would be looking into the use of other laser wavelengths on different cell types and eventually select the most effective wavelength for the irradiation of HIV infected cells. Also, further investigations will be done in order to establish the laser treatment mechanisms that lead to the reduction of HIV infection in TZM-bl cells. The ultimate goal of this study is to develop a device that would be used for HIV treatment at point of care. The work reported here was done *in vitro* with one wavelength and one type of cell line.

Chapter 3 of this thesis was based on the use of optical trapping and transmission spectroscopy for label-free detection of HIV-1 infection in TZM-bl cells. The chapter begins by giving an overview on the various optical trapping modes, followed by a description of forces that govern

optical traps; the influence of wavelengths, particle sizes and the role of the Q value method to determine trapping efficiency in optical trapping systems. Thereafter the assembling of an optical trapping system (Figure 3.7) used in this thesis was provided, followed by a demonstration of trapping 2 μm polystyrene beads (Figure 3.8) and 25 μm TZM-bl cells (figure 3.9) using the newly assembled setup. The ability to trap both the beads and cells showed that the trapping system was working well and of good efficiency. The capably functioning trapping system was then coupled to a transmission spectroscopy in order to analyze individually trapped cells for the detection of HIV-1 infection.

The results obtained revealed that the infected and uninfected cells had different transmittance percentages, with uninfected cells transmitting more light as compared to the infected cells (Figures 3.13 and 3.14). These findings were a clear indication that these two cell populations interacted differently with light and those differences enabled differentiation between HIV infected and uninfected cells without using any labels, stains or bio-markers. The following phase of this study would be to determine scientific reason behind the two cell populations behaving differently in transmitting light. Therefore, factors such as oxygen content, nutrient levels, and cell diameter variations would need to be assessed. So far, it can be said that the presence of the virus in the infected cells caused lesser light to be transmitted in the infected cells due to differences in refractive indices of the infected and uninfected cells. Furthermore, additional measurements and analyzes will be performed through coupling the optical trapping system with Raman spectroscopy, which is more sensitive than transmission spectroscopy applied in the current phase of the study.

The ultimate goal of the work of chapter 3 is to develop a laser driven system that would be used at a point-of-care for HIV diagnosis.

Chapter 4 is about the detection of HIV-1 infection in TZM-bl cells using luminescence spectroscopy. The chapter opens by discussing luminescence mechanism, which involves the processes that lead to the development of luminescence and then specifically touches on bioluminescence; the type of luminescence that was used in this study. The chapter goes on into discussing principles of luminescence spectroscopy as well as the elements that are essential for a luminescence spectroscopy system (Figure 4.5), followed by the summary of where luminescence has been used for analytical purposes. As the chapter continues, it shows that for the first time HIV-1 infection in TZM-bl cells was detected using the Horiba Jobin Yvon Fluorolog spectrometer (Figure 4.7) and the findings are comparable with the use of a luminometer (a widely used system). The use of the Horiba Yvon Fluorolog spectrometer was of great benefit as the luminescence decay was monitored with more ease in comparison with the luminometer.

With the Horiba Yvon Fluorolog the luminescence decay curve was monitored automatically and that cannot be achieved on a luminometer. Besides just being able to detect HIV-1 infection in TZM-bl cells, the ease of working with this system would be of benefit in the assay such as ATP measurement and even in the establishment of other new assays that need luminescence detection. The detection and quantification of the infection in TZM-bl cells using luminescence spectroscopy highlighted the importance of inherent cellular characteristics in disease diagnosis, because the presence of the luciferase gene in TZM-bl cells is what enables the detection of HIV infection as the luciferase gene is only expressed when HIV infection has taken place.

Despite the yet unknown system in human blood cells that could act in a similar manner, the findings of this experiment are an encouragement to continue searching for a molecule or a system in the human blood cells or human cells in general that can only be detected with laser when HIV infection has occurred. The current tests use antibodies and since we are moving towards simplifying diagnostics tests, further improvements are necessary.

In chapter 5, Structured Illumination Microscopy was used for single molecule analysis in HIV-1 infected TZM-bl cells. Firstly, in section 5.1 the overview of super resolution microscopy is discussed by summarizing its development, examining its ability to pass the diffraction limit of light in order to observe nanometer structures and how the passing of the diffraction limit has enabled for many successful investigations to be done in nano and micro scale biological systems. The chapter then focuses on the principles of SIM as it uses Moire fringes in order to provide structured illumination so that a clear distinction between objects separated by 200 nm may be made. Later on in sections 5.4 and 5.5 SIM is used for the detection of HIV-1 molecules in TZM-bl cells. HIV infection in TZM-bl cells was successfully detected or confirmed by picking viral molecules using SIM and confocal microscopy. The detection of HIV molecules in infected cells is an established system, which was used in this study to ensure that viral molecules could be detected by microscopy in TZM-bl cells infected with a pseudovirus.

Furthermore, it was a means of establishing that indeed it will work in our setting before coupling it to an optical trapping system, which is what the next level of the study would focus on. The coupling of an imaging system to our trapping system would enable us to analyze both infected and uninfected cells with confidence knowing that the infected cells are marked. Such a step would then allow us to carefully study and be able to pick up cellular changes between

infected and uninfected cells. As there is a possibility that HIV infection induces changes in some cellular molecules and such changes can be used as means of distinguishing between infected and uninfected cells. Such a finding would bring a different approach to HIV diagnosis as the already established methods focus on antibodies and also on viral molecules. Focusing on host molecules will bring in a different approach, which could simplify HIV diagnosis and even meet the World Health Organization (WHO) required ASSURED (Affordable, Sensitive, Specific, User-friendly, Rapid and robust, Equipment-free and Deliverable to end users) standards.

In this thesis laser driven techniques have demonstrated a great potential in the Biophotonics research area. The major goal of the work reported here is to develop laser driven point-of-care devices for both treatment and diagnosis of various medical conditions. The need to develop such devices was motivated by the lack of diagnostic devices and procedures that can be used by people in low resource settings. The great improvements in the medical field in recent years have brought about an increase in the use of automated laboratory testing procedures with reduction in operation time and improvement in reliability. These improvements have been beneficial especially because diagnostics have become a vital part of medicine. These systems are coupled with the use electronic medical reporting that allows doctors to get results quicker, thereby improving patient care [4]. However, such advanced systems cannot be of benefit across various population groups. These technologies are centralized and can only be operated by highly skilled personnel in specialized facilities. As a result, most laboratory testing is costly and unaffordable to the majority of patients particularly in resource limited countries. Due to that disparity, various organizations including the WHO proposed the development of different diagnostic tools that would be used in situations or locations with poor access to centralized laboratories. Such tools can be used at point of care; that is at sites closer to patient care or

easily accessible to patients and also provide clinicians with results within hours or minutes [5, 6 and 7]. These tools eliminate two major steps between sample collection and availability of results, which are specimen transportation and laboratory processing. The advent of these tools improved health care services for the benefit of the patient. Such devices should meet the WHO's ASSURED criteria as a standard to decide if tests focus on disease control demands: Affordable, Sensitive, Specific, User-friendly, Rapid and robust, Equipment-free and Deliverable to end users. As such scientists from diverse fields are developing point-of-care devices especially for diagnostic purposes [8].

Finally, the outcomes of chapters 3, 4 and 5 illustrate that light-based label free diagnostic techniques are attainable. This is founded on the outcomes of chapters 3 and 4, which show that intrinsic properties of cells can be used for diseases diagnosis. For instance, in chapter 3, by simply measuring transmittance percentage of HIV infected and uninfected cells it was possible to distinguish between the two cell populations. In chapter 4, the capability of TZM-bl cells to express a luciferase gene when infected by HIV caused them to be differentiated from the uninfected ones that do not express the luciferase gene and therefore no luminescence can be detected in them. The findings in chapter 5 confirmed what was observed in chapters 3 and 4. These findings will contribute towards the development of a laser driven HIV point of care device that would not only detect the presence of HIV-1 infection, but it will also detect the presence of HIV drug resistance mutations as well as viral load detection.

References

1. Pace MJ, Agosto L, Graf EH, O'Doherty U. HIV Reservoirs and Latency Models. Virology 2011; 411(2):344-354.
2. https://www.chiroeco.com/low-level-laser-therapy/ 2 October 2018

3. Buell KG, Chung C, Chaudhry Z, Puri A, Nawab K, Ravindran RP. Lifelong antiretroviral therapy or HIV cure: The benefits for the individual patient, AIDS Care. 2016; 28(2): 242-246.

4. Uys PW, Warren R, van Helden PD, et al. Potential of rapid diagnosis for controlling drug susceptible and drug-resistant tuberculosis in communities where Mycobacterium tuberculosis infections are highly prevalent. J Clin Micro. 2009; 47:1484–90.

5. Mabey D, Peeling RW, Ustianowski A, Perkins MD. Diagnostics for the developing world. Nature Reviews. 2004; 2:231–240.

6. Peeling RW, Mabey D. Point-of-care tests for diagnosing infections in the developing world. Clin Microbiol Infect. 2010; 16:1062–69.

7. Mabey D, Peeling RW, Perkins MD. Rapid and simple point-of-care diagnostics for STIs. Sex Transm Infect. 2001; 7:397–98.

8. Gift TL, Pate MS, Hook EW, Kassler WJ. The rapid test paradox: when fewer cases detected lead to more cases treated: a decision analysis of tests for Chlamydia trachomatis. Sex. Transm. Dis. 1999; 26: 232–240.

Appendices

Appendix A

Cell growth conditions, virus production and infection of TZM-bl cells

I. Conditions for cell growth and maintenance

The two cells lines that were used are TZM-bl cells (ATCC, PTA-5659) and HEK 293T/17 cells (ATCC, CRL, 11268). The HEK 293T/17 cell line was used for the production of HIV-1 pseudovirus that was used to infect TZM-bl cells. Both cell lines were grown, maintained and cultured in a cell growth medium made up of Dulbeco's minimal essential medium (DMEM, Sigma-Aldrich, D5796), 10% fetal bovine serum (FBS, FBS Superior, S 0615), 0.5% L-Glutamine-Penicillin-Streptomycin (Sigma-Aldrich, G6784) at 37°C, 5% CO_2 and 85% humidity. Since both cell lines were adherent, trypsin-EDTA solution (Sigma-Aldrich, T4049) was used to bring cells into suspension as they detach from the surface of the culture flask. The cells in suspension were used various experiments.

II. Preparation and titration of ZM53 pseudovirus

For the production of HIV-1 ZM53 pseudovirus, 4 µg of an expression plasmid containing the *env* gene of ZM53 and 8 µg of a plasmid carrying the backbone of HIV-1, but deficient of the *env* gene (pSG3ΔEnv) were used to co-transfect HEK 293T/17 cells. The Superfect transfection reagent (Qiagen, 310305) was added in the mixture of the two plasmids in order to facilitate the entry of DNA into cells with ease due to the interaction between the cell surface charges and charges on the Superfect reagent. Using the 50% tissue culture infectious dose (TCID50), the suitable virus titre was determined.

III. In vitro infection and sample preparation

For the various assays done, the TZM-bl cells were infected with different volumes (50, 100, 150 and 200 µl) of the virus in 35 mm diameter culture dishes, with uninfected cells used as a negative control and the increase in virus volumes added to cells translates to an increase in virus concentration. The infected cells were then incubated for 48 hours in conditions outlined in A*I*. Cells were then rinsed with Hank's Balance Salt Solution (HBSS) (Gibco, Life Technologies, 14170-088), trypsinized, resuspended in growth medium. Following this, cells were divided into various parts in order to perform different assays. For imaging experiments, the TZM-bl cells were grown on 22 mm^2 coverslips in 8 well rectangular culture plates.

Appendix B

Biological assays

I. Cell morphology

The assessment of cell morphology is essential in cell culture experiments, as it is a physical means of determining whether the cells are healthy or unhealthy. In this study, cell morphology was monitored in order to determine the influence of HIV infection, efavirenz and irradiation on the cells. This examination was done using a light microscope (CKX41, Olympus) and images were taken using a digital camera attached to the microscope.

II. Cell viability assay

The CellTiter-Glo® luminescent cell viability assay (Promega, Anatech, G7573) is a means of establishing cell viability in culture by quantifying adenosine triphosphate (ATP), which is an indicator of metabolically active cells within a given cell population. The addition of the

reagent to the cells results in cell lysis, thereby generating a luminescent signal that is proportional to the quantity of ATP cells. Equal volumes of cell suspension and ATP reagent were added together and mixed to induce cell lysis. The mixture was allowed to stabilize at room temperature for 10 minutes in the dark. The luminescence was recorded using the GloMax® Discover System (Promega, Anatech) in relative light units (RLUs).

III. Cell proliferation assay

The CellTiter 96® non-radioactive cell proliferation assay (Anatech, Promega) is a colorimetric assay used to evaluate cell metabolic activity. It makes use of NAD(P)H-dependent cellular oxidoreductase enzymes that reduce the tetrazolium dye MTT 3-(4,5-dimethylthiazol-2-yl) -2,5-diphenytetrazolium bromide, which is yellow in colour to formazan that is purple in colour. The assay was performed in a 96 well plate by mixing 15 µl of the Dye solution with 100 µl of the cell suspension and the mixture was then incubated at 37°C for 4 hours. After 4 of incubation, 100 µl Solubilization solution was added and the plate was allowed to stand at room temperature in the dark for 1 hour. Prior to measuring absorbance by reading the plate at 600 nm using the Glomax® Discover System, the contents were mixed using a multichannel pipette for even distribution of the newly formed substance (formazan).

IV. Membrane integrity assay

The CytoTox 96® non-radioactive cytotoxicity assay (G1780, Anatech, Promega) is a colorimetric assay that measures lactate dehydrogenase (LDH) enzyme. LDH is a stable cytosolic enzyme released by damaged tissues and cells into their environment (cell medium). This assay therefore evaluates the presence of tissue and cell damage.

It was done by mixing equal volumes of the cell medium and LDH assay reagent in a 96 well plate and incubated in the dark at room temperature for 30 minutes. The reaction was terminated by adding 50 µl of the Stop solution and absorbance was measured at 490 nm using the Glomax® Discover System.

V. Luciferase assay

A luciferase (Luc) reporter gene assay which measures the reduction of HIV as a function of Tat-regulated Luc reporter gene expression after a single round of HIV in TZM-bl cells was done using the Bright-Glo™ luciferase assay system (E2610, Anatech, Promega) to evaluate HIV infection in TZM-bl cells. TZM-bl cells are a CXCR4 positive cell line that expresses both CD4 and CCR5, which are essential cellular surface receptors for the entry of HIV-1 into cells. They also contain integrated Tat-inducible luciferase and E.coli β-galactosidase reporter genes and these two reporter genes get expressed when TZM-bl cells are infected with HIV. In the current study, luciferase activity which is measured by RLUs was determined and RLUs are directly proportional to the number of infectious virus particles present in the initial inoculum. During the experiment 100 µl of the luciferase reagent was added to an equal volume of the cell suspension and incubated in the dark for 2 minutes. The luciferase activity was quantified with the GloMax® Discover System.

VI. Flow cytometry

The flow cytometry experiments using Fluorescein isothiocyanate (FITC) Annexin V Apoptosis Detection Kit I (BD Biosciences, Johannesburg, South Africa) were performed to determine the type of cell death experienced by cells following HIV infection.

Following irradiation at different fluences, the cells were incubated for further 24 hours, thereafter flow cytometry experiments were conducted. During flow cytometry experiments, the cell culture medium was removed and placed in a 15 ml centrifuge tube. Following this, cells in the culture dish were rinsed with HBSS, and 500 µl of trypsin was added in each culture dish and placed in the incubator for 5 minutes to allow cells to detach from the culture dish, leaving them in suspension. Once successfully in solution, 1 ml of growth medium was added to the cells and this mixture transferred to a 15 ml tube containing the culture medium and centrifuged for 10 minutes at 2200 rpm. The cell pellet was then rinsed twice with cold PBS and re-suspended by adding 500 µl of 1X annexin V binding buffer. From the 500 µl cell suspension, 100 µl was stained in 5 ml tubes with 5 µl of annexin-V and 5 µl of propidium iodide (PI) and incubated on ice for 30 minutes. The stained cells were suspended in 400 µl of annexin V binding buffer before flow cytometric analysis. For positive controls, apoptosis and necrosis were induced using Dimethyl sulfoxide (DMSO) and ice cold methanol, respectively. The samples were analyzed using the BD Accuri C6 cytometer.

VII. *Reactive Oxygen Species Detection*

Reactive Oxygen Species (ROS) was visualized with CellROX® oxidative stress green reagent (C10444, Life Technologies), which is a DNA dye that binds with DNA upon oxidation and its signal is localized primarily in the nucleus and mitochondria. After irradiation at different fluences, the cells were incubated for 1 hour under normal cell growth conditions. After incubation, 750 µl of the growth medium was removed and only 250 µl remained in the culture dish. To the 250 µl medium, 1 µl of 25 mM CellROX green reagent was added and the contents of the dish were mixed by gently swirling to ensure even distribution of the reagent throughout the plate and incubated for 30 minutes. The cells were washed three times with 1X Phosphate

Buffered Saline (PBS) and 500 µl of PBS was left in the dish to prevent desiccation during sample viewing under the fluorescent microscope (CKX41, Olympus).

Appendix C

Luminescence spectroscopy and imaging experiments

I. Luminescence Spectroscopy

The steady state spectra of photoluminescence emission were obtained using a Horiba Jobin Yvon Fluorolog 3 photoluminescence spectrometer. For luminescence spectroscopy work, equal volumes of the cell suspension and the luciferase agent were mixed and incubated for 2 minutes before transferring into a plastic cuvette. The cuvette was then transferred into the Horiba Jobin Yvon Fluorolog 3 photoluminescence spectrometer system. The emission resulting from the expression of the luciferase gene in infected TZM-bl cells was then recorded with a fast photomultiplier tube detector coupled to the Horiba Jobin Yvon Fluorolog 3 system.

II. Imaging

Cells were fixed with 4% formaldhehyde, washed with phosphate buffered saline (PBS) and blocked for 10 minutes with 5% donkey serum. Cells were incubated at 4°C with primary antibodies (anti-HIV1 p24 antibody and anti-HIV1 gp41 antibody) overnight. The cells were washed with PBS before incubating them for an hour with the secondary antibody; donkey anti-mouse IgL H&L (Alexa Flour 488) pre-adsorbed (Abcam, ab150109) and washed with PBS. For nucleus staining, the cells were incubated with Hoechst for 10 minutes and washed with PBS. The coverslips were then mounted on microscope slides using the fluorescence mounting media.

All samples were visualized and imaged using the Carl Zeiss Confocal LSM 780 Elyra S1 with SR-SIM at the Central Analytical Facility, University of Stellenbosch.